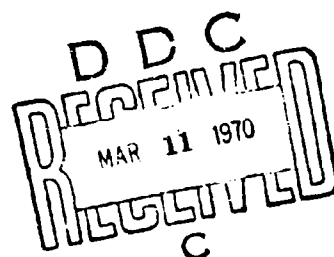AD702490

SPECIFICATION OF THE WIND DISTRIBUTION
IN THE MARINE BOUNDARY LAYER
FOR WAVE FORECASTING

by

Vincent J. Cardone

New York University

School of Engineering and Science

University Heights, New York, N.Y. 10453

Geophysical Sciences Laboratory TR69 -1

Department of Meteorology and Oceanography

Research Division

D D C

MAR 11 1970

C

This document has been approved
for public release and sale; its
distribution is unlimited.

144

New York University
School of Engineering and Science
Department of Meteorology and Oceanography

Geophysical Sciences Laboratory TR-69-1

SPECIFICATION OF THE WIND DISTRIBUTION
IN THE MARINE BOUNDARY LAYER
FOR WAVE FORECASTING

by

Vincent J. Cardone

December 1969

ERRATA for

Specification of the Wind Distribution in the Marine Layer for Wave Forecasting

by
Vincent J. Cardone

	<u>for</u>	<u>read</u>
p. 13, line 16	duration or fetch	fetch or duration
p. 19, eq. (2.9)	$L = \dfrac{-U_*^3 K C_p \overline{\rho}_a}{gH}$	$L = \dfrac{-U_*^3 C_p \overline{\rho}_a T}{KgH}$
p. 19, line 8	where C_p ...	where T is temperature, C_p is ...
p. 29, line 8	amplitude a.	amplitude G.
p. 31, eq. (3.17)	$e^{-\vec{k}\,\eta}$	$e^{-k\eta}$
p. 31, eq. (3.20)	$\nu/1.09$	$\nu/1.09\,U_*$
p. 95, line 13	ane	and
p. 101, line 21	tha	the
p. 103, line 22	correlation	correction
p. 103, line 23	incorporated	incorporates
p. 126, line 16	.LT.05	.LT..05
p. 126, line 20	SLN = 0	SL = 0
p. 128, 1 below 1110	(B*G/F*S)	(B*G/(F*S))
p. 128, 1 below 1114	LOG(B*G/F*	LOG(B*G(F*
p. 128, 2 below 1114	-FI	-FI)
p. 128, 1 below 1140	5.15*TD	(5.15*TD)
p. 129, 1 above 1155	INDEX=2	INDEX=2 GO TO 1110

Preface

This technical report describes research by Dr. Cardone that began in 1966 and has been sponsored by three different contracts as its scope increased and as the many applications that it will have become apparent.

The first application of this work is to use available data more intelligently in the development of numerical wave hindcasting and forecasting procedures. In 1964, a wave climatology for the North Atlantic was produced that used ship reports to generate the wind fields for the wave hindcasts. It took one half an hour on a CDC 1604 to generate the wind fields for every six hours for a year. Although the hindcasts gave quite good results, it was clear that higher resolution wind fields and a better theory for the winds in the planetary boundary layer would improve the quality of wave predictions. This report more than adequately makes up for the naïveté of previous wind field models in the planetary boundary layer.

A second goal for this study was to aid in the development of the software to be used should radar scatterometry and passive microwave data become available from a spacecraft. The definition of the winds over the ocean depends on many factors. Work is actively in progress to combine the results of this paper with simulated data such as might be obtained from remote sensing techniques so that an optimum analysis of the planetary boundary layer can be made. This report makes it possible to develop ways to use the widely scattered ship reports over the ocean obtained on a synoptic basis in an intelligent way for the extrapolation and interpolation of spacecraft data into areas not observed by ships.

A numerical model of the North Atlantic Ocean is presently under development for the Office of Naval Research. For this model, the wind stress at the sea surface and the sensible and latent heat fluxes at the air sea boundary are needed. The procedures described in this report define the wind stress at the sea surface, the atmospheric stability and the air sea temperature differences on an oceanic scale.
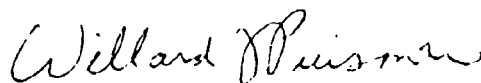
i

Although not described in this report, Dr. Cardone is developing the extensions needed to compute evaporation from the sea surface and sensible heat exchange. This report is thus a basic building block in the development of procedures for modeling the oceans.

For all of 1966 and the first eight months of 1967, this work was sponsored by the U.S. Naval Oceanographic Office under Contract N62306-1589, Task Order No. 3 in connection with our still uncompleted efforts to develop a wave climatology for the North Pacific.

From September 1967 to August 1968, this work was supported by the Office of Naval Research under Contract Nonr 285(57).

Since September 1968 this work has been supported about equally by the Spacecraft Oceanography Project of the U.S. Naval Oceanographic Office and by the Office of Naval Research under the above ONR contract and under Contract N62306-68-C-0249.

In my opinion, this report provides a firm foundation for all of these efforts. It serves as the first important step in interpreting the wealth of micrometeorological data for global scale application over the oceans in the practical problems of making better weather forecasts and wave forecasts, and developing oceanographic forecasts.

Willard J. Pierson, Jr.
Professor of Oceanography

Table of Contents

Table of Contents (cont.)

iv

List of Figures

List of Figures (cont.)

vi

List of Figures (cont.)

Acknowledgments

Abstract

The operational application of spectral ocean wave specification models to wave forecasting is limited mainly by the inadequacy of the meteorological input supplied to these models by existing meteorological analysis techniques. One of the more successful models, whose spectral growth formulation is based upon the Miles-Phillips resonance and instability wave generation mechanisms, is shown to require no less than a specification of the wind distribution in the marine surface boundary layer. This study demonstrates how this requirement can be satisfied in a computerized objective format from routinely available meteorological data and prognostic fields.

Wave generation theory is employed to develop a quantitative formulation for the effects of atmospheric stability upon the development of the wave spectrum. In terms of this stability dependent spectral growth formulation, the effects of stability on wave generation are found to be significant and compare well with observational studies of the dependence of wave height and whitecap production on air-sea temperature difference.

A simple model of the non-neutral, baroclinic planetary boundary layer over a sea surface described in terms of an internally prescribed roughness parameter is derived. The model is shown to provide a suitable framework for the diagnosis of the marine surface boundary layer wind distribution from prognostic fields of sea level pressure, air temperature and sea surface temperature.

The model is consistent, as the surface is approached, with a surface
boundary layer model constructed around similarity profile forms
that are shown to be applicable, at least under active wave generating
conditions, to the flow near the sea surface. Finally, it is shown how these
models can be objectively applied to ships' weather observations and
routine prognostic fields to satisfy the requirements of wave hind-
casting and forecasting.

1. Introduction

The introduction of the spectral concept to the study of water waves by Pierson and Marks (1952) led to new methods of describing and predicting ocean surface waves. A practical wave forecasting technique employing spectral concepts was developed by Pierson, Neumann and James (1955) and was based on the fully developed spectral form and spectral growth rates proposed by Neumann (1953). The latter were derived from data collected by Neumann on the vessel "Heidberg" where the wind velocities were measured at a height of 7.5 meters above sea level. The method was eventually incorporated into a large-scale numerical wave specification model (Baer, 1962) capable of diagnosing the two-dimensional wave spectrum on a grid array representing the North Atlantic Ocean every two hours, given the meteorological input. In that limited study, the meteorological input consisted of grid point values of surface wind speed and direction read from hand-analyzed streamflow-isotach charts.

The application of the similarity theory of S. A. Kitaigorodskii to a large sample of wave recorder data collected on the British weather ships enabled Pierson and Moskowitz (1964) to develop a spectral form that rather successfully described the spectra of fully developed seas in terms of the wind speed at 19.5 meters above mean sea level. Further, it was shown that a consideration of the variation of wind with height through the use of logarithmic profile and the drag coefficient proposed by Sheppard (1958) brought the results of Neumann, Pierson and Moskowitz and others into close agreement (Pierson, 1964). The study also demonstrated that the lack of consideration of the variation

of wind with height in the formulation of the PNJ method and in the cal-
culation of the wind field for Baer's model was clearly to their detriment
and affected resulting wave forecasts in an uncontrollable way.

The fully developed spectral form of Pierson and Moskowitz
forms the basis of an improved wave specification model (Pierson,
Tick and Baer, 1966), an important aspect of which is that the spectral
growth is specified in terms of wave generation theory. Theoretical
work during the past decade has revealed the two dominant physical
processes responsible for wave generation in the frequency range of
practical interest. On the one hand, Phillips (1957) proposed that
pressure fluctuations on the sea surface associated with atmospheric
turbulent eddies being convected by the mean wind excite, by resonance,
a wide range of frequencies in the wave spectrum with a corresponding
linear growth rate of a spectral component. Miles (1957) proposed a
mechanism whereby the pressure field induced on the sea surface by a
sheared air flow over a wave disturbed surface results in a transfer of
energy to the waves and an exponential growth rate of a spectral com-
ponent. Miles' theory has since been improved (Miles, 1959), and
extended theoretically (Phillips, 1966) to include certain aspects of
turbulent air flows.

It may be concluded from the results of several recent field
and wind tunnel studies that the above body of theory is at least in out-
line correct and relevant to the description of the dominant modes of
generation by wind of a large portion of the wave spectrum. Further,
it appears that Phillips' resonance mechanism is significant only for
the initial excitation of gravity waves, with the feedback mechanisms

accounting for most of the energy input. Inoue (1967) analyzed data on
wave growth from many sources and working within the framework of
the theory was able to develop expressions for wave generation that
proved to be superior to earlier methods when applied to sample wave
hindcasts for the North Atlantic Ocean.

Implicit in the increasing sophistication of wave specification
models is the need for a more accurate and detailed meteorological
input. Indeed, what is required by state of the art wave prediction
models is a specification of the wind distribution in the surface boundary
layer over the sea on as small a time and space scale as possible. The
challenge to provide such meteorological analyses in an objective,
computerized format must be met if existing models are to be made
operational and utilized to their fullest extent. Such analyses may also
provide a base of meteorological information from which future even
more complex wave specification models can be tested and evaluated.

One can distinguish between two broad applications of wave
specification models. First, they may be applied to meteorological
forecasts to produce wave forecasts. Until such time as time-dependent
and highly detailed boundary layer models are integrated into numerical
weather prediction schemes, the meteorological forecast prod'·ts ·:ost
adaptable to wave forecasting are sea level pressure and temperature
prognoses such as those currently produced by primitive equation pre-
diction models. Secondly, wave specification models may be applied
to wave hindcasting; that is, the calculation of wave fields from an
historical record of meteorological data. Wave hindcasting has been
employed to test wave specification models, as well as to calculate

wave spectrum climatologies. Also, since it is currently impossible
to specify the initial conditions for a wave forecasting model from data,
the initial conditions are calculated through a wave hindcasting procedure
operating on initial meteorological analyses.

A meteorological analysis procedure for wave forecasting
must then be capable of specifying the required input from both forecasted
meteorological fields and from routine observations. An analysis scheme
is proposed in this study that satisfies these requirements by incorporat-
ing models of the surface and planetary boundary layers of the marine
atmosphere into an objective computerized analysis procedure.

A simple two-layer model of the marine planetary boundary
layer has been developed that includes the effects of atmospheric stability,
baroclinicity and a realistic description of the lower boundary. The
model makes possible the specification of the meteorological input for
wave forecasting from prognoses of sea level pressure and temperature
and a knowledge of sea surface temperature. The lower layer of the
planetary boundary layer model is consistent with a surface boundary
layer model that is employed to utilize routine ships' observations of
wind and air-sea temperature difference to the specification of the re-
quired meteorological input.

The inclusion of the effects of atmospheric stability in the
analysis procedure allows such effects to be incorporated into the
wave forecasting model. As a part of this study, a spectral wave
forecasting model is extended to include the effects of stability on wave
growth, and the results are compared with empirical studies revealing
the effects of stability on wave height and whitecap production.

The analysis model is particularly well suited to the utilization

of new sources of marine data that are likely to become available in the near future. For example, as a part of IGOOS*, an international marine data-gathering buoy system is under active development, and it is possible that a prototype network of such a system could be in operation as early as 1973. The part of this study that deals with the treatment of the several existing types of observations at sea should help in the utilization of buoy data for an accurate definition of the wind field near the sea surface.

Another important source of data that may become routinely available is measurements of radar sea return from an orbiting satellite. It has been demonstrated experimentally that such measurements are a measure of sea state and that they may reflect largely the high frequency part of the wave spectrum (Moore and Pierson, 1967). Should this be the case, radar measurements would provide an indirect observation of the local wind field. To infer the wind speed at any height near the sea surface from such measurements will require the application of surface boundary layer theory as is done in this study.

When they become available, these new sources of data should greatly improve our knowledge of the low level wind field over the world's oceans. Part of the analysis procedure outlined in this study could be applied to such analyses to yield improved analyses of wind and pressure in the marine planetary boundary layer. These analyses could in turn be coupled with satellite infrared spectroscopic measurements to provide the three-dimensional distribution of geopotential in the marine atmosphere, a basic input to numerical weather prediction models. The most immediate benefit of such analyses, however,

---

*International Global Oceanic Observing System.

is to wave specification. Hence, before describing the analysis model in more detail, it would be fruitful to describe in detail the meteorological requirements of the wave specification model under development at New York University.

2. Meteorological Aspects of a Spectral Wave Specification Model

2.1 Spectral growth formulation

In the absence of nonlinear effects, the growth of a wave spectral component can be expressed as (see, e.g., Snyder, 1965)

$$\frac{d}{dt} S(f, x, t) = A(f, x, t) + B(f, x, t) S(f, x, t) \qquad (2.1)$$

where $S(f, x, t)$ is the one-dimensional spectral density of the component at frequency f at the point x and time t, and A and B represent functions of the wind field. The quantity A has been given physical significance through the theory of Phillips (1957) which explains the initial generation of gravity waves on an undisturbed sea surface through a resonant excitation of gravity waves by incoherent atmospheric turbulent pressure fluctuations. Snyder and Cox (1966) conducted a field study in which they measured the growth rate of waves seventeen meters long. Utilizing measurements of the atmospheric turbulent pressure spectrum (over mowed grass) by Priestly (1965), they concluded that Phillips' resonance mechanism was probably responsible for the initial excitation of tne 17 meter waves.

In the formulation of the wave growth for a wave specification model, Inoue (1967) utilized the measurements of Priestly and Snyder and Cox, and following the method developed by Barnett (1967) formulated a general expression for A as a function of frequency and wind speed. In the process, the wind data were corrected to 19.5 meters through the use of a logarithmic profile, since atmospheric stability was near neutral in the field conditions encountered. By the very nature of the formulation, then, at least for neutral conditions, it is

important that the meteorological input to Inoue's model be designed so as to produce winds representative of 19.5 meters. Failure to do so introduces errors in both the amplitude and peak frequency of the implied atmospheric pressure spectrum. It should be noted, however, that the calculations of spectral growth by both Snyder and Cox (1966) and Barnett and Wilkerson (1967) suggest that in most instances of practical significance, only a very small portion of energy input to waves by the wind is done so through a resonance mechanism. It appears that the mechanism acts merely to trigger growth by an instability mechanism which in turn is responsible for most of the wave energy.

The quantity B in equation (2.1) has been given dynamical and physical significance through a series of studies beginning with the pioneering work of Miles (1957). In that study, Miles was the first to calculate the amplitude of the component of atmospheric pressure, induced by a prescribed free surface wave, in the air flow over the wave and in phase with the wave slope, but the model was rather idealized in that the air flow over the waves was regarded as quasi-laminar, atmospheric turbulence being neglected except in the sense that the mean wind profile was specified as logarithmic. The main conclusion of that work was that energy is transferred from the air flow to a wave of a given phase speed at a rate proportional to the ratio of wind profile curvature to slope at the elevation where the wind speed equals the phase speed, the so-called critical or matched layer. Miles (1960) then presented a more accurate version of this model and combined it with the resonance model to show that the two were rather complementary, each generating mechanism dominating in different states of wave development. Phillips (1966) was successful in extending Miles' model to include

some aspects of atmospheric turbulence and showed that these effects were most important in determining the energy transfer by an instability mechanism from wind to wave components possessing phase speeds near or above anemometer height wind speeds.

The important result of the combined Miles-Phillips instability theories is that the spectral density of a wave component increases exponentially with time or fetch (until dissipative effects become important) with the magnitude of the dimensionless growth rate given as

$$\frac{B}{f} = \frac{\rho_a}{\rho_w} \frac{2\pi}{C^2 k} \left\{ \frac{A_m \Gamma^2 k^4}{\cos^2 a} \left(-\frac{U''}{U'^3} \right)_{z_m} \left(\int_{z_m}^{\infty} [U \cos a - C]^2 e^{-kz} dz \right)^2 \right.$$

$$\left. + A_p \int_{o}^{\infty} \Gamma^2 (-U'') \cos a |U \cos a - C| e^{-2kz} dz \right\} \qquad (2.2)$$

where ρ_a and ρ_w are air and water density respectively, C is phase speed, k is wave number, U'' and U' the mean wind profile curvature and slope, a the directional difference between wind and wave, and z_m the elevation where wind speed and phase speed are equal. A_m and A_p are constants and Γ^2 is a number taking on the value $+1$ below the matched layer and is less than one above. The first integral on the right-hand side of (2.2) and its coefficient is Miles' solution, and the second integral is Phillips' contribution, with the range at integration limited to the fully turbulent region of the flow.

To compare the theory with available observations of wave growth, of course, requires estimates of the constants A_m, A_p and Γ above the matched layer. Miles' quasi-laminar analysis gives $A_m = \pi$ and $\Gamma^2 = 1/3$. Phillips (1966) remarks that they are probably of the same order in turbulent flow as well. The value of A_p can only be

found by experiment and Phillips (1966) employed Motzfeld's (1937)
measurements of the air flow over solid wave models to show A_p is
about 1.6×10^{-2} with an uncertainty of roughly $\pm 30\%$. The intro-
duction of the logarithmic profile

$$U = \frac{U_*}{K} \log \frac{z}{z_o} \tag{2.3}$$

where $U_* = \sqrt{\tau_o / \rho_a}$, where τ_o is the surface stress, K is von
Kármán's constant, and z_o is the virtual origin of the logarithmic
profile, and Charnock's (1955) relation for z_o

$$z_o = \frac{a U_*^2}{g} \tag{2.4}$$

where a is a constant and g is the gravitational acceleration,
reduces (2.2) to a relation between B/f and U_*/C (Phillips, 1966).
Values for a have most often been suggested between .01 and .035
and in this range, the calculation is not too sensitive to a. Figure 1
indicates the theoretical form (2.2) calculated under these assumptions
with the value of the constants A, A_{in}, and Γ used as cited above and
a value of a of .02. Also shown is the collection of experimental
data analyzed by Inoue (1967) and the growth rate proposed in that
study. It is seen that the theory in its unmodified form provides at
least order of magnitude agreement with the available data in the
range of U_*/C above .03, but the predicted growth rates are too low
by a factor of 4 at high U_*/C and somewhat too high at lower U_*/C.
Below U_*/C of about .03, the theoretical predictions depart consider-
ably from the data, but it is   possible that these data represent
conditions in which strong dissipative mechanisms are operating.[*]

_____

[*]For a detailed account of the criteria employed to determine the
  data points shown, see Inoue (1967), p. 20.
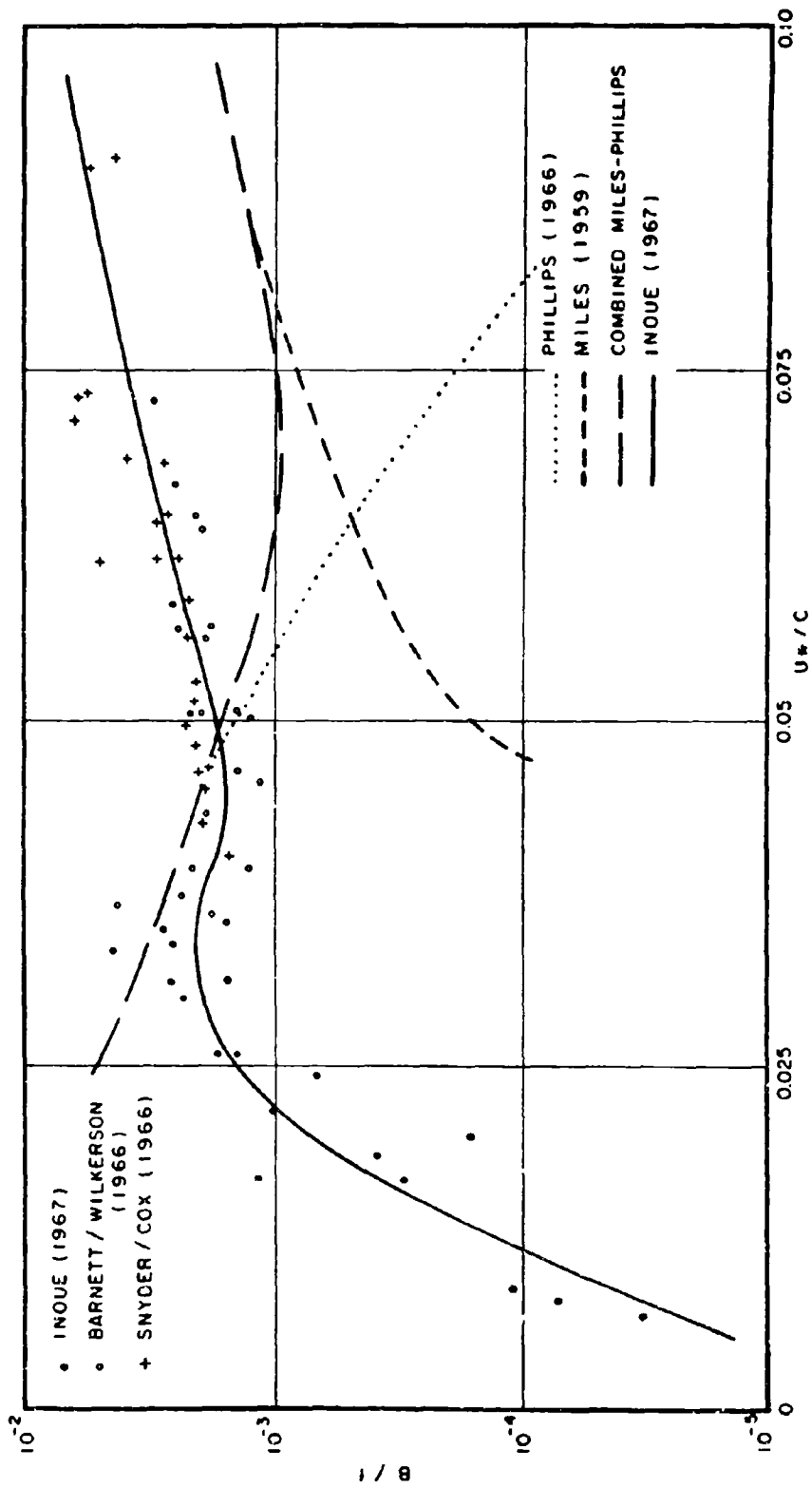
FIG. 1

Dimensionless growth rate, B/f, of the instability mechanism versus dimensionless friction velocity, U_*/C.

11

An increase of the factor $(A_m l^2)$ in equation (2.2) by about 4, and a
slight adjustment of A_p will produce essentially the best fit curve of
Inoue above U_*/C of .03.

In comparing their experimental results with theory, Snyder
and Cox and Barnett and Wilkerson concluded that though an instability
mechanism was clearly operative, Miles' theory was inadequate, since
its predictions disagreed with the experimentally determined growth
rates both in order of magnitude and in the trend of the data. When
their data are plotted as in Figure 1, however, it can be shown that
most of their data were in a range of U_*/C such that the matched layer
was high on the mean wind profile, in a region of relatively low profile
curvature. The consequent energy transfer implied by this mechanism
is small. Indeed, it appears that Phillips' turbulent instability mech-
anism contributes to the growth rate as effectively as Miles' mechanism
at U_*/C of about .06 or above most of the data collected by Snyder-Cox
and Barnett-Wilkerson. It may be argued that the discrepancy between
theory and observation is due to the assumption of a logarithmic profile.
However, wind tunnel/wave tank studies designed to check Miles'
theory have also found the Miles theory to yield growth rates lower
than observed even when the mean wind profile was suitably represent-
able by the logarithmic form in the region of the matched layer (Shem-
din and Hsu, 1966). In these studies, theoretical growth rates three
to five times lower than observed were found, confirming the oceanic data.

To complete the formulation of wave growth according to (2.1),
the concept of a fully developed sea is introduced. That is, it is assumed
that if the wind blows uniformly in speed and direction over a sufficiently

large area and for a sufficiently long period of time, the wave spectrum
in the area will attain the fully developed form (of Pierson and Moskowitz,
1964) given as

$$S_\infty(\omega) = \frac{a_\infty g^2}{\omega^5} e^{-\beta(\omega_0/\omega)^4} \qquad (2.5)$$

where $\omega = 2\pi f$, $a_\infty = 8.1 \times 10^{-3}$, $\beta = .74$ and $\omega_0 = g/U_{19.5}$ where
$U_{19.5}$ is the wind speed as would be measured at 19.5 meters above
sea level. Based on this limiting state, all nonlinear dissipative effects
that would act during wave generation are modelled implicitly by modify-
ing (2.1) according to

$$\frac{d}{dt} S = \left[A \left\{ 1 - \left(\frac{S}{S_\infty}\right)^2 \right\}^{1/2} + BS \right] \left[1 - \left(\frac{S}{S_\infty}\right)^2 \right], \qquad (2.6)$$

the solution to which for zero initial conditions can be written

$$S(\omega, t) = A \left\{ \frac{\exp(Bt) - 1}{B} \right\} \left[1 + \left\{ \frac{A \exp(Bt) - 1}{B S_\infty} \right\}^2 \right]^{-1/2} \qquad (2.7)$$

Inoue (1967) used (2.6) and the representations for A and B
to compute partially developed sea spectral shapes for the special cases
in which the solution to (2.6) can be considered to be independent of
either wind duration or fetch. In the former case, (2.7) can be summed
over all frequencies for varying time to yield the development of the wave
spectrum as a function of wind duration. In the latter case, the sea is
independent of time and (2.1) becomes

$$C_g \frac{\partial}{\partial x} S(\omega, x) = A + B S(\omega, x)$$

where C_g is group velocity.

With the transformation $t = x/C_g$, (2.7) may then be used to calculate the development of the wave spectrum for varying fetches.

An example of a computation of the development of the wave spectrum fetchwise is shown in Figure 2. The wind was specified to be 40 knots at 19.5 meters. The quantity B was computed according to the procedure that will be presented in Section 3.5, assuming neutral stability conditions. Also shown in Figure 2 is the fetchwise variation of significant wave height, $\overline{H}_{1/3}$,

$$\overline{H}_{1/3} = 2.83 \sqrt{E}$$

where E is twice the variance of the spectrum. The curve is found to lie between the empirical relations proposed by Sverdrup-Munk (1947) and Pierson, Neumann and James (1955).

Inoue (1967) also applied the spectral growth formulation outlined above to a numerical wave specification computer program to hindcast wave conditions over the North Atlantic Ocean during December, 1959. The time history of hindcasted significant wave height verified well with observed data collected at the position of the British weather ship equipped with a wave recorder. More significant, however, was the fact that the predicted wave spectrum verified better than any model previously run, particularly at the more important lower frequencies.

It is apparent from the above that a wave specification model employing a carefully formulated spectral growth such as the model of Inoue requires an especially precise meteorological input. The Inoue growth formulation requires estimates of the surface stress and the wind speed as would be measured at 19.5 meters. Of course, wind direction

FETCH IN n. MILES
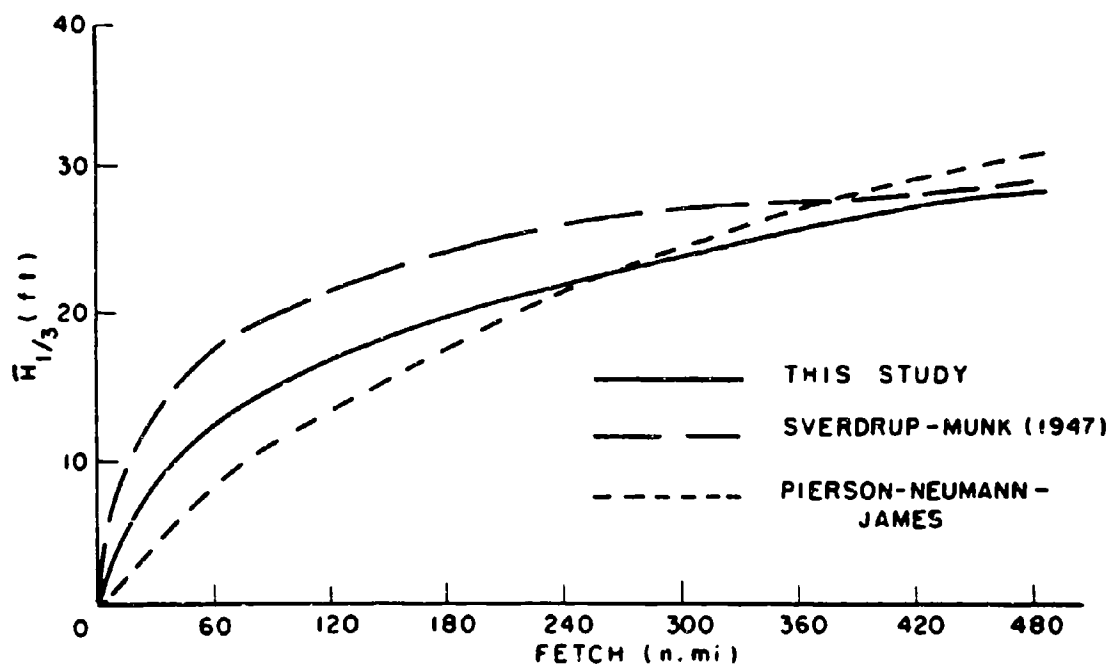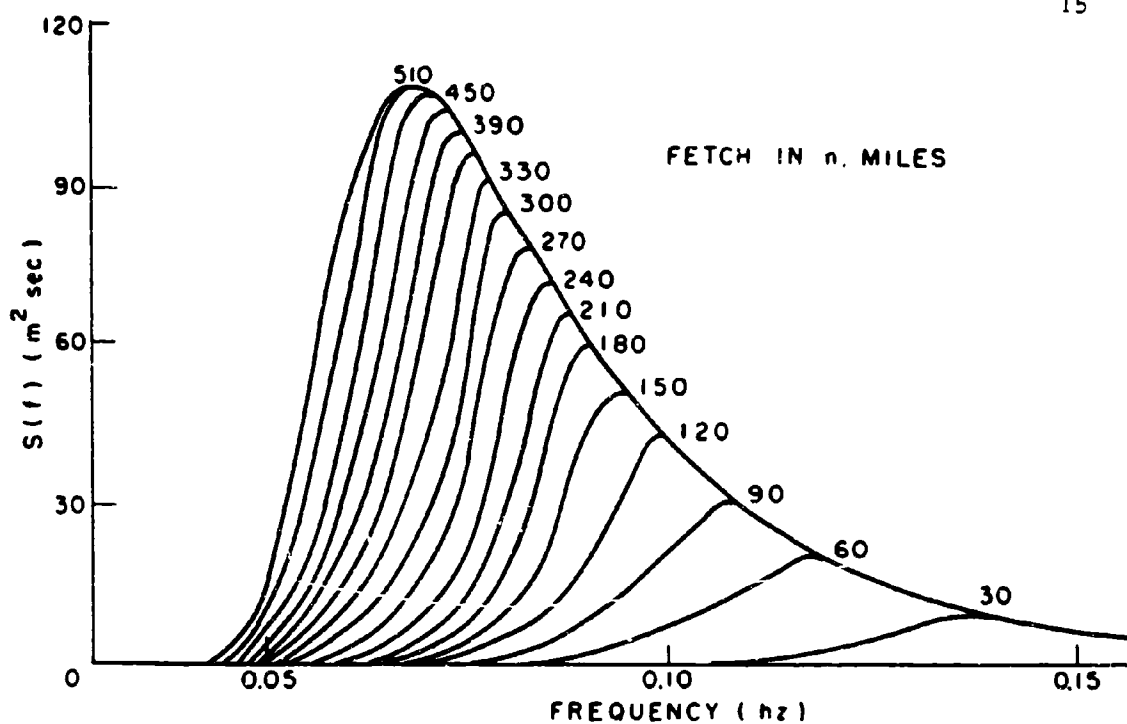
FIG. 2

Growth of the spectrum, S(f), and significant wave height, $\overline{H}_{1/3}$, with fetch for 40 knot winds at 19.5 meters and neutral stability.

must be specified, inasmuch as the spectral representation in the model is two-dimensional. With regard to wave hindcasting, the computation of these parameters from routinely available synoptic ship reports implies a knowledge of the wind distribution over the sea up to the heights of the highest anemometers (~40 meters). In the range of wind speeds of practical significance, surface boundary layer theory would be expected to be applicable to this specification. Wave forecasting, however, requires the calculation of these input parameters from routinely available prognostic fields and implies a knowledge of the wind distribution in the planetary boundary layer over the sea. An important part of this study is the application of surface and planetary boundary layer theory to the marine atmosphere such that the wind distribution in that atmosphere as required by sophisticated wave specification models can be obtained in an objective computer-based procedure from routinely available meteorological sources.

2.2 The effects of atmospheric stability

It is widely held by mariners that for a given anemometer height wind speed, sea surface waves develop more rapidly and reach greater heights when the air is colder than the underlying sea surface than when the reverse is true. The phenomenon, however, has not been studied extensively from a scientific point of view. Roll (1952) analyzed data collected at certain North Atlantic weather ships and found that for the same measured wind speed, the mean wave height was about 20% higher during unstable conditions (water temperature 6.7°C above the air temperature) than during neutral conditions. Fleagle (1956) has criticized Roll's conclusion on the grounds that the observed relation

between air-sea temperature difference and wave height might be due to a correlation of fetch with stability rather than stability and wave generation. Recently, a wind tunnel-wave tank experiment was conducted in which the growth rates of the wind generated waves were determined for varying water temperatures (Hidy*). Growth rates were found to be higher when the temperature of the water was higher than that of the air. The experiment was designed to check Miles'** viscous theory of wave generation and the effect was attributable to the dependence of the molecular viscosity coefficients on temperature.

Fleagle (1956) analyzed wave height and wind speed data at certain weather ships in a way designed to eliminate possible correlations between fetch and stability. He concluded that significantly higher waves are generated in unstable conditions than in stable conditions and that the effect is of practical importance with the extremes of air-sea temperature differences sometimes encountered in certain regions of the major oceans.

In light of these results, it seems appropriate to include the effects of atmospheric stability in a wave specification model. Such effects could be included most basically by some modification of the three components of the spectral growth formulation: the resonance

---

* Personal communication.

** The theory presented by Miles (1962) appears to explain the growth of gravity waves whose phase speeds are so low such that their matched layers lie inside the viscous sublayer. These spectral components are of little consequence in a practical wave specification program since they contribute little to the total wave energy present under real conditions and can be assumed to be in equilibrium with the local wind field.

growth, the instability growth, and the fully developed spectral form.
Though it is likely to be sensitive to the prevailing atmospheric stability,
little is known about how the atmospheric turbulence pressure spectrum
varies with stability in any quantitative way. Such knowledge must
await careful measurements of the fluctuating pressure field near the
surface such as those carried out by Priestley but over widely varying
stability conditions. However, the relative unimportance of this mech-
anism to energy transfer in most cases of practical significance suggests
that the exclusion of a stability dependency from this parameter speci-
fication would not be serious. The sensitivity of the instability theories
of wave generation to the characteristics of the wind profile, and the
success of the application of profile theory to the fully developed spectral
form in explaining the discrepancies between various proposed forms,
however, do indicate that realistic stability modifications can be made
to these aspects of the spectral growth, since the shape of the wind
profile in the surface boundary layer is known to depend on stability.

The effect of atmospheric stability on the generation of free
surface gravity waves by an instability mechanism can be investigated
by examining the departure from the neutral growth rates shown in
Figure 1 when a stability-dependent non-logarithmic profile is intro-
duced into the theoretical relation (2.2). Since stable conditions pro-
duce more significant deviations from the purely logarithmic profile
than equivalent* unstable conditions, any sensitivity of the growth
rate to stability should be more apparent under stable conditions.

---

*Equivalent in the sense that the Richardson numbers near the
surface are equal in absolute magnitude.

Under these conditions, the wind profile in the surface boundary layer
is well represented (except in extreme stability) by the so-called
log + linear relation*

$$U = \frac{U_*}{K}\left(\log\frac{z}{z_0} + a\,\frac{z}{L}\right) \tag{2.8}$$

where L is the so-called Lettau-Monin-Obukov stability length
defined as

$$L = \frac{-U_*^3\,K\,C_p\,\bar{\rho}_a}{gH} \tag{2.9}$$

where C_p is the specific heat of air at constant pressure, H is
the heat flux and $\bar{\rho}_a$ is the mean density of the surface boundary
layer, wherein L is considered to be constant. The substitution of
(2.8) into (2.2) yields

$$\frac{B}{f} = 2\pi\frac{\rho_a}{\rho_w}\left(\frac{U_*}{CK}\right)^2\left\{A_m\Gamma^2\left(\frac{kz_m}{1+\frac{akz_m}{kL}}\right)^3\left(\int_1^\infty\left(\ln\mu + \frac{akz_m}{kL}(\mu-1)\right)^2 e^{-kz_m\mu}\,d\mu\right)^2\right.$$

$$\left. + A_p\int_{\mu_0}^\infty\frac{\Gamma^2}{kz_m\mu^2}\left|\ln\mu + \frac{akz_m}{kL}(\mu-1)\right|e^{-2kz_m\mu}\,d\mu\right\} \tag{2.10}$$

where the substitution $\mu = z/z_m$ has been made and $\mu_0 = h_0/z_m$,
h_0 marking the lower limit of the fully turbulent flow. The dimension-
less height of the matched layer kz_m can be expressed as a function
of the ratio U_*/C and the dimensionless stability parameter kL since

$$C = \frac{U_*}{K}\left(\log\frac{z_m}{z_0} + \frac{az_m}{L}\right)\qquad z_0 \ll L \tag{2.11}$$

---

*The validity of this form as well as the applicability of profile theory
in general over the sea surface is discussed in the next chapter.

so that

$$z_m = z_o e^{(KC/U_* - az_m/L)} \tag{2.12}$$

Through the use of Charnock's relation for z_o, (2.12) can be written

$$kz_m = a(U_*/C)^2 e^{(KC/U_* - ak_m/kL)} \tag{2.13}$$

As in the calculation performed for neutral conditions, the lower extent of the fully turbulent region can be chosen as the height where $U = 10 U_*$. Then, since

$$U = 10 U_* = \frac{U_*}{K} \left(\log \frac{h_o}{z_o} \right) \qquad h_o << L$$

we can write

$$\mu_o = \frac{kh_o}{kz_m} = a(U_*/C)^2 e^{4.0} \cdot \frac{1}{kz_m} \tag{2.14}$$

In general, then, B/f is a function of the ratio U_*/C and the dimensionless parameter gL/C^2. The sensitivity of (2.2) to stability was determined in the following way. For a chosen value of U_*/C and gL/C^2, the dimensionless matched layer height was calculated by applying the Newton-Raphson iterative scheme to (2.13). Then, μ_o was calculated from (2.14) and (2.10) evaluated numerically, employing the same values for the constants A_p, A_m and Γ used in the neutral calculation. The significant result of these calculations was that for typical values of U_*/C and gL/C^2, the growth rates for a given U_*/C were insensitive to the stability parameter, deviations never exceeding 10% of the neutral growth rates. The reason lies in the fact that stability affects the wind profile (2.8) only at appreciable height. With regard to Miles' contribution to (2.10), stability does

indeed produce significant departures from the neutral growth rates but only at relatively low values of U_*/C, where the contribution of the mechanism to the total growth rate is negligible. On the other hand, contributions to the first integral in (2.1C), representing Phillips' contribution, arise mainly from the region of high profile curvature, just above the lower limit of integration but well below the matched layer.

The fact that the relation between B/f and U_*/C appears to be a "universal" one, independent of the atmospheric stratification is not necessarily inconsistent with the studies of Roll and Fleagle cited above, which imply higher growth rates during unstable rather than under stable conditions, since these studies used as a measure of the wind field the wind speed as measured at typical anemometer levels (20 to 25 meters). To demonstrate this point clearly, consider the three hypothetical profiles shown in Figure 3. The friction velocity and the roughness parameter are the same ($\tau_o = 1$ dyne/cm^2) for all three profiles but the purely logarithmic profile is valid for neutral conditions while the other two represent moderate departures from neutrality ($|L| = 3000$ cm). Note that the profiles for all three stability regimes are nearly identical below one meter but that significant differences appear at the height at which wind speed is normally measured. If winds were measured at 20 meters, for example, it would take a wind of about 24 knots under stable conditions to produce the effective wave generating ability of a wind speed of only about 19 knots during neutral conditions and 17 knots under unstable conditions Conversely, the inclusion of atmospheric stability in the determination
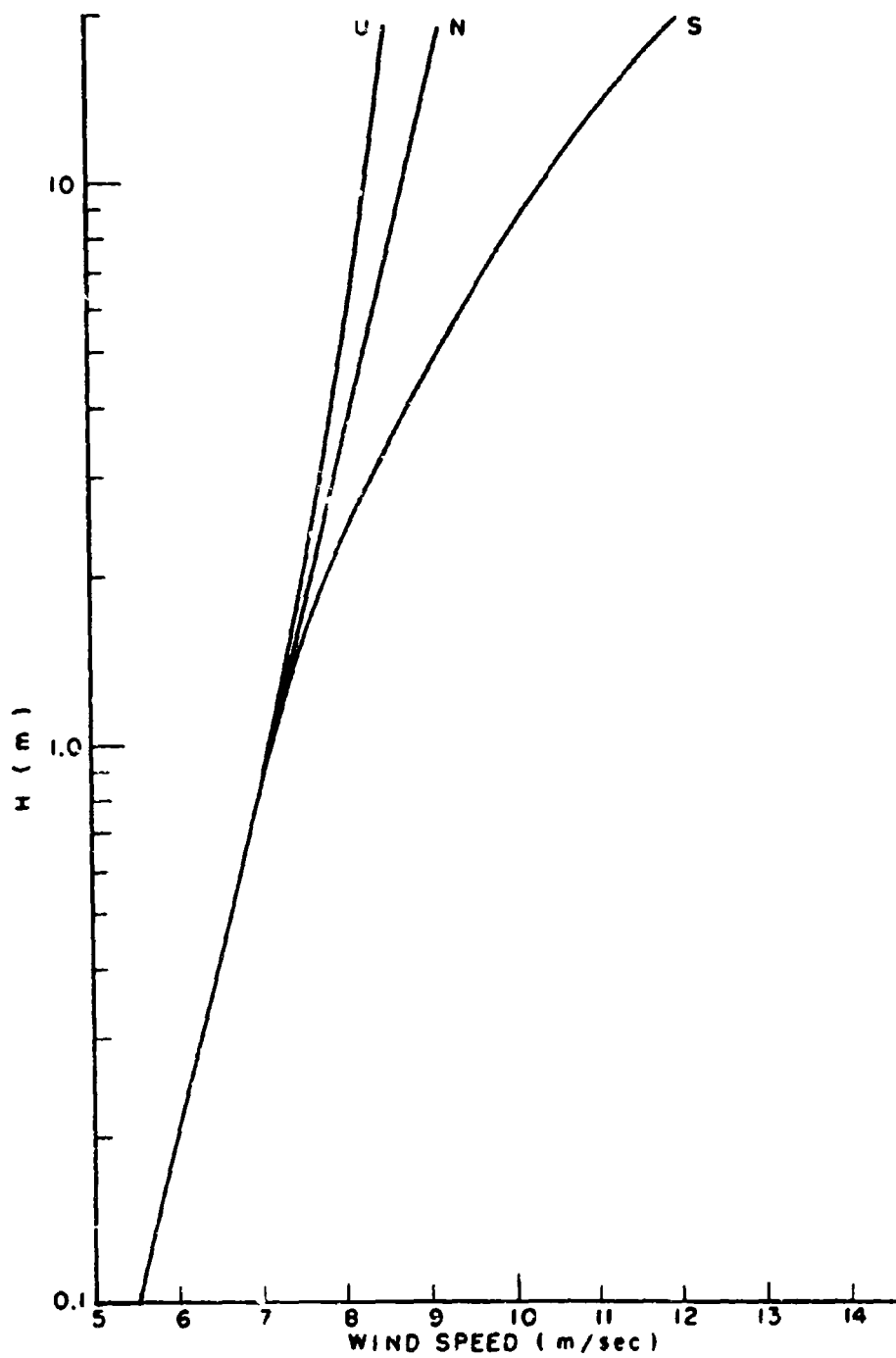
FIG. 3

Theoretical wind profiles in the marine surface boundary layer for a surface stress of 1 dyne/cm^2 and neutral (N), unstable (U), and stable (S) stratification.

of friction velocity from measured winds yields higher friction velocities and in general more rapid development of the spectrum on the whole for unstable conditions than for neutral conditions.

An important aspect of the spectral growth formulation under discussion is the fully developed spectral form. The latter is based upon wave recorder data analyzed by Moskowitz (1964) and provides a nested family of curves for the wave spectrum in terms of the 19.5 meter wind speed. The relationship also implies that the significant wave height for fully developed seas is proportional to the square of the 19.5 meter wind speed. Serious discrepancies apparently existed between the Pierson-Moskowitz spectrum and the theoretical spectrum proposed by Neumann (1953) upon which the Pierson, Neumann, James (1955) forecasting manual was based. Pierson (1964) showed, however, that the differences between the two theories largely reflected differences in the heights of the anemometers used to measure wind speeds for the data sets that formed the basis of the two proposed spectral forms.

The theory of wave generation suggests that the rate at which energy is transferred from wind to wave is determined largely by the properties of the wind field very near the surface. This in turn suggests that the definitive parameter in a fully developed spectral form should be the wind profile very near the surface and not necessarily a wind speed at some height high above the surface. With regard to Figure 3, for example, this implies that all three profiles should produce the same fully developed sea, although the 19.5 meter wind speeds vary by 7 knots over the range of stabilities represented.

The fully developed spectral form can then be easily extended to non-neutral conditions by incorporating into the Pierson-Moskowitz

spectrum the simple notion of an equivalent wind speed, U_E, where

$$U_E = U_E(U_m, L)$$

defines a procedure which, for a measured wind U_m and prevailing stability, yields the wind speed that would exist at 19.5 meters if the surface stress were unchanged but the surface boundary layer exhibited neutral stability. The procedure effectively relates the Pierson-Moskowitz spectrum to the wind profile and for a given measured wind speed produces higher fully developed seas for unstable conditions than for stable conditions.[*]

The wave data analyzed by Roll and Fleagle in the studies noted above allow at least a rough test of the proposed stability modifications to the spectral growth formulation. Before the theoretical predictions can be compared with the data, however, it is necessary to specify in detail the wind profile representations applicable to the surface boundary layer over the sea surface. Further, it must be shown how these forms can be specified in terms of standard ships' weather observations.

---

[*]An alternative approach would have been to redefine the fully developed spectral formulation in terms of U_*, as had been originally suggested by Kitaigorodskii (1961). It is shown in Section 3, however, that $(U_*/U_{19.5})^2$ increases nearly linearly with wind speed in the range 20 to 40 knots. A dimensionally consistent spectral form in terms of U_* would then imply that the fully developed significant wave height was proportional to the cube of the wind speed, a result in serious disagreement with the data of both Neumann and Moskowitz.

3. Surface Boundary Layer Model

3.1 The profile method

A great deal of progress has been made in recent years in
our understanding of the distribution of wind and temperature in con-
stant flux boundary layers over solid boundaries through the application
of the Monin-Obukov similarity theory. The extent to which the theory
is applicable to the analysis of the flow near the sea surface depends
on the extent to which the concepts developed in the analysis of
neutral boundary layers over solid boundaries can be transferred to
the sea.

The sea surface is basically different from a solid boundary
in that a fluid interface cannot support a stress discontinuity. More
significantly, the fluid interface is characterized by travelling waves,
whose momentum is typically derived from the air flow above the
interface through wave generation mechanisms. Hence, serious ob-
jections have sometimes been raised to the application of models, such
as the logarithmic profile, to the flow near the sea surface. To
justify the application of profile methods to the flow near the sea sur-
face, it is useful to review first the properties of air flow over solid
boundaries and then examine the nature of the air flow over the sea
surface in the light of the recent developments in wave generation
theory.

Consider the flow over a horizontal plane surface, with the
mean wind taken to be parallel to the surface with instantaneous wind
components $u_i (i, j = 1, 2)$ and w. The x_1 axis is in the direction
of the mean wind, the z-direction is directed opposite to the direction

of gravity, and the x_2 axis is directed so that a right-handed orthogonal coordinate system results. The horizontal components of the momentum equation can be written as

$$\frac{\partial u_i}{\partial t} + \frac{\partial u_i u_j}{\partial x_j} + \frac{\partial u_i w}{\partial z} = -\frac{1}{\rho}\frac{\partial p}{\partial x_i} + \nu \nabla^2 u_i \qquad (3.1)$$

where ν is the kinematic viscosity, and the continuity equation for a constant density fluid

$$\frac{\partial u_i}{\partial x_i} + \frac{\partial w}{\partial z} = 0 \qquad (3.2)$$

has been employed.

For turbulent flows, the velocity and pressure can be decomposed into an average value and an instantaneous fluctuation as

$$u_i = U_i + u_i'$$
$$w = W + w' \qquad (3.3)$$
$$p = P + p'$$

Substitution of (3.3) into (3.1) yields

$$\frac{\partial U_i}{\partial t} + \frac{\partial U_i U_j}{\partial x_j} + \frac{\partial}{\partial x_j}\overline{u_i' u_j'} = -\frac{1}{\rho}\frac{\partial P}{\partial x_i} + \nu \nabla^2 U_i + \frac{\partial}{\partial z}(-\overline{u_i w}) \qquad (3.4)$$

after the average of the resulting equation is taken. Imposing the restrictions that the mean flow is steady and that all averaged quantities are functions of z only reduces (3.4) to

$$\frac{\partial}{\partial z}\left(\rho \overline{u_i w} - \mu \frac{\partial \overline{U_i}}{\partial z}\right) = 0 \qquad (3.5)$$

The quantity $-\rho \overline{u_i w}$ represents the horizontal components of the Reynolds stress and equation (3.5) implies that the total stress, τ_i

$$\tau_i = \rho \overline{u_i w} - \mu \frac{\partial \overline{U}_i}{\partial z} = \text{constant} \tag{3.6}$$

and hence is equal to the stress at the boundary τ_o.

An analysis of the typical scales of atmospheric motions
and the magnitudes of the terms in (3.1) indicates that the assumptions
leading to (3.6) are justifiable in the neutral boundary layer near the
surface to the heights of 20 to 200 meters for typical surface stresses
($1 - 10 \text{ dynes/cm}^2$) (Lumley and Panofsky, 1964). Except very near the
surface where the viscous stress may be appreciable, the surface
stress is supported entirely by the turbulent Reynolds stress and the
velocity scale, U_*, may be defined, which alone characterizes the
flow in the turbulent regions of the neutral surface boundary layer.
This implies (see, e.g., Lumley and Panofsky, 1964) that the mean
wind shear in such a region is logarithmic,

$$\frac{\partial \overline{U}}{\partial z} \sim \frac{1}{z} \tag{3.7}$$

but a more complete description of the wind profile requires a con-
sideration of the nature of the lower boundary.

Turbulent flow in the constant stress layer has generally
been described in terms of two limiting cases: aerodynamically
smooth, in which the total stress is supported near the boundary
enitrely by viscosity; and aerodynamically rough, in which case the
viscous stress is considered to be negligible everywhere and the total
stress is exerted on the boundary through the action of pressure forces
on the roughness elements. In the former case, the air flow is nearly
laminar near the surface[*] and the mean velocity increases linearly

---

[*]The region called the viscous sublayer.

from zero at the boundary according to

$$\overline{U}_z = \frac{U_*^2 z}{\nu} \tag{3.8}$$

The upper limit for the linear profile in smooth flow has been variously reported as lying at $z = 10\nu/U_*$ (Nikuradse, 1933), $5\nu/U_*$ (Schlichting, 1951), and $6.6\nu/U_*$ (Miles, 1957). Above this limit the profile becomes

$$\overline{U}_z = \frac{U_*}{K} \log \frac{z}{z_0} \tag{3.9}$$

with the roughness parameter z_0 given as

$$z_0 \propto \nu/U_* \tag{3.10}$$

as required by continuity of the profile at the outer edge of the viscous sublayer. If the flow is aerodynamically rough, (3.9) is again applicable away from the region of the roughness elements but in this case z_0 is proportional to the characteristic height of the roughness elements and ranges from about .01 cm for sand to several meters for cities. In the region in which the logarithmic law is valid, it is possible to determine, in principle, the stress from a knowledge of z_0 and a measurement of wind speed since (3.9) can be rewritten

$$\tau_0 = \rho C_z \overline{U}_z^2 \tag{3.11}$$

where C_z, the drag coefficient, is

$$C_z = K^2 / (\log z/z_0)^2 \tag{3.12}$$

The instability theories of Miles and Phillips, described in Section 2, and the viscous wave generation theories of Benjamin (1959) and Miles (1962) have indicated, as will be shown below, to what extent the concepts just presented can be applied to the flow near

the sea surface .

In the formulation of the instability theories, the air flow was considered as a shear flow over one component of a wave field composed of an infinite sum of infinitely long-crested sinusoidal components of infinitesimal amplitude. The horizontal coordinates (x_1, x_2) were translated in the direction of wave propagation (and mean wind direction) with the appropriate phase speed C of the component of frequency ω and wave number k and amplitude a. Under these conditions, the free surface can be taken as

$$\zeta = a \cos kx_1 \tag{3.13}$$

and the instantaneous horizontal velocity field decomposed as

$$u_i = U_1 - C + u_i' + u_i \tag{3.14}$$

where u_i, the wave induced perturbation, represents the velocity fluctuations in fixed phase with respect to the water surface elevation, u_i' are the random velocity fluctuations of the atmospheric turbulence and U_1 is the mean wind velocity. With a similar decomposition for vertical velocity and pressure, the mean stress balance over the sea surface can be shown to be

$$\frac{\partial}{\partial z} \left\{ \overline{u_i w} + \overline{u_i' w'} - \nu \frac{\partial \overline{U}_1}{\partial z} \right\} = 0 \tag{3.15}$$

which indicates that the total stress above the water surface is constant with height and composed of the turbulent Reynolds stress, the viscous stress, and a wave-induced Reynolds stress

$$\tau_w = - \rho \overline{u_i w}$$

The mean flux of momentum to the wave arising from induced pressure

fluctuations on the surface, ρ_o, is

$$F_w = \overline{\rho_o \partial \zeta / \partial x_1} \tag{3.16}$$

and Phillips (1966) showed that $-\rho \overline{u_1 w_o}$, the wave induced Reynolds
stress at the level $z = 0$, was a good approximation to F_w even for
turbulent flows, when the viscosity is neglected.

The first successful analytical expression for the wave-induced
Reynolds stress at the surface was derived by Miles (1957). Stewart
(1961) considered the effects of Miles' mechanism of wave generation
on the mean wind flow near the surface and speculated that the mean
wind profile near the sea surface should depart significantly from the
logarithmic. The argument was based upon the expectation that τ_w
associated with the dominant wave components in typical wind seas con-
tributed significantly to τ_o ($\tau_w / \tau_o \geq 0.2$). Hence, since the motions
contributing to τ_w are of a too highly organized nature to be called
turbulence, the friction velocity, U_*, no longer alone characterizes
the flow and the simple similarity argument leading to the logarithmic
profile may not be applied.

Miles (1965) considered the question raised by Stewart from a
slightly different aspect by investigating the reduction in mean wind
profile curvature and slope owing to momentum transfer from a turbulent
wind to surface waves by the Miles mechanism and concluded that these
effects should be small for typical wind speeds. He also suggested, as
had been done earlier by Neumann (1956), that the shorter waves were
especially significant in determining the ratio τ_w / τ_o. Phillips (1966)
strengthened the argument considerably by calculating the magnitude of
τ_w / τ_o for all wave components for which $U_* / C < .1$ on the basis of the

combined Miles-Phillips instability mechanisms and conservatively estimated[*] the ratio to be less than .1. An immediate consequence is that in statistically steady and neutral stability conditions, the mean wind profile near the sea should be logarithmic.

Before the mean properties in the air flow over the sea can be compared to similar flows over solid boundaries, the definition of the vertical coordinate must be considered. Benjamin (1959) expressed the mean properties of the wind over the sea in terms of a modified height, η, above the free surface, where η and z are related by

$$\eta \equiv z - \sum_{\vec{k}} G(\vec{k}, t) e^{-\vec{k}\,\eta} e^{\sqrt{-1}\,\vec{k}\,\vec{x}_i} \qquad (3.17)$$

Benjamin argued that the vertical coordinate must be taken as η and that the mean wind profile over the sea surface should be

$$\overline{U}_\eta = \frac{U_*}{K} \log \eta/\eta_0 \qquad (3.18)$$

η_0 being the roughness length. Benjamin's formulation embodies the notion that to a first approximation, the surface boundary layer over the sea is merely bent to follow the larger scale surface undulations, for which direct experimental support is provided by Motzfeld's (1937) flow visualization experiments.

Measurements of the wind profile over the sea surface have generally been taken with probes mounted at fixed heights above mean sea level. Phillips (1966) showed that very near the surface these profiles

___

[*]The estimate is so conservative that employing the modified Miles-Phillips growth (figure 1) does not alter the result that $\tau_w/\tau_0 < .1$.

should exhibit deviations from the logarithmic law but that since the wave-induced undulations in the boundary layer decrease exponentially with height, well clear of the surface, the mean properties of the boundary layer determined with measurements from fixed probes should be comparable to those over a solid boundary.

Experimental results tend to confirm these ideas. Careful measurements of the wind profile over the sea with probes well clear of the surface in the overwhelming majority of cases indicate a logarithmic variation (see e.g., the reviews by Deacon and Webb, 1962; Roll, 1965; and more recent measurements of Paulson, 1968). Takeda (1963) and Shemdin (1967) measured the profile with fixed probes to very low levels and observed deviations from the logarithmic law as the surface was approached that might be attributed to the effects of the undulations in the boundary layer. On the other hand, there have been a few careful measurements of mean wind velocity very near the sea surface with moving probes which should be expected to approximate the coordinate η rather than z. Deardorff (1962) showed a single determination of the mean wind profile with fixed probes at 90, 155, and 275 centimeters and a moving probe at 14 centimeters that closely approximated a logarithmic distribution even though the significant wave height was 25 centimeters. Recently Seesholtz (1968) obtained many wind profiles in Buzzards Bay with a floating array of anemometers at 30, 50, and 70 centimeters combined with similar anemometers mounted at several fixed heights above the highest wave crests. Under neutral stability conditions, the profiles were closely approximated by a logarithmic distribution down to the lowest level even when the mean wave height exceeded 100 centimeters.

Though the experimental data are generally limited to moderate
wind conditions (< 15 meter/second), the theoretical estimates of the
ratio τ_w/τ_0 do not indicate that it should increase markedly at higher
wind speeds. Disregarding the possibly significant (but impossible to
consider at the current state of the art) effects of wave breaking and
extensive sea spray, the process of wave generation itself, then, does
not seriously affect the nature of the surface boundary layer in that
under neutral and steady conditions a logarithmic shear zone should be
established. However, the existence of surface waves and of wave
generation processes is significant to a description of the whole flow
near the surface inasmuch as they determine the effective roughness
parameter of the sea surface.

3.2 Roughness parameter specification

By analogy to flow over a smooth flat plate, it may be expected
that for the case of very light winds over a flat calm sea, the stress
at the sea surface is supported entirely by viscosity and the flow may
be classified as aerodynamically smooth. Of course, the action of the
wind soon initiates undulations in the interface, but the flow may con-
tinue to be classified as smooth if the unaulations remain everywhere
covered by a viscous sublayer which itself undulates to adhere to the
boundary (no form drag) and if the viscous stress overwhelms the
wave-induced stress at the surface.

Kraus (1967) has considered the nature of the roughness of the
sea surface for aerodynamically smooth flow by noting that for such a
flow regime, the wind profile will be laminar if the Reynolds number
is smaller than a critical Reynolds number.

$$R_c = \frac{dU_d}{\nu}$$

where d is the depth of the viscous sublayer. The depth d is determined by matching the eddy viscosity distribution in the turbulent regime

$$K_m = KU_* z$$

to the kinematic viscosity ν at the height d on the assumption that, on the average, the flow will become viscous as the boundary is approached at that height. Then,

$$d = \nu / K U_* \tag{3.19}$$

and it may be shown by a match of the laminar and logarithmic profiles at d that

$$z_o = \nu / 1.09 \tag{3.20}$$

which is somewhat larger than the relation usually shown to hold in flow near a smooth wall. Equation (3.19) also implies that the mean velocity at the top of the viscous layer is U_* / K. Kraus further argued that the flow over the sea surface can be characterized as aerodynamically smooth until form drag associated with separation of the flow becomes significant. Boundary layer separation should not be expected until air parcels in the viscous sublayer are moving fast enough to overtake the roughness obstacles--in this case, the free surface waves. Since the minimum free surface wave phase velocity, C_m, is 23 cm/sec, and the average translational speed of the viscous sublayer is $U_* / 2K$, separation is not possible when

$$U_* < 2K C_m = 18 \text{ cm/sec}$$

which together with (3.20) and (3.9) implies a wind at 10 meter height of about 6 meters/second.

The above argument neglects the effects of a pressure field induced on the sea surface in association with the generation of shorter wave components ($C < U_d$) by a generating mechanism other than flow separation. The instability theories discussed in Section 2 are clearly unable to explain the amplification of components whose matched layers lie inside the viscous sublayer, a region of zero profile curvature. The studies of Benjamin (1959) and Miles (1962), however, showed that the inclusion of viscous effects in their shear flow models could produce a component of induced pressure in phase with the slope of these components and thus provided a mechanism for producing wave drag that does not require flow separation. The viscous theories of wave generation have been well verified in the wave tank experiments of Plate et al. (1969) and Hires (1968).

The experimental studies of wind set-up in a model yacht pond conducted by Van Dorn (1953) and their interpretation by Munk (1955) and Miles (1965) suggest that the total wave supported stress at the sea surface could easily exceed 25% of the total stress for typical wind speeds. Since the larger wave components can account for at most 10% of the total stress, it appears that the high frequency part of the spectrum, draining momentum from the viscous sublayer, is responsible for most of the wave drag. For the conditions present under Hire's (1968) experiment, this was indeed found to be the case. Phillips (1966) has in fact employed the term "aerodynamically rough" to describe the limiting form that the flow near the sea surface may achieve as the wind speed increases, the density of short gravity waves increases, and the momentum flux to these waves becomes large

compared to the molecular viscous stress.

Whether the momentum flux at high wind speeds is due to the viscous shear flow mechanism or to flow separation, the part of the wave spectrum involved will always lie at such high wave numbers that the spectrum can be expected to be saturated and in equilibrium with the local wind. An important consequence of rough flow, then, is that the roughness parameter becomes independent of fetch and viscosity and is proportional to the root mean square height of those spectral components whose phase speeds are less than the velocity at the outer edge of the viscous sublayer. If the effects of capillary waves are neglected, and Phillips' (1958) equilibrium range spectral form is assumed to apply, it can be shown simply that Charnock's relation (2.4) must apply for aerodynamically rough flow.

Observational studies of the roughness parameter have generally been concerned with the dependency upon wind speed at a certain height (usually 10 meters) of the drag coefficient referred to that height. For aerodynamically smooth flow, eq. (3.20) applies and the drag coefficient referred to 10 meters, C_{10} decreases with increasing wind speed. For aerodynamically rough flow, if (2.4) applies, C_{10} increases with wind speed. Many functional forms for C_{10} versus U_{10} have been proposed in the literature, some reflecting each of the above views and others indicating that C_{10} is independent of wind speed. The forms have usually been based upon the investigators own set of measurements of the wind stress at the sea surface with a particular method for stress determination, a particular kind of sensor, in generally limited fetch conditions, and over a narrow range of wind speeds. The results of most existing studies have been summarized

in considerable detail in the reviews of Roll (1965), Wilson (1960),
and Wu (1968) and it is unnecessary to repeat the individual results
here. The collection of Wu is shown in Figure 4 and serves as a use-
ful presentation for the purposes of this discussion.

The data in Figure 4 are the results of 30 field investigations
conducted between 1876 and 1962. The scatter is large and typical of
the scatter usually observed in each individual set of measurements.
Some of the scatter can be attributed to the fact that the surface boundary
layer may not have been in a state of neutral stability. The effect is
especially important at low wind speeds. Also shown in the plot is the
drag coefficient for smooth flow based upon (3.20) and the drag co-
efficient for rough flow based upon Charnock's relation with the constant
chosen as .035. It is seen that the data at low wind speeds are not
inconsistent with the concept of aerodynamically smooth flow but that
at wind speeds above about 6 meters/second, the drag coefficient is
significantly higher than predicted for smooth flow and increases with
wind speed in agreement with the predictions of Charnock's relation.

Many recent determinations of the drag coefficient over the
sea have employed rapid response anemometers to measure the
Reynolds stress directly. Notable are the measurements of DeLeonibus
(1966), Smith (1966), Weiler and Burling (1967), Hasse (1966), and
Zubkovski and Kravchenko (1967). The data from these studies are
generally limited to wind speeds (at 10 meters) between 2 and 12
meters/second and when grouped together show even more scatter
than the data of Figure 4, and one is inclined to believe that the eddy
correlation data reflect considerable sampling variability and
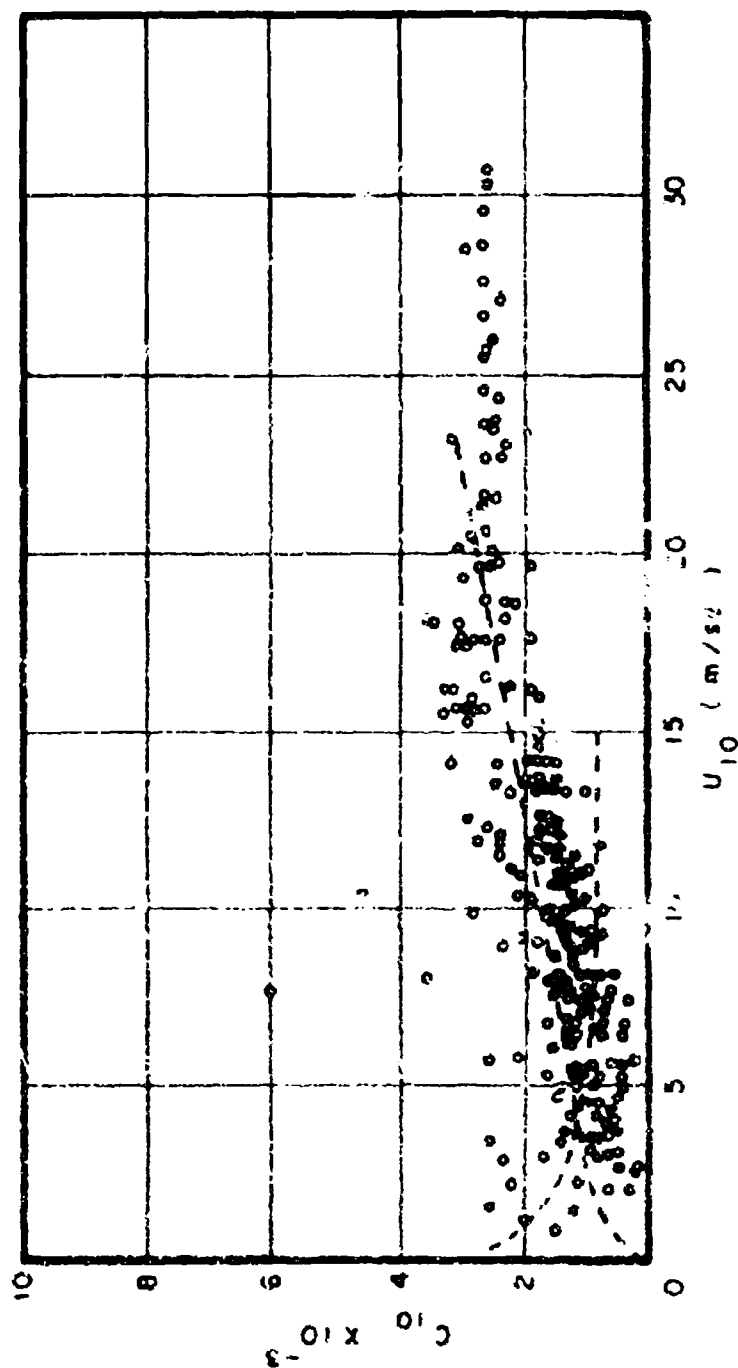
Wu's (1969); collection of oceanic drag coefficient measurements and the functional form for C_{10} for aerodynamically smooth and rough flow

FIG. 4

instrumental error.

For the purpose of a wave forecasting analysis model, it is proposed on the basis of physical reasoning and the limited empirical evidence noted above that at least for situations in which the high frequency part of the wave spectrum is a reflection of the local wind[*], the roughness parameter can be expressed in terms of physical constants and U_* only. A simple expression for z_o covering a wide range of wind speeds and interpolating between smooth and rough flows is

$$z_o = C_1/U_* + C_2 U_*^2 + C_3$$

where C_1, C_2, and C_3 are constants (not dimensionless) to be determined. The constants were chosen so that C_{10} is a minimum at the 10 meter wind speed of 6 meters/second under neutral conditions and so that above this speed the relation is close to Charnock's relation with the constant of .035, as suggested by the statistical analysis of 18 sets of data by Kitaigorodskii and Volkov (1965). For U_* in cm/sec and z_o in cm, the resulting expression is

$$z_o = .684/U_* + 4.28 \times 10^{-5} U_*^2 - 4.43 \times 10^{-2} \tag{3.21}$$

and is shown in Figure 5 expressed as C_{10} versus U_{10}. The drag coefficient at 20 m/sec is 2.6×10^{-3}, in agreement with the data analyses of Wu and Wilson. Further, above 6 m/sec, the region of interest to wave forecasting, the relation has a slope close to Sheppard's (1958) relation, which was shown to be the most successful drag coefficient relation in explaining the discrepancies between different proposed wave height versus wind speed theories (Pierson,

---

[*]A condition common to active wave generating situations.
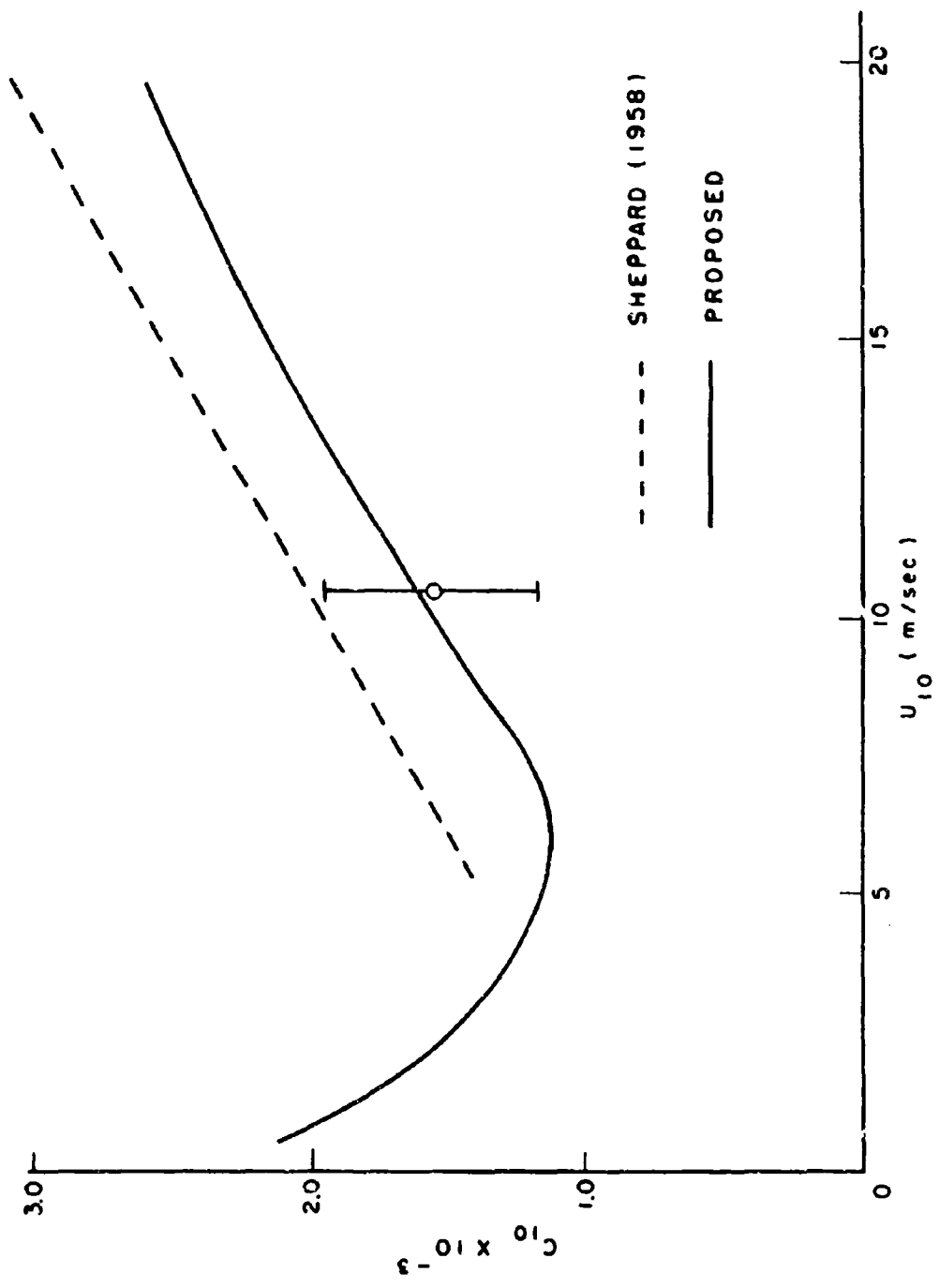
FIG.5

Drag coefficient with respect to 10 meters as a function of 10 meter height wind speed for neutral conditions and roughness parameter specification (3.21).

1964).

After the above relation had been developed, the author learned of a series of eddy correlation determinations of the drag coefficient taken at Argus Island between 1800Z 22 March 1967 and 0515Z 23 March 1967 (DeLeonibus, personal communication). The result of five runs in which the stability was near neutral is plotted in Figure 5 (mean and root mean square spread). The wind field during the period was unusually steady with constant wind direction (235°) and wind speed varying between 9.8 meters/second and 11.2 meters/second (average = 10.6 meters/second). The agreement between the proposed relation and the data is encouraging, particularly since the Argus Island site is representative of open ocean conditions.

3.3 Profile representations

The similarity theory of Monin and Obukov has been quite successful in providing a framework for the description of the mean structure of the surface boundary layer over solid boundaries and the conclusions of the last two sections indicate that it may also be valid over the sea surface. The theory was, in fact, applied in this study with this view in mind and with the realization that the few observations of wind profiles over the sea under non-neutral conditions (Brocks, 1959; Fleagle et al., 1958; Deacon, 1962) showed at least qualitatively the same effects of stability on the profiles as had been observed over land. More recent analyses of accurate wind profile measurements over the sea under non-neutral conditions by Paulson (1967) and Hoerber (1968) have indeed shown that the theory is applicable.

According to the theory, a universal relation should exist between

the non-dimensionalized wind shear and temperature gradient

$$\phi_u = \frac{Kz}{U_*} \frac{\partial U}{\partial z} \tag{3.22}$$

$$\phi_t = \frac{z}{T_*} \frac{\partial \theta}{\partial z} \tag{3.23}$$

and the dimensionless ratio z/L, where θ is potential temperature, T_* is a scaling temperature defined as

$$T_* = -\frac{1}{KU_*} \frac{H}{C_p \rho_a}$$

and L is defined by (2.9). It follows from the definition of the eddy viscosity K_m and the eddy conductivity K_h that the non-dimensional parameters are related by

$$\phi_u = a_h \phi_t$$

where $a_h = K_h/K_m$.

The calculation of L from data requires a knowledge of the heat flux and since this quantity is not easily measured, investigators have often followed the suggestion of Panofsky (1963) and analyzed wind and temperature profiles in terms of a modified stability length L' defined as

$$L' = \frac{U_*(\partial U/\partial z)T}{Kg(\partial \theta/\partial z)} \tag{3.24}$$

and which can be easily calculated fro· profile data alone. Since $L' = a_h L$, the assumption that L' is independent of height implies that a_h is constant, a condition usually referred to as similarity of wind and temperature profiles.

The behavior of a_h with stability is currently a very controversial topic in micrometeorology. There is considerable evidence

that a_h is higher in unstable conditions than in neutral or stable conditions and functional forms between ϕ_u, ϕ_t, and z/L have been proposed for unstable conditions by Businger (1966) and Pandolfo (1966). Nevertheless (as shown, for example, by Panofsky's (1965) analysis of Swinbank's Kerang data), the analysis of profile data from land sites with a_h assumed constant yields good results when compared to the more complicated analysis in terms of L. For wind and temperature profiles over the sea under unstable conditions, Paulson's (1967) study demonstrated that the profile representations in terms of L' with a_h assumed constant provided as good a description of the observations as did representations in terms of L. For stable conditions over land McVehil (1964) found that profiles may well be represented in terms of L' with a_h treated as constant up to z/L' near 0.3, and Paulson's (1967) profile measurements within this stability range confirmed this conclusion.

Since the departure of the surface boundary layer from neutrality over the sea surface is generally smaller than that over land, especially at the wind speeds of interest to wave specification, it will be assumed in this study that wind and temperature profiles are similar. The similarity theory then requires

$$\frac{Kz}{U_*} \frac{\partial U}{\partial z} = \phi_u (z/L')$$
(3.25)

$$\frac{z}{T_*} \frac{\partial \theta}{\partial z} = \frac{\phi_u (z/L')}{a_h}$$
(3.26)

The integration of (3.25) and (3.26) yields the wind and temperature profile formulas

$$U_z = \frac{U_*}{K} \left[\ln \frac{z}{z_o} - \psi(z/L') \right] \qquad (3.27)$$

$$z \gg z_o$$

$$\theta_z - \theta_o = \frac{T_*}{a_h} \left[\ln \frac{z}{z_o} - \psi(z/L') \right] \qquad (3.28)$$

where the relation between ψ and ϕ_u is

$$\psi(z/L') = \int_0^{z/L'} \frac{1 - \phi_u(\xi)}{\xi} d\xi \qquad (3.29)$$

To date, no "universal function" between ϕ_u and z/L' (or z/L) has been found that describes observations well in the whole range of stabilities normally encountered in the surface boundary layer. Monin and Obukhov expanded $\phi_u(z/L)$ into a Taylor series and since $\phi_u(o) = 1$ (neutral conditions) wrote for small z/L (z/L' in our case)

$$\phi_u = 1 + \beta'(z/L') \qquad (3.30)$$

The integrated profile stability parameter ψ corresponding to (3.30) is simply $-\beta' z/L'$ and the wind profile may be written

$$U = \frac{U_*}{K} \left[\ln \frac{z}{z_o} + \frac{\beta' z}{L'} \right] \qquad z \gg z_o \qquad (3.31)$$

This form has been found to describe profiles in stable conditions over land (McVehil, 1964) and over the sea (Paulson, 1967) up to $z/L' = 0.3$ with $\beta' = 7$ providing the best fit to the observations. For unstable conditions, however, (3.30) and (3.31) fail at relatively slight instability and the so-called KEYPS function (Panofsky, 1963) has been found to apply to a broad range of unstable conditions, from near neutral to z/L' of about -.5. The relation between ϕ_u and z/L' according to the KEYPS formulation is implicit in (3.32):

$$\phi_u{}^4 - \gamma' z/L' \phi_u{}^3 - 1 = 0 \qquad (3.32)$$

with $\gamma' = 18$ generally providing a good description to land and marine profiles. The function ψ implied by (3.32) has been evaluated numerically and expressed graphically as a function of z/L' by Panofsky (1963). Alternatively, ψ may be computed from ϕ_u directly since (3.29) can be transformed into a function of ϕ_u and the integrand can be expanded into integrable partial fractions.

$$\psi = \int_1^{\phi_u} \left(-1 + \frac{2}{1+\xi} + \frac{2}{1+\xi^2} + \frac{2\xi}{1+\xi^2} - \frac{3}{\xi} \right) d\xi$$

which yields after integration

$$\psi = 1 - \phi_u - 3 \ln \phi_u + 2 \ln\left(\frac{1+\phi_u}{2}\right) + 2\tan^{-1}\phi_u - \frac{\pi}{2} + \ln\left(\frac{1+\phi_u{}^2}{2}\right) \qquad (3.33)$$

3.4 The variation of drag coefficient with stability

The drag coefficient, defined by (3.11) may be expressed as a function of stability by rearranging and squaring (3.27) to yield

$$C_z = \frac{U_*^2}{U_z^2} = \frac{K^2}{[\ln z/z_0 - \psi(z/L')]^2} \qquad (3.34)$$

Since the effects of stability on distorting the mean wind profile become significant only at appreciable heights, the roughness parameter specification (3.21) can be employed for any stability, thus allowing one to use (3.34) to calculate the dependence of the drag coefficient upon wind speed and stability. The calculation is most easily performed by specifying L' and U_*, computing ϕ_u from (3.32) or (3.30), ψ from (3.33), z_0 from (3.21), and C_z and U_z from (3.34).

Figure 6 shows the results of such calculations for the drag coefficient with respect to 7.5 meters and for two stability cases. The unstable case corresponds to a stability length of 6000 cm and the stable case to a stability length of 2500 cm. The height and stability parameters were so chosen so that the curves could be compared to the extensive set of drag coefficient data collected at Argus Island and reported by DeLeonibus (1966). The data shown in Figure 7 were determined from direct measurements of the turbulent Reynolds stress and mean wind speed at the fixed height of 7.5 meters above mean water level. The data were grouped into stable and unstable classes, the stability being determined through a calculation of the Richardson number (referred to 7.5 meters)

$$Ri = \frac{\frac{g}{\theta} \frac{\partial \theta}{\partial z}}{(\frac{\partial U}{\partial z})^2} \tag{3.35}$$

from measurements of wind and temperature at 10 and 6 meters. The stability lengths employed in the determination of the theoretical curves were calculated from the average Richardson numbers for the classes from

$$\frac{z}{L'} = \frac{Ri}{1 - \beta' Ri} \tag{3.36}$$

for stable air, and

$$\frac{z}{L'} = \frac{Ri}{\sqrt[4]{1 - \gamma' Ri}} \tag{3.37}$$

for unstable air (Lumley and Panofsky, 1964).

The drag coefficient data in Figure 7 represent means of measurements classed by half-meter/second wind speed intervals,
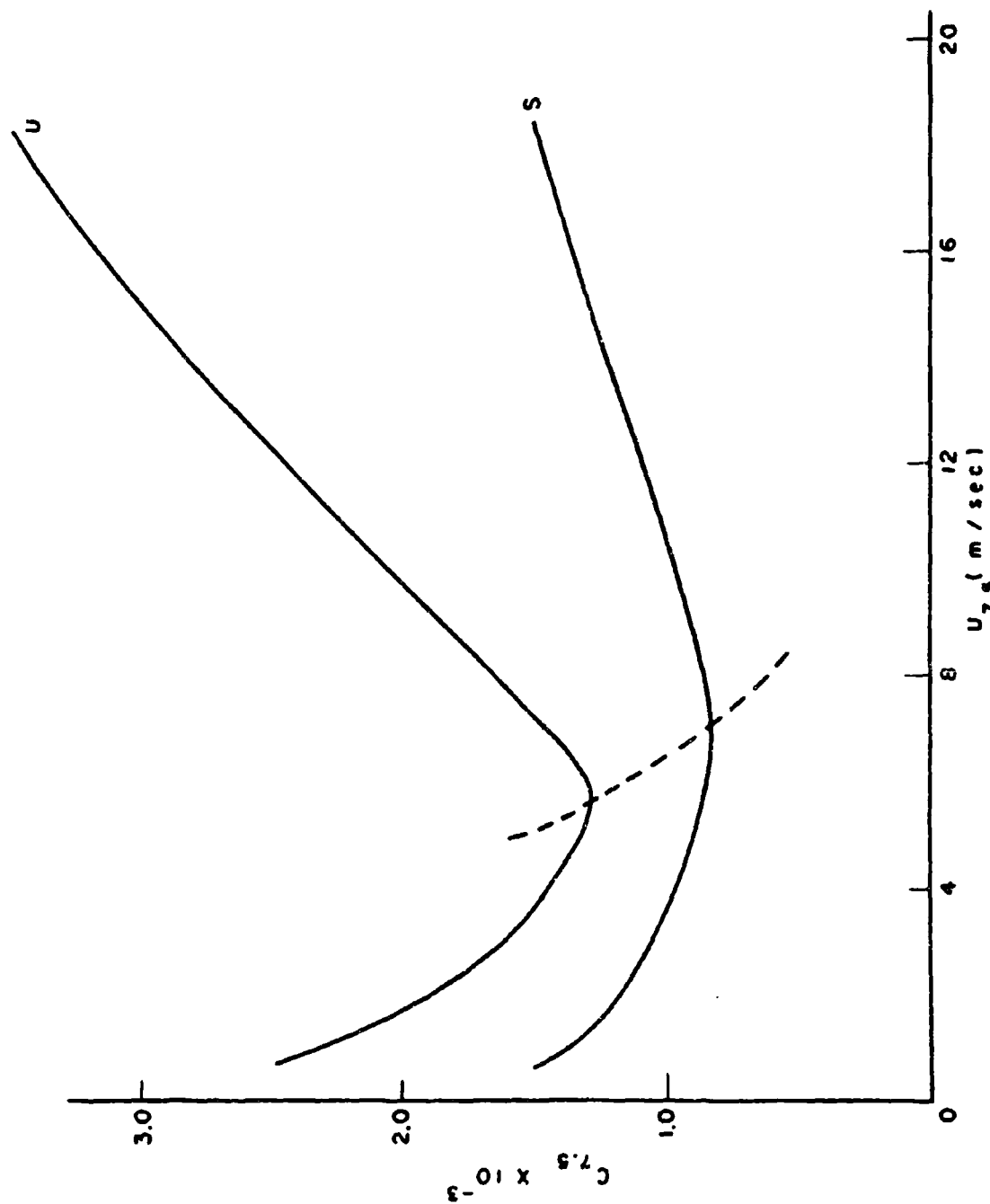
Drag coefficient with respect to 7.5 meters for unstable (U) and stable (S) conditions
corresponding to mean stabilities encountered at Argus Island.
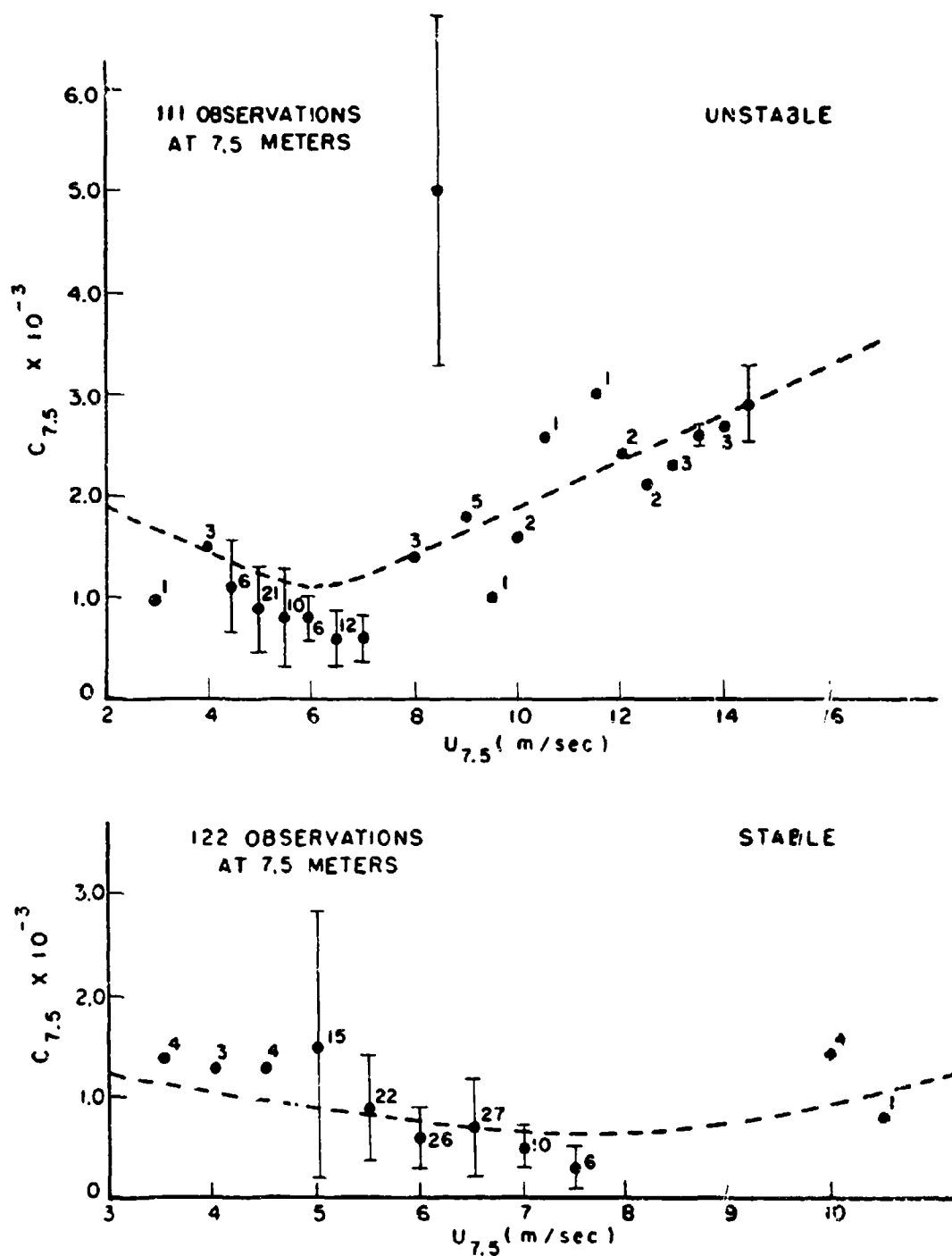
FIG. 7

Drag coefficient with respect to 7.5 meters for unstable
(-.28 ≤ Ri ≤ -.02) and stable (.02 ≤ Ri ≤ .24) conditions from
DeLeonibus (1966).   Dashed lines are drawn from Figure 6.

and are plotted with the root mean square spread and number of observations indicated. The data for stable conditions clearly suggest that the drag coefficient decreases as wind speed increases to at least 8 meters/second with perhaps a slight increase thereafter. The data for unstable conditions also suggest that the drag coefficient decreases with increasing wind speed. This behavior is not as well marked, however, and ceases near 6 meters/second above which the drag coefficient increases sharply with increasing wind speed. The calculated drag coefficient relations qualitatively predict this kind of behavior and in fact between 8 and 14 meters/second, the theoretical curve for unstable conditions provides nearly the best fit to the data. A quantitative comparison at the lower wind speeds is complicated by the fact that at such wind speeds (and low wind stresses) the surface boundary layer is quite shallow, with the 7.5 meter height perhaps in a region in which the stress decreases with height. The general agreement, however, may be taken as additional evidence that the roughness parameter specification proposed in (3.21) is realistic and that similarity theory can be applied successfully to the marine surface boundary layer.

The dashed line in figure 6 is drawn to indicate how the wind speed at which the drag coefficient is a minimum increases with increasing stability. This wind speed also increases with increasing height and the continuing controversy in the literature as to whether the drag coefficient increases or decreases with wind speed may be at least partially due to the fact that the variation of C_z with height and stability was not properly considered.

3.5 Application of the surface boundary layer model to ships' weather observations

The analysis of the marine surface boundary layer presented above implies that with observations of wind and temperature at two heights in the layer near the sea surface (to calculate Ri) one can apply the similarity theory to the calculation of the wind stress at the sea surface and to the specification of the wind profile to the heights to which the theory is applicable. In practice, however, such data are not available and the best that can be routinely obtained from a ship's weather observation is a measurement of wind at one level and a measurement of the air-sea temperature difference. The success with which the theory can be utilized to provide the meteorological data for wave prediction thus depends on how well one can estimate the stability from such data. The method developed below for this purpose uses the theoretical profile forms and the additional assumption that the sea surface temperature is a sufficient approximation to θ_o. The solution requires the use of an iterative procedure but this is of little importance within the context of a computerized analysis model.

The stability length involves gradients of potential temperature and wind speed. The potential temperature gradient can be expressed in terms of the air-sea temperature difference $(\theta_a - \theta_s)$ by the elimination of T_*/a_h between (3.28) and (3.26). This yields

$$\frac{\partial \theta}{\partial z} = \frac{\phi_u(z_a/L') \cdot (\theta_a - \theta_s)}{z[\ln(z_a/z_o) - \psi(z_a/L')]} \tag{3.38}$$

where z_a is the height at which θ_a, air potential temperature, is measured. The substitution of (3.38) and (3.25) into (3.24) yields

$$L' = \frac{U_*^2 \overline{\theta}[\ln(z_a/z_o) - \psi(z_a/L')]}{K^2 g(\theta_a - \theta_s)} \tag{3.39}$$

Equation (3.27) can be rearranged as

$$U_* = \frac{KU_m}{[\ln(z_m/z_o) - \psi(z_m/L')]} \tag{3.40}$$

where z_m is the height at which wind speed is measured. Since z_o can be expressed in terms of U_* through (3.21), (3.39) and (3.40) can be solved for the unknowns U_* and L'. The following procedure converges rapidly and is programmed as PROPAR in Appendix I:

1. Compute an initial guess of L' from (3.39) assuming $\psi = 0$ and $U_* = .04 U_m$.

2. Use this first estimate of L' to solve (3.40) iteratively, calculating ψ from (3.30) or (3.33), to compute U_*.

3. Use U_* to recompute the stability length from (3.39) iteratively.

4. Repeat the procedure from step 2 until $L'(n) - L'(n - 1) \leq \epsilon$, where ϵ is some preassigned convergence criterion.

When convergence has been achieved, $U_*(n - 1)$ is the appropriate value for friction velocity and z_o from (3.21) is the appropriate roughness length. The output of PROPAR is then U_*, L', and z_o, which together define the surface boundary layer wind distribution.

There are surprisingly few data available with which one can attempt to verify the procedure since experiments designed to measure the profiles of temperature and wind simultaneously over

the sea surface in varying stability conditions are difficult to carry
out successfully. Further, in two of the more recent successful pro-
grams (Paulson, 1967; Hoerber, 1968) sea surface temperature was
not available. The twenty-nine published wind and temperature profiles
of Fleagle et al. (1958), however, meet the data requirements in that
a wide range of stabilities is represented, wind and air temperature
profiles and sea surface temperature were measured simultaneously
and averages were taken over sufficiently long periods for the quantities
to be representative. The measurements were taken over a salt water
inlet with an over-water fetch of five miles. The curvature of the wind
and temperature showed qualitatively the same variation with stability
that had been demonstrated previously over land but some of the wind
profiles indicated anomalies of 1 or 2 percent of the wind speed. These
anomalies were always associated with readings from anemometers
located on the opposite side of the mast from the others (there were
eight levels in all) and may have been associated with mast interference
or horizontal inhomogeneities. These levels were not used in the
following analysis.

To verify the stability parameter determination procedure
proposed above, Richardson numbers were computed from the 29 wind
and temperature profiles by a finite difference analogue of (3.35). The
derivatives were approximated by (Panofsky, 1965)

$$\frac{\partial F}{\partial z} = \frac{F_2 - F_1}{\sqrt{z_1 z_2} \ln z_2/z_1}$$

where z_1 and z_2 are the lower and upper measurement levels for
F (U or θ), and the derivative applies at the height $\sqrt{z_1 z_2}$. To

evaluate $\partial\theta/\partial z$, the heights $z_1 = 40$ cm and $z_2 = 160$ cm were used, and to evaluate $\partial U/\partial z$, the heights $z_1 = 31$ cm and $z_2 = 171$ cm were used, the derivative corrected to 80 cm logarithmically. To compute Ri from single level wind data, the highest level wind observation ($z = 442$ cm), and the difference in temperature between the highest air temperature measurement (320 cm) and the sea surface temperature were used. Since sea surface temperature was measured by the bucket method, a correction for the cool skin effect was determined by extrapolating an observed adiabatic temperature profile to the sea surface. The correction was found to be 0.26°C which is in good agreement with Saunders' (1967) formulation for the conditions encountered in the experiment.

The wind profile for the neutral case was used to determine a z_0 of .0014 cm, a value that yields a drag coefficient about 20% less than that predicted by (3.21). Since the experiment was conducted in a range of wind speeds in which z_0 changes relatively little with wind speed, the value of z_0 was held constant in the computation of L' from single level data through (3.39) and (3.40). Richardson numbers were computed from computed L''s by solving (3.36) and (3.37) for Ri using $z = 80$ cm, $\beta' = 7$, and $\gamma' = 18$.

A comparison between observed (profile) Richardson numbers and those computed by the above iterative scheme is shown in figure 8a. The agreement is quite good generally, with the scatter increasing expectedly at greater deviations from neutrality.

The simplest stability parameter that can be computed from ship data is the so-called bulk Richardson number
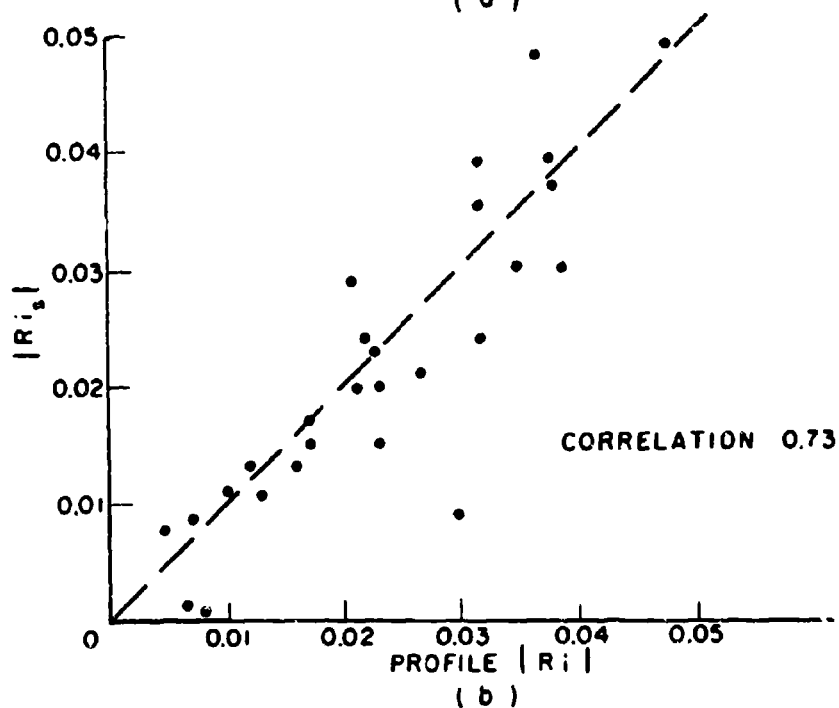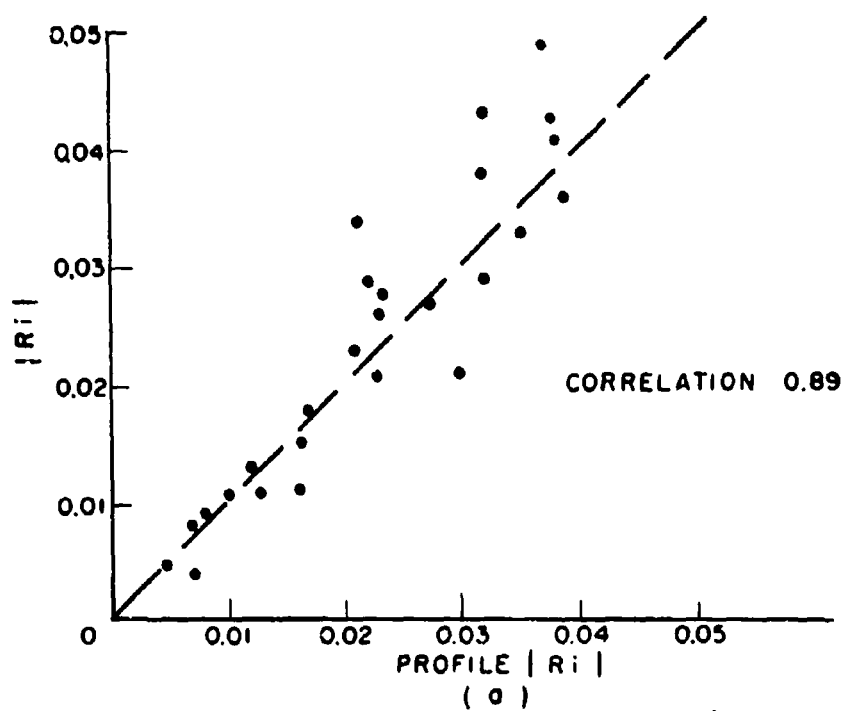
FIG. 8

(a) Scatter diagram of profile Richardson numbers and those
computed from single level data through (PROPAR). (b) Scatter
diagram between profile Richardson numbers and those determined
from statistically derived bulk relation from Fleagle et al. (1958)
profile data.

$$R_b = \frac{\theta_a - \theta_s}{U_m^2} \qquad (3.41)$$

To test its usefulness as a measure of the profile Richardson number, R_b was computed from the Fleagle et al. (1958) data and related to the profile Richardson numbers by a linear least squares fitting procedure. A scatter diagram between the Richardson numbers predicted by this procedure, Ri_s, and the profile Richardson numbers is shown in figure 8b. It is seen by comparison with figure 8a, that this procedure is not as successful as the iterative procedure as evidenced by the greater correlation coefficient for the latter. Furthermore, a simple statistical relation between R_b and Ri should not be as successful over a wider range of wind speeds becuase of the relatively large variations of z_o with wind speed above 8 m/sec and below 3 m/sec.

Data on the behavior of the drag coefficient during stable fetch limited conditions have been recently obtained on Long Island Sound by means of thrust anemometer measurements of the turbulent Reynolds stresses by Adelfang (1969). The results of that study are shown in Figure 9, where the drag coefficient is related to the bulk stability parameter defined exactly as (3.41). The solid curve is an empirical relation proposed by Adelfang and is based upon a quadratic least squares fit to the data. The range of wind speeds was quite small (6 to 8 meters/sec at 2 meter height), but the difference in temperature between the sea surface and 3.2 meters varied between 0.8 to 3.8°C, thus allowing the relatively wide range of R_b to be encountered.

To compare the predictions of the similarity theory to Adelfang's measurements, (3.39) and (3.40) can be combined to relate
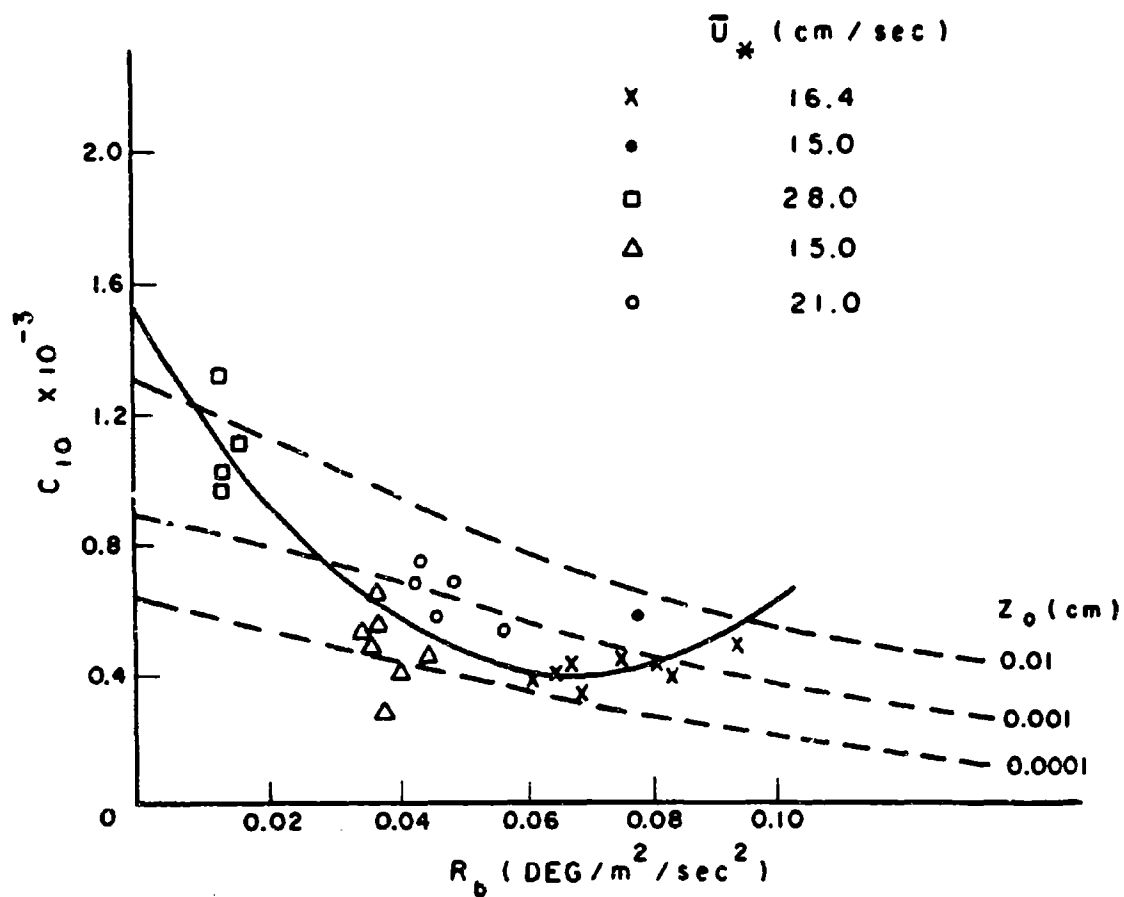
FIG. 9

Thrust anemometer determinations of the drag coefficient
(Adelfang, 1969) versus bulk stability.

L' to R_b since

$$L' = \frac{\bar{\theta}}{g} \cdot \frac{1}{R_b} \cdot \frac{[\ln(z_a/z_o) + 7(z_a/L')]}{[\ln(z_m/z_o) + 7(z_m/L')]^2} \qquad (3.42)$$

The drag coefficient can be written for stable conditions

$$C_{10} = \frac{K^2}{[\ln(z_{10}/z_o) + 7(z_{10}/L')]^2} \qquad (3.43)$$

It is seen that the relation between L' and R_b is not unique but depends upon z_o, as does the relation between C_{10} and L'. Profile measurements were not made during the experiment nor were drag coefficients measured during neutral conditions; hence, data from which an appropriate z_o could be measured or inferred are not available. Therefore relationships between C_{10} and R_b were computed from (3.42) and (3.43) for several values of z_o and these are also indicated in figure 9.

Though the observations appear to indicate greater effects of stability than given by (3.43), this may be due to variations in z_o between the one near neutral and the other more stable sets of measurements. The mean friction velocities observed for the latter suggest that z_o may indeed have been lower, within the context of the discussion in Section 3.3. Qualitatively, however, the measurements confirm the marked effects of stable conditions in reducing the drag coefficient as predicted by the use of the log-linear model.

3.6 Some effects of stability on wave generation

The procedure just outlined allows a comparison to be made between Fleagle's (1956) observational study of the dependence of wave

generation on stability and the modifications proposed in Section 2.2.
Figure 10(a) shows the relationship found between air-sea tempera-
ture difference and wave height with observations at ship "Hotel"
(36°N, 70°W), each point representing an average wave height and wind
speed for ten observations in the indicated air-sea temperature range.
The criteria employed in the selection of cases by Fleagle were meant
to insure that the fetch was approximately equal to the distance of the
ship from shore (270 nautical miles) and cases of reported wind and
wave direction differing by more than 20° were excluded. The same
kind of analysis was done for 77 cases at ship "Sierra" (48°N, 162°E)
as for "Hotel" except that smaller differences were observed, cor-
responding to a smaller range of air-sea temperature differences
observed there.

It is difficult to compare any predictions of wave height in
ship "Hotel" with Fleagle's data because the observed data are visual
estimates of wave height and because of uncertainties in the height at
which the wind speed was measured. Also, the air-sea temperature
differences observed at the ship may not be representative of the
differences upstream of the ship. They most probably are under-
estimates for the cases selected by Fleagle. Furthermore, there is
no assurance that in the cases selected the waves had actually reached
full development for the fetch involved; hence, the cases probably
represent a wide range of duration-limited as well as fetch-limited
states of wave development. For comparison, however, relationships
between wave height and wind speed as would be observed at a fetch of
270 nautical miles were computed for the stability cases analyzed by
Fleagle. The wave spectrum was assumed to be fully developed for
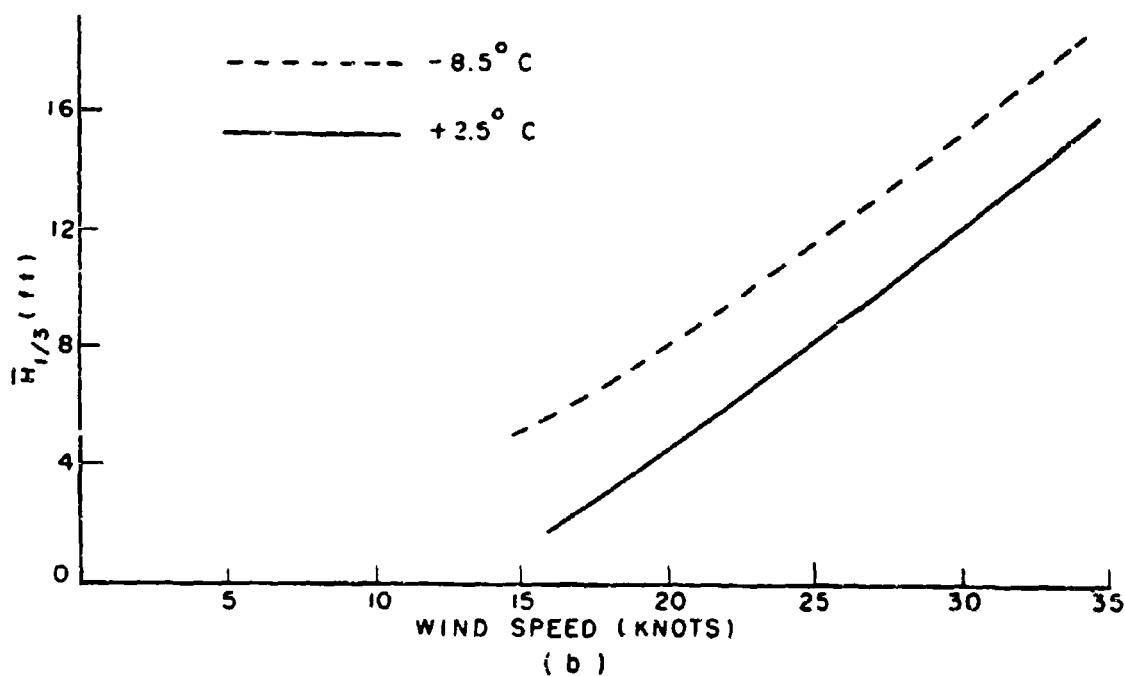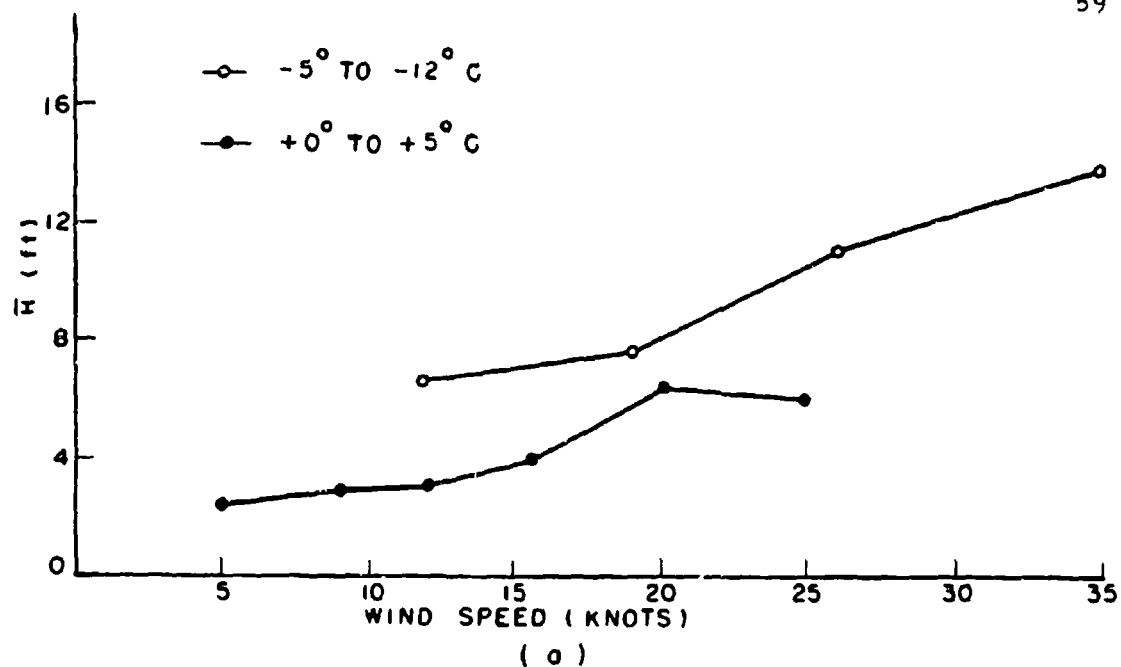
(a) Observed influence of air-sea temperature difference on mean wave height at ship "Hotel" from Fleagle (1956). (b) Computed variation of significant wave height at a fetch of 270 n. mi. with wind speed and air-sea temperature difference from stability dependent spectral growth formulation.

the fetch involved and the method outlined in Section 2.2 was used to
compute the spectrum and the significant wave height. The wind
speeds were assumed to have been measured at 25 meters, the average
anemometer height on U. S. Coast Guard vessels that man the U. S.
ocean stations. The stability was determined by specifying an air-sea
temperature at the middle of the range analyzed by Fleagle and com-
puting L' and U_* on the basis of the surface boundary layer model.
Referring to (2.7) the quantity B could then be computed from U_*, A
from the wind speed at 19.5 meters and the fully developed spectral
energy, S_∞, from a wind speed corresponding to an upward extra-
polation to 19.5 meters of a logarithmic profile based upon the com-
puted U_* (and hence z_0).

The computed relations are shown in figure 10(b). There is
considerable disagreement between the actual magnitudes of the reported
and calculated heights for low wind speeds, and this may be due in large
part to the deficiencies in the method of estimating wave heights from
ships under these conditions. The percentage differences between
stable and unstable computed wave heights, however, are in rough
agreement with the data. Also, for both the observed and computed
cases, the variation of wave height with fetch is more nearly linear
than quadratic, reflecting the effect of fetch limitation.

It is significant that at wind speeds below 20 knots, the fetch is
sufficient for the spectrum to attain nearly full development for the
wind speeds regardless of the stability. The observed differences at
these low wind speeds could only be explained, within the context of
the Inoue spectral growth formulation, in terms of a stability dependent
fully developed sea. At higher wind speeds, the differences reflect

both this factor as well as the effect of stability on the growth rates.

At high wind speeds, the effect of stability in terms of signi-
ficant wave height is a 20% increase in significant wave height for
unstable conditions over stable conditions. In terms of the more
sophisticated applications of wave spectrum predictions, however,
the effects of stability are more pronounced. Referring to Figure 11
which shows the spectra for the same lapse rate conditions of Fleagle's
analysis, with a wind speed at 35 knots, it can be seen that the 20%
difference in wave height corresponds to a 40% difference in the total
area under the spectrum, a shift in the spectral peak toward lower
frequencies, and significant differences in the spectral density of com-
ponents at frequencies near and below that of the spectral peak.

As an example of the effects of stability on modifying the vari-
ation at significant wave height with wind speed for fully developed
seas, the surface boundary layer model was employed to calculate
such relationships for air-sea temperature differences of -8°, 0°,
and +4°C. The results of these computations are shown in figure 12.
Between 20 and 40 knots the significant wave height for the unstable
(stable) case averages about 20% higher (25% lower) than for the neutral
case. Stated another way, in terms of air-sea temperature difference,
stable conditions are more than twice as effective as unstable conditions
in modifying the fully developed spectrum. The differences in the spectra
discussed above for the fetch limited case of course also apply to the
fully developed spectrum.

Indirect evidence of the effects of stability on wave generation
has been provided by recent observations of whitecap coverage by
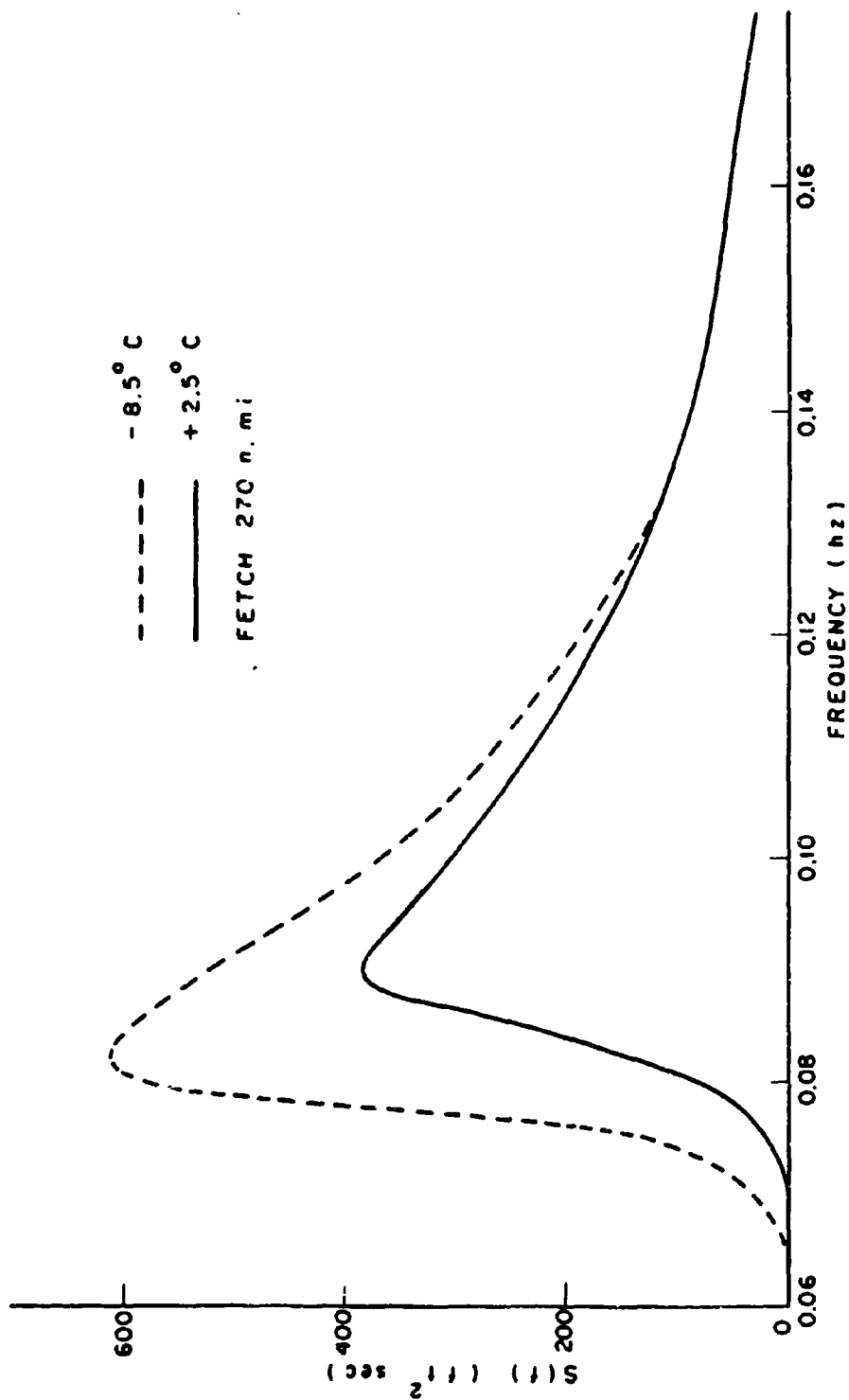
Fetch limited spectra corresponding to 35 knot winds at 25 meter height and the stability conditions employed in Fig. 10.
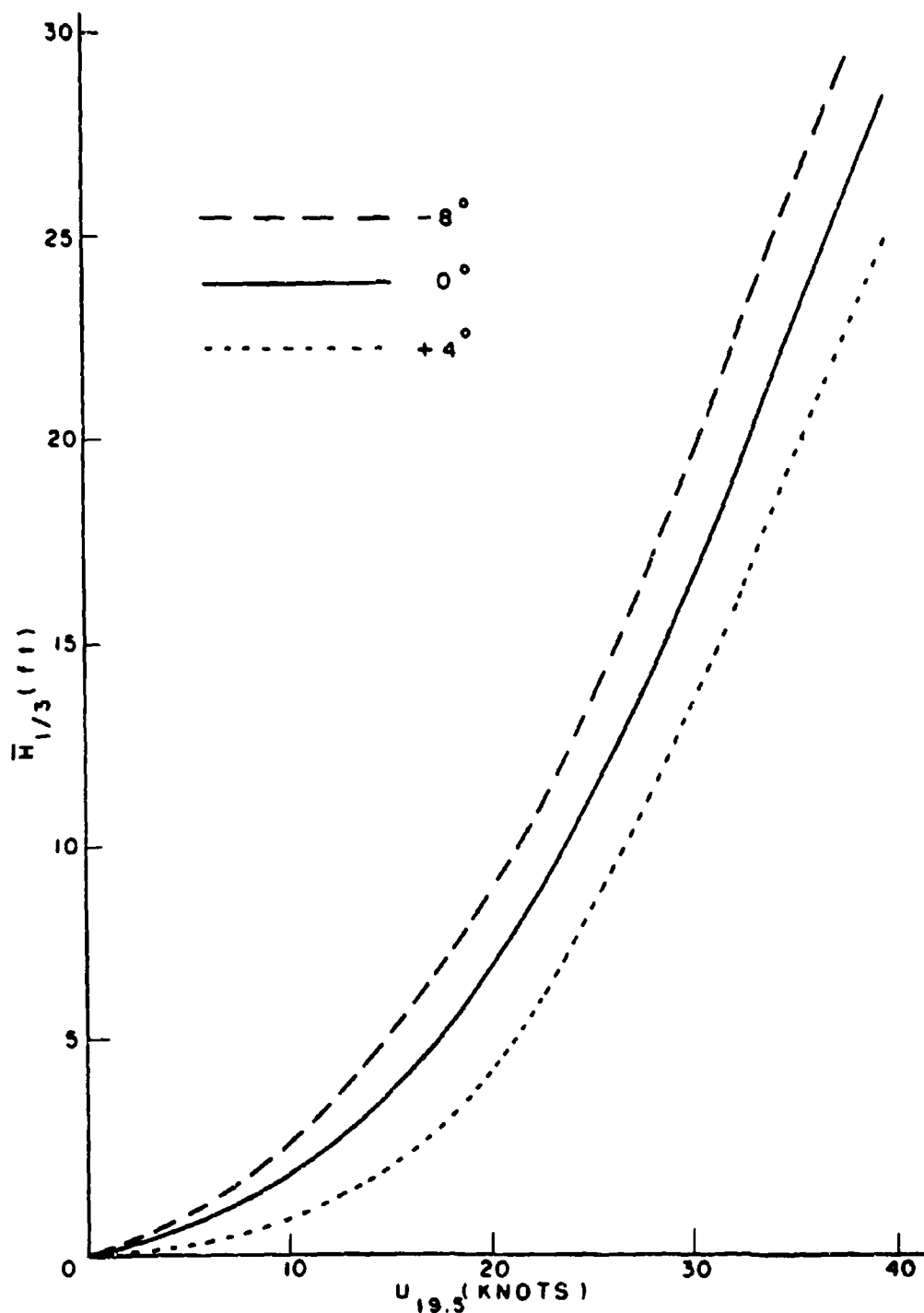
FIG. 12

Variation of significant wave height with 19.5 meter wind speed for fully developed seas and various air-sea temperature differences.

Monahan (1969). Observations of the percentage of the sea surface
covered by whitecaps were determined photographically from vessels
on the Great Lakes. The observations; shown in figure 13, cover a
fairly wide range of wind speeds and air-sea temperature differences,
though most of the observations, particularly at the lower wind speeds,
represent very stable stratification.

Monahan suggests that the abrupt increase of whitecap coverage
at about 7 m/sec may be evidence for the existence of the legendary
critical wind velocity for air-sea boundary layer processes. He also
notes that for the same wind speed, whitecap coverage is higher for
unstable conditions than for stable conditions. The latter observation
is consistent with the stability modifications proposed in Section 2.2.
Whitecaps are a manifestation of wave breaking, which may be thought
of as a process whereby energy transferred through wave generation
processes to spectral components that are fully developed is made unavail-
able to wave motion. An instability mechanism is responsible for most
of this energy transfer, and it was shown in Section 2.2 that in terms of
the Miles-Phillips instability theories, the transfer is in general higher
for unstable conditions than for stable conditions for a given anemometer
level wind speed. The transfer, however, also depends upon the
spectrum and as such, should be expected to depend sensitively upon
other factors such as fetch and duration.

To check this model more quantitatively with Monahan's data,
the simple hypothesis is made that the percentage of the sea surface
covered by whitecaps, which is related to the rate of energy dissipation
in a generating wave spectrum, is directly related to the rate of energy
transfer from the air flow to the fully developed spectral components
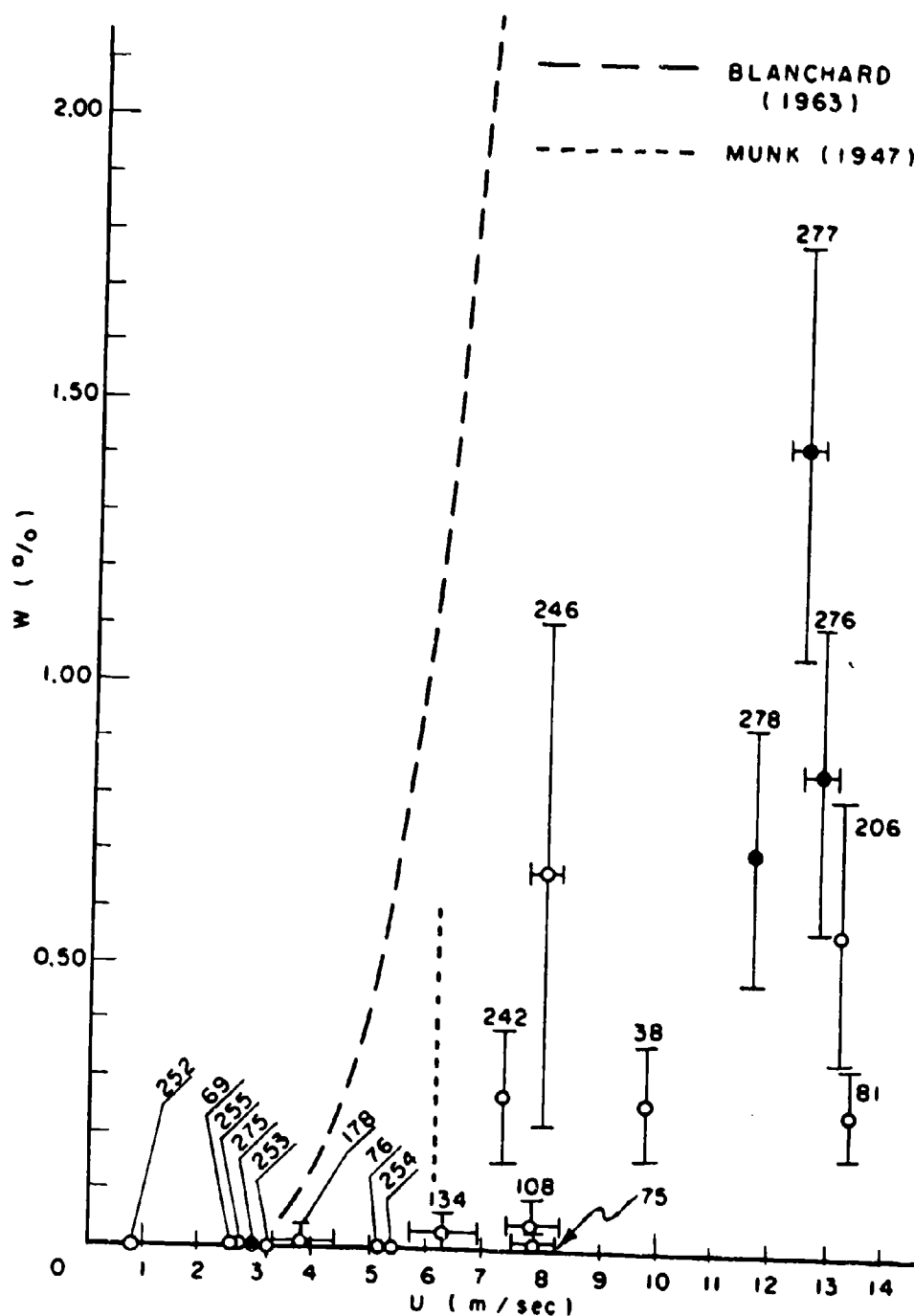
FIG. 13

Monahan's (1969) measurements of percent whitecap coverage (W) versus deck height wind speed (V) with observation number and standard deviation (vertical bars) indicated. Filled circles represent observations in unstable conditions and open circles represent observations in stable conditions.

through a combined Miles-Phillips type instability mechanism. The latter is given by the expression

$$E_t = \rho_w g \int_0^{f_g} \frac{dS}{dt} \, df = \rho_w g \int_0^{f_g} B \cdot S(f, x, t) \delta \, df \qquad (3.43)$$

where $\delta = 1$, $S = S_\infty$,

$\delta = 0$, $S < S_\infty$,

f_g indicates that the integration is to be limited to the gravity wave frequency domain, and E_t has the units energy/area/time.

Observations of fetch, air-sea temperature difference and wind speed by Monahan for each observation of whitecap coverage, make possible an evaluation of equation (3.43) with the assumption that the wind speed and stability conditions were uniform over the entire fetch and that the duration was sufficient for the wave spectrum to be fully developed, for the observed fetch. The anemometer height was taken to be nominally 40 feet[*] for all observations. The results of these calculations are shown in Figure 14. The considerable scatter that remains may be due in part to variability in wind and stability along the fetch, duration limitations, variability in the anemometer height and, perhaps, as noted by Monahan, to unknown variations in surface tension caused by organic films. It can be seen, however, that whitecap coverage is considerably better correlated with E_t than with wind speed alone.

To demonstrate the effects of fetch and stability on whitecap coverage, within the context of the proposed model, a linear least squares fit was employed to relate whitecap coverage to energy transfer, E_t.

---

[*] The author is indebted to Prof. Monahan for providing this valuable piece of information.

$$W (\%) = -0.0185 + 0.893 \times 10^{-3} \times E_t \ (ergs/cm^2/sec)$$
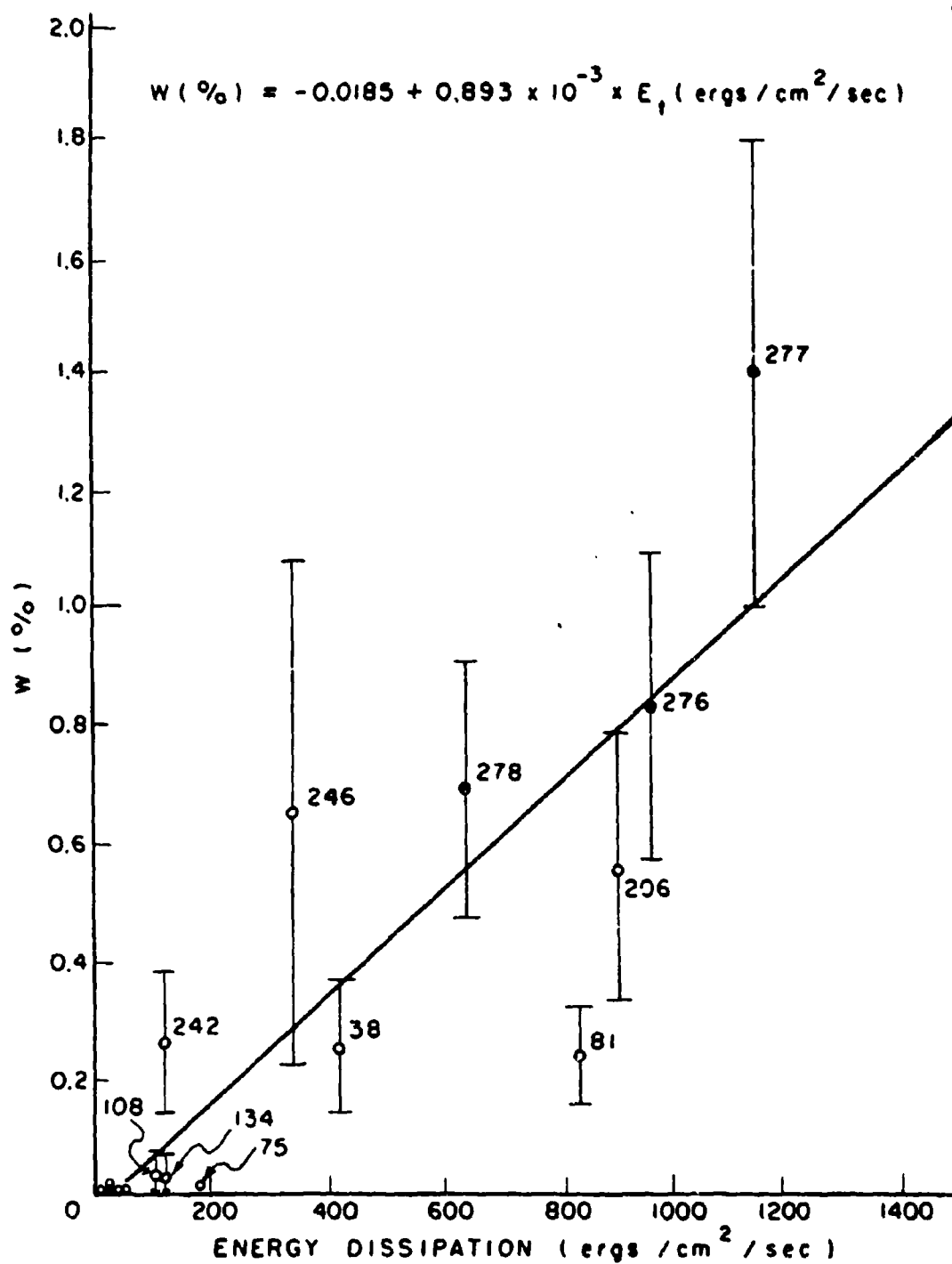
FIG. 14

Energy dissipation calculated according to (3.43) for the conditions of Monahan's (1969) observations versus observed whitecap coverage.

Then the spectral growth model was used to calculate the percentage

of the sea surface covered by whitecaps as a function of wind speed

(at 19.5 meters) at a fetch typical of Monahan's observations (25 km)

for unstable $(\theta_a - \theta_s = -8°C)$ and stable $(\theta_a - \theta_s = 4°C)$ conditions.

These relations are shown in Figure 15, where they show the significant

effects of stability. It is also important to note in these curves the

abrupt nature of increase in whitecap coverage with wind speed above

a speed which depends on stability. This behavior is not a reflection

of any discontinuity in the drag coefficient and, in fact, would have

been quite evident had z_o been assumed constant between 2 and 10 m/sec.

Also shown in Figure 15, is a calculated wind speed-whitecap

coverage relation corresponding to neutral conditions and fully developed

seas. This curve lies much closer to Blanchard's (1963) curve

(Figure 14) which is representative of oceanic whitecapping and hence

of characteristically longer fetches than those encountered over the

Great Lakes. Blanchard's data also differ in that they represent

salt water whitecapping. It has been shown (Monahan, 1966) that the

size spectra of fresh water and salt bubbles produced by the same

mechanical mixing processes are markedly different and that this pro-

duces differences in whitecap stabili r. The quantity, E_t, is more

directly related to wave breaking. Thus if salt water whitecaps were

more persistent than fresh water whitecaps for the same wave break-

ing conditions, whitecap coverage would be expected to be greater in

salt water than in fresh water for the same wind stability fetch and

duration conditions. Hence, the quantitative results obtained here should

not be applied to salt water until sufficient observations of salt water

whitecapping are obtained and analyzed as above.
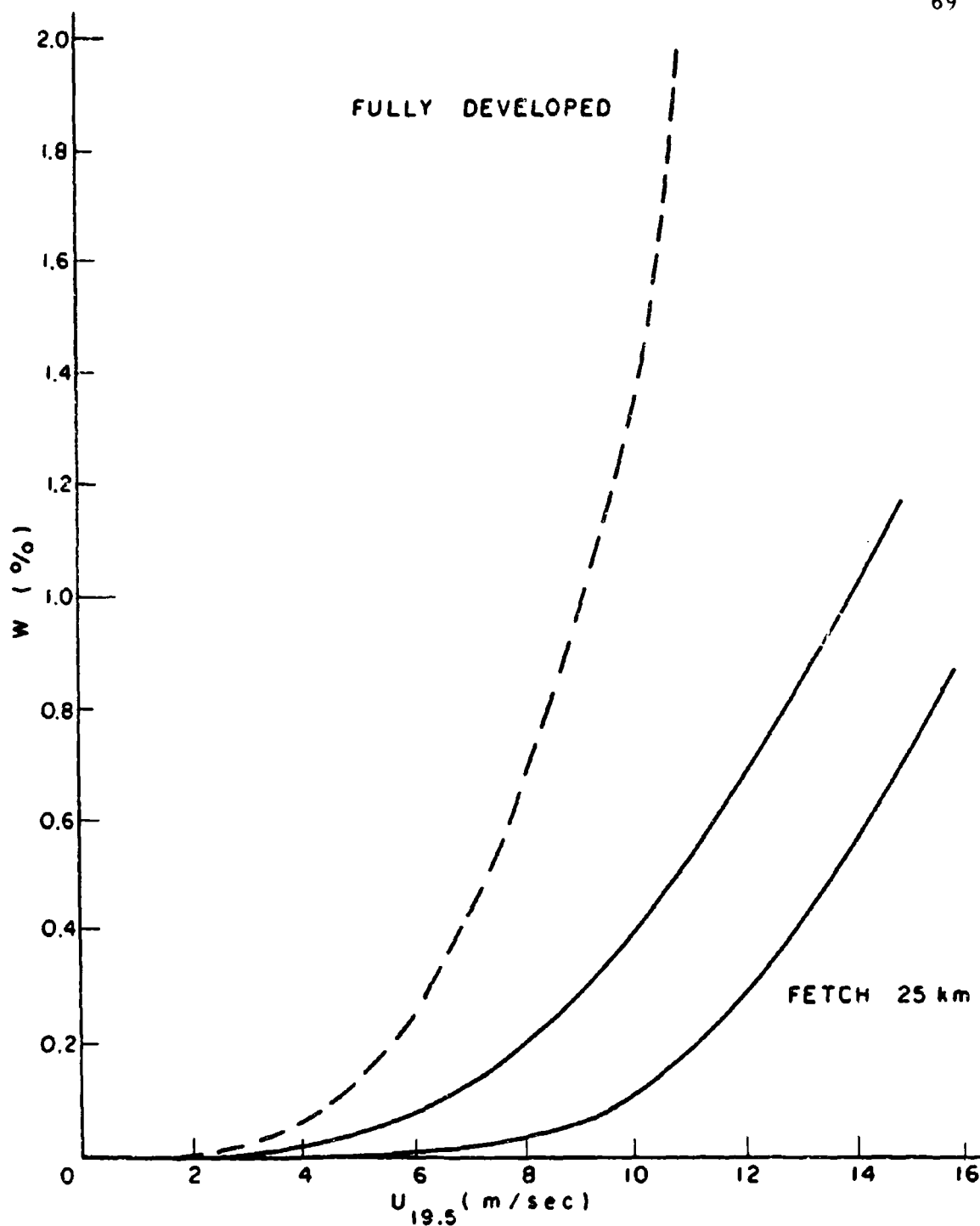
FIG. 15

Whitecap coverage versus 19.5 meter wind speed and stability
for fetch limited seas, and versus wind speed for neutral
conditions for fully developed seas, computed on the basis of a
linear least squares fit to Monahan's data (see Fig. 14).

4. The Planetary Boundary Layer Model

4.1 Review of past research

The past decade has been a period of active research in the problem of determining the characteristics of the wind distribution in the planetary boundary layer. This interest stems basically from the fact that in many areas of meteorology, such as urban air pollution dynamics, numerical weather prediction, and general circulation studies, there is being evidenced a need for a better description of this region of the atmosphere. Much of the research, however, appears to have been inspired by the publication of a paper on the subject by Lettau (1959). In that paper, Lettau presented an empirical relation between the geostrophic drag coefficient U_*/G, where G is the surface geostrophic wind speed, and the so-called surface Rossby number, G/Fz_0 where F is the Coriolis parameter. That such a unique relationship should exist in a steady, neutrally stratified boundary layer was first proposed by Rossby and Montgomery (1935) and Lettau employed available measurements of U_*/G (see Figure 16) to show that this may indeed be the case. Available measurements of another important characteristic of the planetary boundary layer, the angle between the surface wind and the surface geostrophic wind, ψ_0, indicate that this property may also depend systematically on G/Fz_0, and more recent planetary boundary layer models have produced such expressions for comparison with data.

Thus far, nearly all attempts at the problem of the approach to the geostrophic wind have utilized assumptions simplifying the atmospheric boundary layer to a region in which the mean motion is in a

LETTAU (1959)

BLACKADAR (1965 b)

APPLEBY AND OHMSTEDE (1966)

BLACKADAR (1965 a)

LETTAU (1962)

BLACKADAR (1965 b)

log_{10} R_O
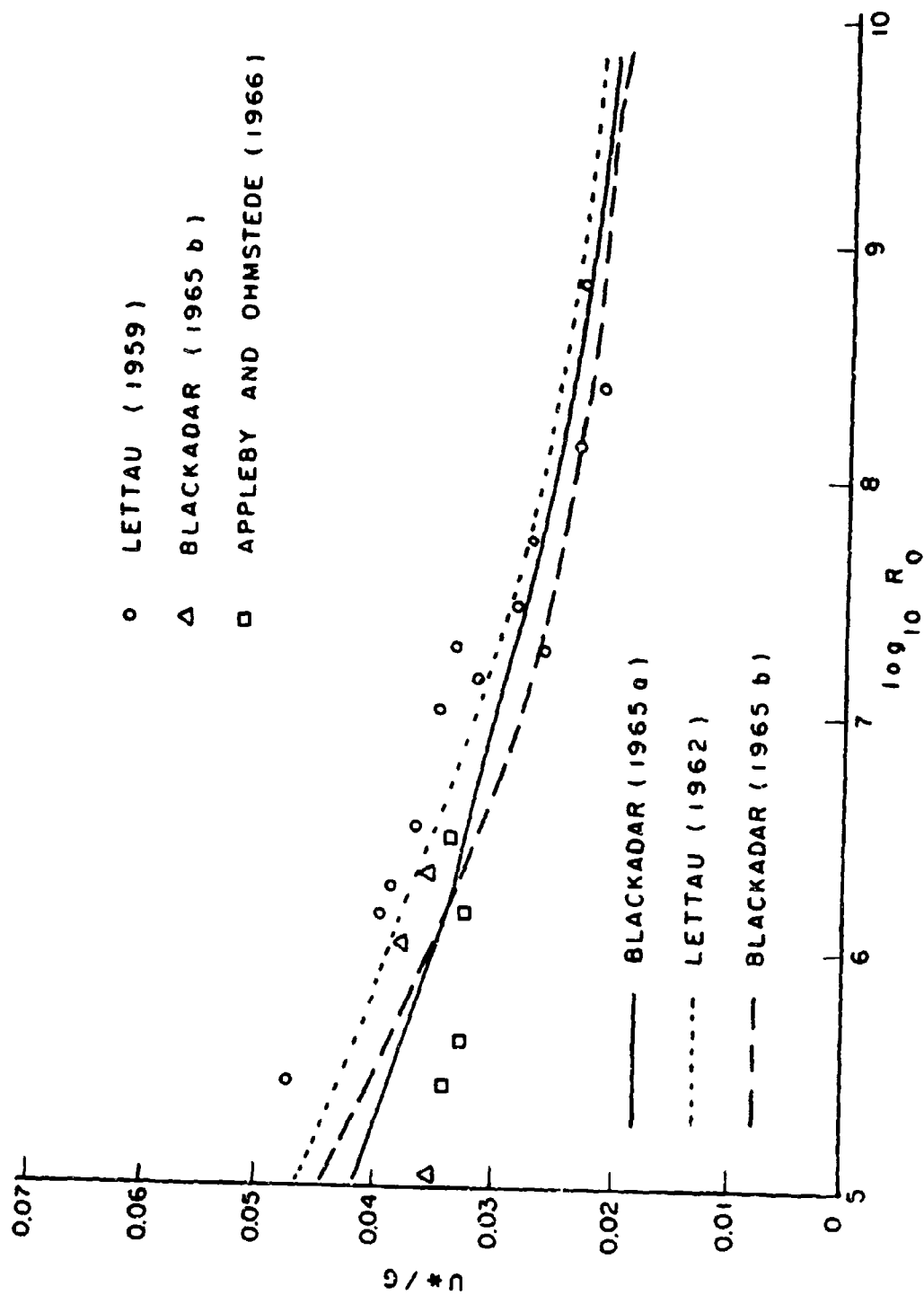
$F I G. 16$

Published measurements and proposed theoretical forms for the variation of the surface geostrophic drag coefficient (U_*/G) with surface Rossby number (R_O).

steady state and is entirely homogeneous and uniform at every level and in which the density may be considered independent of height. The equations of motion are then written

$$f(v - v_g) + \frac{d}{dz}\left[K_m \frac{d}{dz}(u - u_g)\right] = 0$$

$$-f(u - u_g) + \frac{d}{dz}\left[K_m \frac{d}{dz}(v - v_g)\right] = 0$$

$$(4.1)$$

where u, v are the horizontal wind components and u_g, v_g are the corresponding geostrophic wind components. The first solutions to this system were reached independently by Ekman and G. I. Taylor and applied to the case where K_m is independent of height. The familiar solution to this problem under the boundary conditions

$$u = u_g \qquad z \to \infty$$
$$u = v = 0 \qquad z = 0$$

can be written

$$u = u_g(1 - e^{-az} \cos az)$$

$$v = u_g(e^{-az} \sin az)$$

$$(4.2)$$

where $a = \sqrt{F/2K_m}$ and the x-axis coincides with the geostrophic wind direction. The theory predict the commonly observed veering of the wind vector with height and a suitable choice of K_m for a given situation often allows the theory to fit observed wind profiles closely away from the surface boundary layer. The theory breaks down in the surface layer, predicting an unrealistic wind profile as well as a constant value of ψ_0 of 45°.

The cause of the unrealistic behavior in the surface boundary layer in the Taylor-Ekman model is the unrealistic assumption of

constant K_m there since, according to Prandtl,

$$K_m = KU_* z \qquad (4.3)$$

near the ground in thermally neutral conditions. Kibel (see Belinski, 1948) was the first to solve (4.1) with the form (4.3) applied throughout the boundary layer. Ellison (1956) employed the same assumption but incorporated the effects of ground roughness and showed that the wind profile approached a logarithmic form as the surface was approached. The predictions of the behavior of U_*/G and ψ_0, however, verified poorly with available observations, the discrepancies no doubt due to the fact that (4.3) is valid only in the lower 20-200 meters or so and leads to unrealistically high values of K_m when extrapolated to the upper part of the boundary layer.

Kohler (see Sutton, 1953) presented a solution to (4.1) based on the assumption of a power law distribution for K_m of the form

$$K_m = K_1 z^m \qquad 0 < m < 1$$

where K_1 is the value of K_m at $z = 1$. The solution indicates that near the ground

$$U = U_1 z^{1-m}$$

and

$$\psi_0 = \frac{1-m}{2(2-m)} \pi$$

where U_1 depends on F, m, K_1, and G. Since the eddy viscosity is known to increase more rapidly with height in unstable conditions than in stable conditions, Kohler's analysis indicated how ψ_0 might vary with stability. The analysis was successful in demonstrating many features of the wind structure in the boundary layer but it is difficult

to apply in any quantitative sense. There is no way to take into account the effect of ground roughness since K_1 and m must be chosen on the basis observations to fit the profile of K_m in the entire boundary layer. Also, the profile laws for the lower part of the boundary layer do not agree with the similarity forms presented in Section 3.3.

The failure of any model utilizing a single analytical expression for K_m led several workers to develop models based on two-layer representations for K_m. Indeed, the two-layer model of Rossby and Montgomery (1935) represented a landmark in boundary layer research and was the first study to demonstrate the importance of the non-dimensional number G/Fz_o. The model divided the boundary layer into a lower layer in which the stress was considered constant and in which K_m was specified according to Prandtl and an upper layer in which K_m decreased with height. The predicted relations between U_*/G, ψ_o, and R_o, however, are not in good agreement with observations.

Yudin and Shvetz (see Belinski, 1948) combined a Prandtl surface layer with an Ekman upper layer. Estoque (1959) combined a Prandtl surface layer with an upper layer in which the eddy viscosity gradually decreases and solved the system of equations numerically. Both models are of academic interest only, however, since in each case the height of the surface layer was arbitrarily specified.

Blackadar's (1965a) model utilizes a structure similar to that of Yudin and Shvetz but specifies the height of the surface layer explicitly in terms of external parameters. In particular, a dimensional argument is applied and a simple form for the height of the surface layer n is postulated as

$$h = B_o G/F \qquad (4.4)$$

where B_o is a dimensionless constant. Since the model employs an Ekman type upper layer, the value of K_m at the internal boundary and above is

$$K_m = K U_* G/F \qquad (4.5)$$

The solution in the upper layer can be written

$$W = W_h e^{-a(z-h)} e^{-ia(z-h)} \qquad (4.6)$$

where $W = (u - u_g) + i(v - v_g)$ and W_h is the value of W at $z = h$.

The solution is determined by applying the outer boundary conditions

$$u = 0 \qquad z = z_o$$

$$u = u_g \qquad z \rightarrow \infty$$

and the conditions that at h, continuity of wind, wind shear and stress is required. The solutions for U_*/G and ψ_o, which together with z_o completely define the surface boundary layer wind distribution in neutral conditions, are given as

$$U_*/G = \sqrt[3]{2KB_o \sin^2 \psi_o}$$

$$U_*/G = K\sqrt{2} \sin(\pi/4 - \psi_o) \ln B_o R_o$$

where $R_o = G/F z_o$, which indicates that U_*/G and ψ_o are uniquely related to R_o. Blackadar chose a value for B_o of 3.0×10^{-4} as providing the best fit to observations and the predicted relation between U_*/G and R_o is indicated in Figure 16.

It was noted by Lettau (1962) that none of the approaches which explicitly specify the distribution of eddy viscosity can meet with complete

success since the eddy viscosity can be defined as a product of a length and a velocity as

$$K_m \equiv \ell \cdot v^* \equiv \ell \cdot \sqrt{\tau/\rho} \tag{4.7}$$

where τ is in general a function of height. Only the length term can be expected to be an explicit function of height. The velocity term depends on the shear stress distribution which in turn depends on the solution of the differential equation governing the problem. Thus the problem is essentially nonlinear and Lettau uses a numerical approach to solve the nonlinear system of equations that results from the use of (4.7). The mixing length specification chosen was

$$\ell/X = \frac{kz/X}{(1 + 4z/X)^{5/4}}$$

where X is a scaling height. With the additional assumption that the level of maximum eddy viscosity and maximum cross isobar flow occur at .5X, a non-dimensionalized form of (4.1) is solved by numerical integration. The hodograph of the solution is again a spiral much like the Ekman model, but the wind profile approaches a logarithmic form close to the surface. The characteristics of the solution are found to be dependent upon R_o with the predicted relation for U_*/G indicated in Figure 16.

Nearly concurrently with the publication of Lettau's model, Blackadar (1962) introduced a boundary layer model based on the implicit specification of the eddy viscosity. The model differs basically in the specification of the mixing length. Blackadar chooses the form

$$\ell = Kz/(1 + Kz/\lambda)$$

where λ is the value of ℓ in the free atmosphere and was related to the external parameters G and F through

$$\lambda = .00027\, G/F \qquad (4.8)$$

the constant chosen so that the predictions of the model fit well with some careful observations of ψ_0 at Brookhaven. In a later version (Blackadar, 1965b) the mixing length was specified according to (4.8) but with

$$\lambda = .0063\, U_{*}/F$$

The resulting solution differs little from the earlier model and the predicted relation between U_{*}/G and R_0 is also shown in Figure 16.

Yet a fourth solution employing the mixing length approach has been offered by Appleby and Ohmstede (1966). Their expression for the mixing length is derived from the differential equation

$$\frac{d\ell}{dz} = K - \ell/L_0 \qquad (4.9)$$

which embodies the notion that the mixing length increases with height at a rate given by von Karman's constant but that there is a direct linear feedback that prevents unbounded growth. The solution to (4.9) is

$$\ell = \ell_0 (1 - e^{-z/L_0})$$

where $L_0 = \ell_0/K$, ℓ_0 representing the limiting value of ℓ. The length ℓ_0 was specified to be 32 meters on the basis of the Leipzig wind profile (Lettau, 1950). The predictions of this model lie between those of the numerical solutions of Lettau and Blackadar.

It can be seen by referring to Figure 16 that all the recent solutions are very similar and that it is possible, on the basis of

available observations, to determine which of the models is more correct. The solutions are especially similar over the range of Rossby numbers characteristic of the marine boundary layer ($R_o \sim 10^8 - 10^{11}$). The same conclusions could be drawn from a comparison of the predicted relationship between ψ_o and R_o and available data. Apparently, only very accurate determinations of U_*, G, and ψ_o under neutral conditions and over a wide range of Rossby numbers will be able to distinguish between the several approaches. It is also required of such measurements that a steady state regime be established. Such a regime is rare over land because of inertial oscillations in the boundary layer wind field set up by the normal diurnal range of stability. The diurnal variation of stability over the oceans is much smaller and a quasi-steady state regime is more likely to be established, but there are many practical difficulties involved in making accurate measurements of the wind profile in the entire planetary boundary layer there and the range of Rossby numbers encountered there is also relatively small.

None of the models discussed above can be directly applied to the marine boundary layer since each considers the roughness parameter as an external parameter. Over the oceans, this parameter is a characteristic of the flow and as such, is a quantity to be predicted by the model. Aside from this complexity, little work has been done on generalizing boundary layer models by relaxing the assumptions usually made. The effects of baroclinicity can be taken into account relatively simply but it is not clear how the important effects of a non-neutral stratification may be included. The mixing length approach

may be irrelevant during unstable conditions since it is known that in those conditions convection is a much more effective momentum transporting mechanism than transport by turbulent eddies.

Blackadar and Ching (1965) extended Blackadar's numerical model to unstable conditions by modifying the eddy viscosity formulation for unstable conditions and obtained qualitative agreement with observation of the behavior of U_*/G with stability. The solution, however, requires a time-consuming and delicate numerical integration of the equations of motion and furthermore cannot be applied to stable conditions. The success of Blackadar's two-layer model in predicting the essential characteristics of the neutral surface boundary layer and its relative ease of application when compared to the numerical solutions recommends its extension to the non-neutral marine boundary layer.

4.2 Extension of Blackadar's two-layer model

The two-layer approach to the modelling of the eddy viscosity distribution in the neutral planetary boundary layer can be generalized to model in a simple way the effects of non-neutral stratification. Realistic profiles for K_m can be specified in the constant stress layer by employing forms consistent with the similarity profiles presented in Section 3. At the same time, within the context of the two-layer modelling, the eddy viscosity distribution would also be affected above the surface, with higher (lower) values specified for unstable (stable) conditions than would be specified with neutral conditions, all other things being equal. This again is realistic and in agreement with the few available determinations of K_m above the surface boundary layer.

In the constant stress layer, the eddy viscosity can be written

$$.K_m = \frac{U_*^2}{\partial \overline{U}/\partial z}$$

and can be expressed in terms of the non-dimensionalized wind shear as

$$K_m = KU_* z (\phi_u (z/L'))^{-1}$$

Within the context of Blackadar's two-layer model, the value of K_m at and above the internal boundary h is

$$K_m = KU_* B_o G (F \phi_u (h/L'))^{-1}$$

and the parameter a takes the value

$$a = F\sqrt{\phi_u (h/L')/2KU_* B_o G} \qquad (4.10)$$

The wind profile in the constant stress layer is given by (3.27) from which the wind speed at the level h can be written

$$U_h = (U_*/K)\left[\ln B_o R_o - \psi(h/L')\right] \qquad (4.11)$$

The internal boundary conditions are fitted by referring to the diagram which applies at the level h and
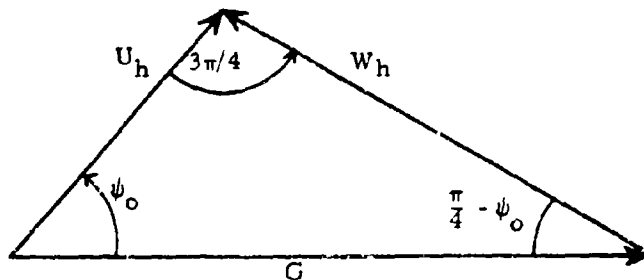
which follows from the fact that $\partial W/\partial z$ always makes an angle of $3\pi/4$ to W and that $\partial U/\partial z$ is parallel to U in the constant stress layer. From the law of sines the following two relations are obtained (satisfying the directional aspects of the continuity conditions):

$$\frac{U_h}{G} = \sqrt{2}\, \sin(\pi/4 - \psi_o) \tag{4.12}$$

$$\frac{|W_h|}{G} = \sqrt{2}\, \sin\psi_o \tag{4.13}$$

The requirement of continuity of wind shear at h is then satisfied by differentiating (4.6) and equating it to the wind shear at h in the surface boundary layer. The condition is written

$$W_h = F U_* \phi_u(h/L')/\sqrt{2}\, B_o G a \tag{4.14}$$

When G, F (and hence h) and z_o are regarded as assignable parameters, (4.10) through (4.14) are five equations in as many unknowns and can be reduced to

$$\frac{U_*}{G} = \sqrt{2K B_o \sin^2\psi_o \phi_u(h/L')}$$

$$\frac{U_*}{G} = K\sqrt{2}\, \sin(\pi/4 - \psi_o)/[\ln B_o R_o - \psi(h/L')]$$

which can be solved simultaneously for U_*/G and ψ_o from the external parameters G, f, z_o, and L'. The solution depends upon the dimensionless parameters R_o and a dimensionless stability parameter

$$L_* = B_o G/FL'$$

which represents the ratio of the mixed layer h to the stability length and is approximately the result obtained in the numerical model of Blackadar and Ching (1965).

The basic characteristics of the dependence of U_*/G and ψ_o are shown in Figures 17 and 18. It is seen that at all Rossby numbers, the model predicts U_*/G to increase with decreasing stability though the effect in terms at L_* is more pronounced at lower R_o. The cross isobar angle decreases with decreasing stability. In general, stable conditions have a more pronounced effect on the surface layer wind characteristics than unstable conditions.

The characteristics predicted by the model are in qualitative agreement with observations. For example, in a statistical study of frictional veering in the planetary boundary layer, Mendenhall (1967) concluded that veering is decreased slightly in steep lapse rate conditions over a mean neutral value of about 20° over land and 10° over the oceans, but that veering increases greatly in inversion conditions characteristic of nighttime conditions over land.

It is more difficult to establish through observation the behavior of the geostrophic drag coefficient with stability. Lettau (1959) has collected data on the ratio of U_*/G to its value in neutral conditions, say C_r, at O'Neill, Nebraska, 1953, and the data are plotted in Figure 19, where the points represent class means of direct measurements of surface stress and wind profile data. For comparison, the theoretical curve is drawn for typical conditions $G = 10$ m/sec, $F = 10^{-4}$ sec^{-1}, and $z_o = 1$ cm, corresponding to $R_o = 10^7$. Lettau used as a stability parameter the Richardson number at 1 meter. We may relate L_* to this quantity since at 1 meter the approximation

$$Ri = z/L'$$

is quite good. Hence, for the stated conditions,

$$L_* = 30 Ri$$
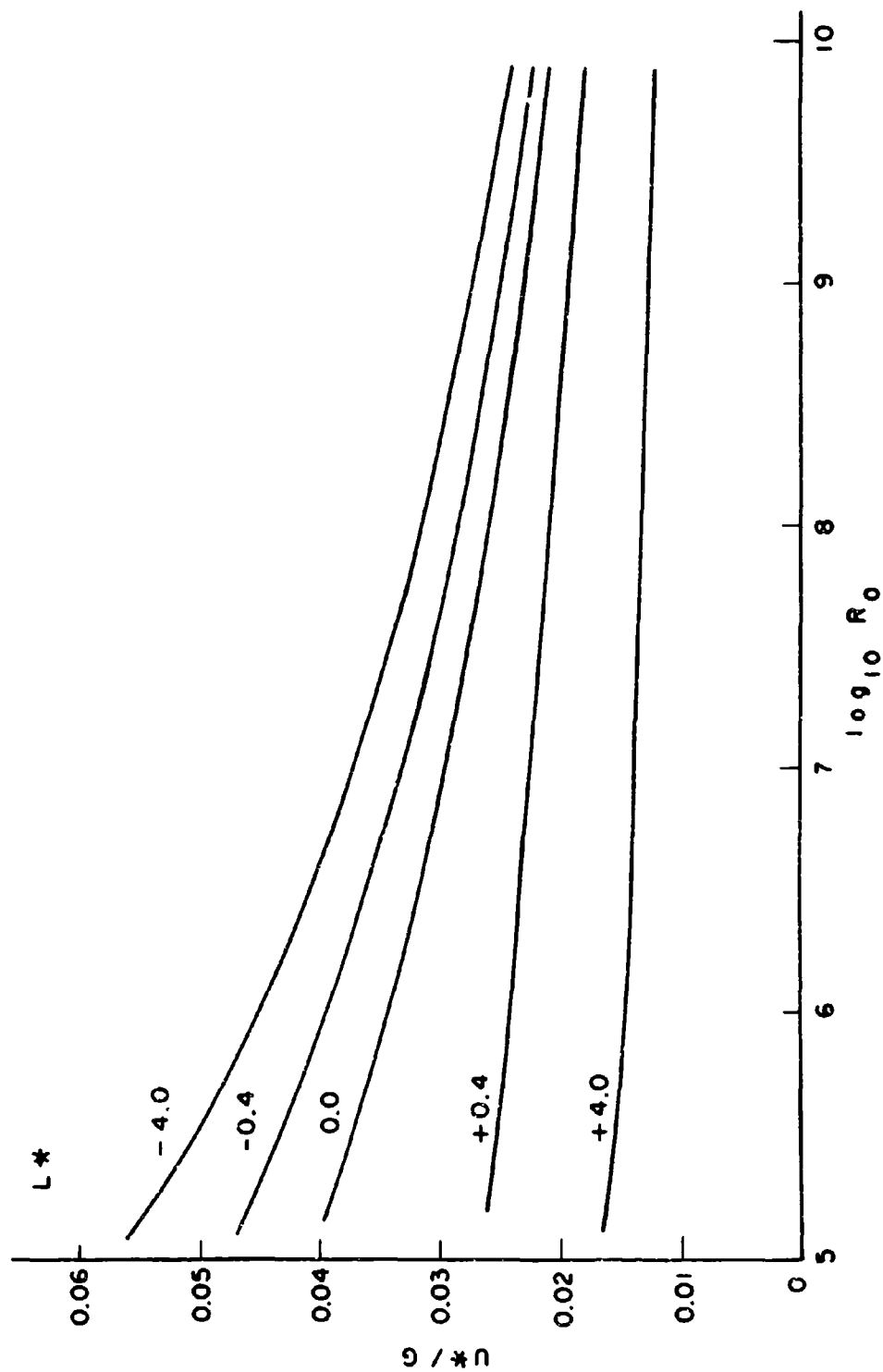
Variation of the geostrophic drag coefficient with surface Rossby number and dimensionless stability length, L_*

FIG. 17

83
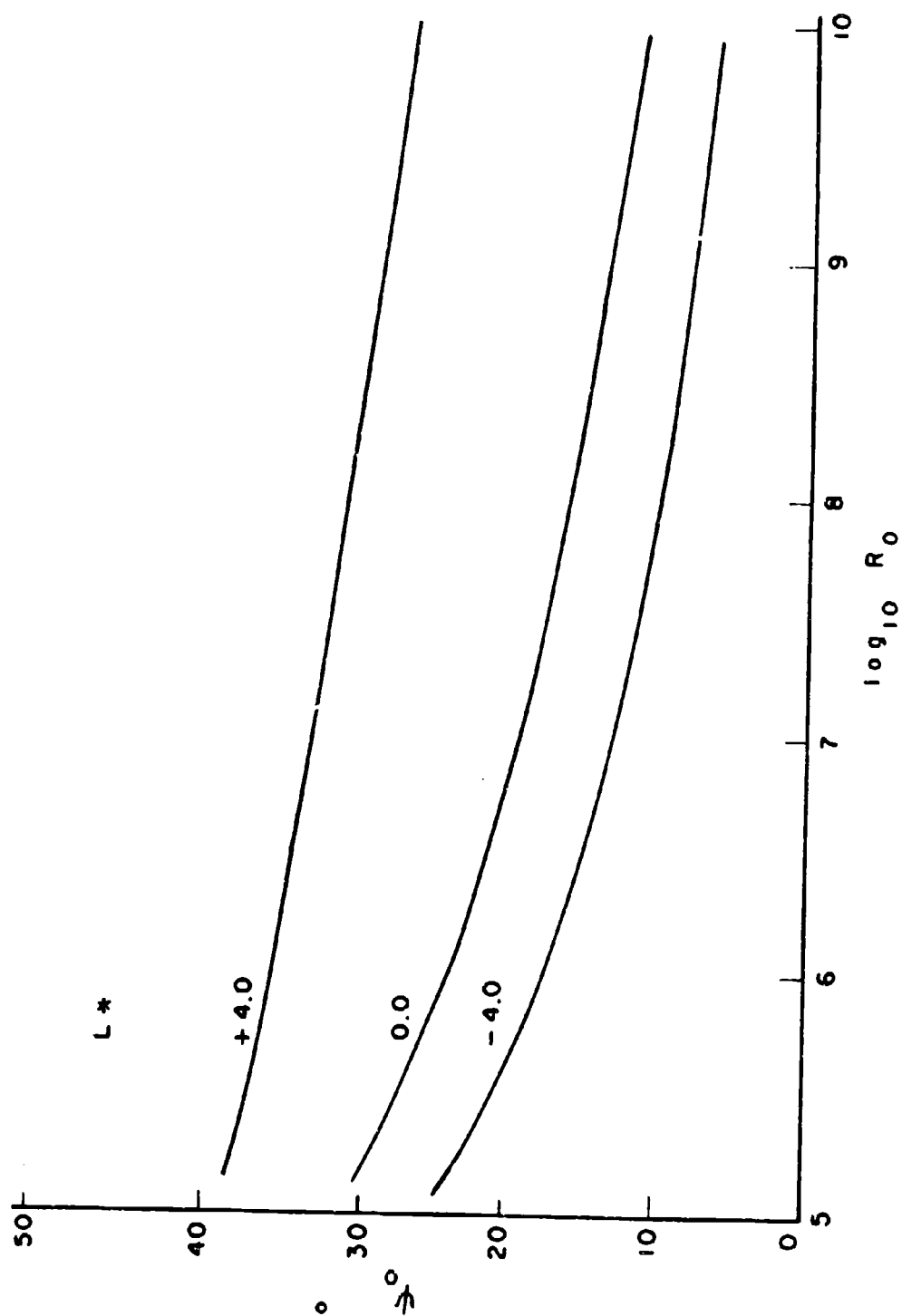
FIG. 18

The variation of surface cross isobar angle with surface Rossby number and stability.
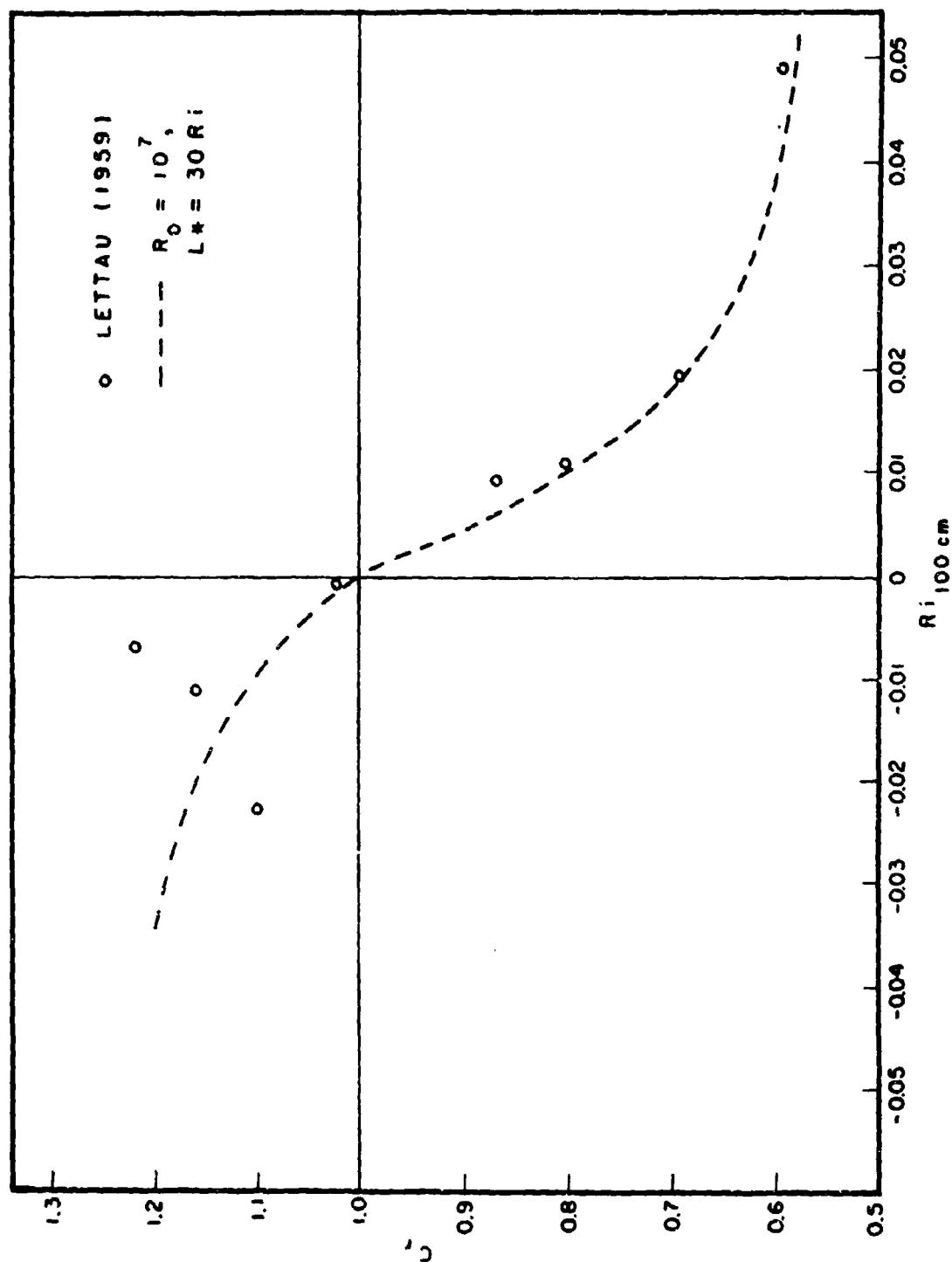
FIG. 19

Comparison of the two-layer model predictions of the variation of the normalized drag coefficient (C_r), with stability and Lettau's (1959) data.

The agreement for stable conditions is remarkable and quite good for unstable conditions unless one accepts Lettau's interpretation of the data that the drag coefficient at first increases for unstable conditions but decreases at further instability. Neither was this behavior predicted by the model of Blackadar and Ching (1965). Further evidence that the geostrophic drag coefficient does not respond to thermal instability in this manner may be inferred from the measurements of Clarke (Priestley, 1967). Clarke accumulated data at Hay, Australia, on the dependence of the ratio

$$U_*/V_{500}$$

where V_{500} is the 500 meter wind speed, on the stability factor

$$\frac{\Delta_{50}\theta}{V_{500}^2}$$

where $\Delta_{50}\theta$ is the potential temperature difference over the 50 millibar layer with base at 1 meter. The measurements were presented, as in Figure 20, normalized by a geostrophic drag coefficient as derived from Lettau's empirical expression. Since 500 meters is likely to be below the geostrophic level, even if appropriate, the normalization factor would yield drag coefficient ratios higher than expected for C_r. Baroclinicity would also affect the measurements, and in fact, a curve drawn through Clarke's data tends to cross neutral stability near 1.3. We may infer, then, that the geostrophic drag coefficient increases by roughly 30% in unstable conditions with no marked tendency to decrease at great instability, and decreased by roughly 70% in stable conditions, in good agreement with the predictions of the model except during the most stable conditions. These conditions are likely to be associated

87
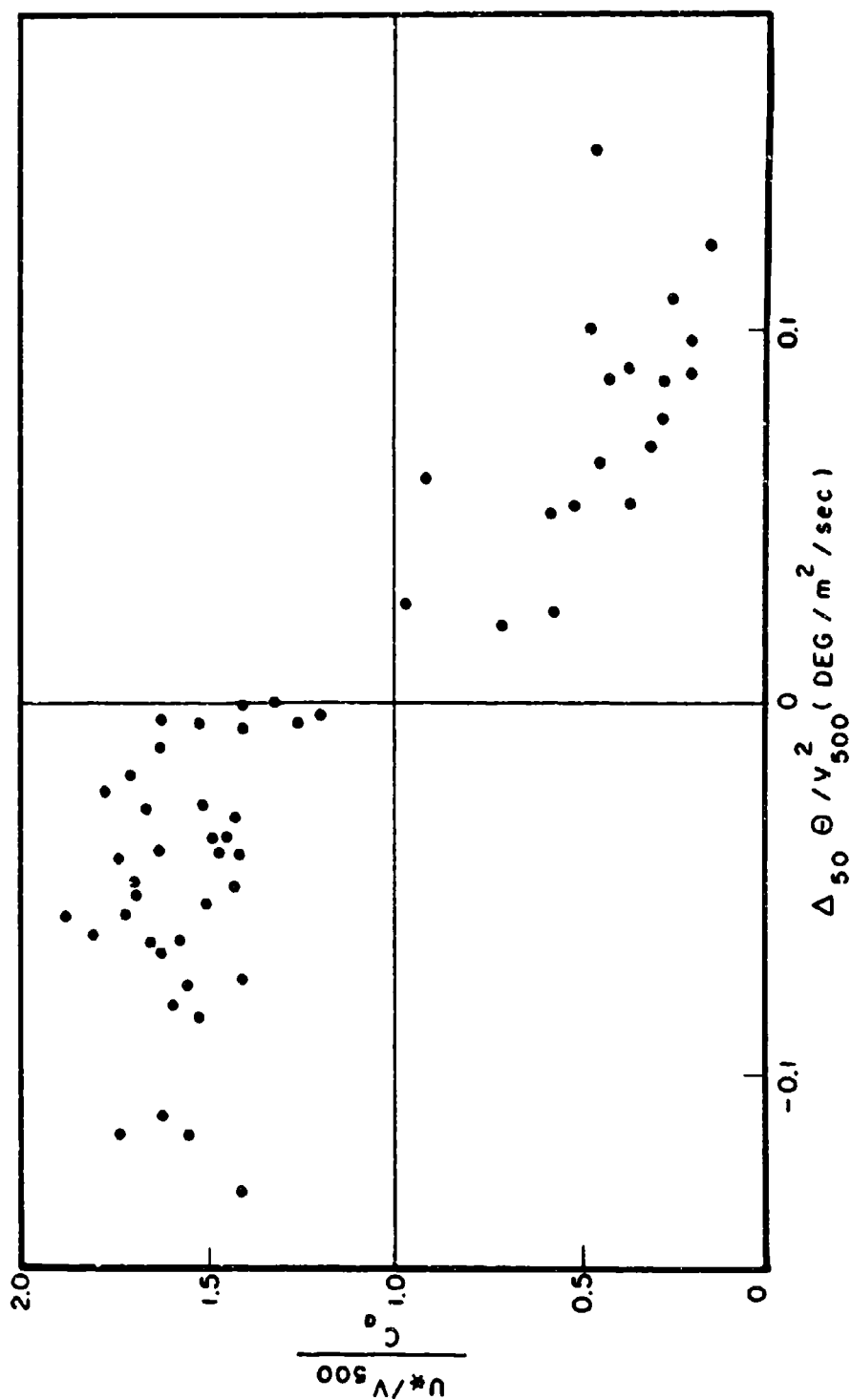
FIG. 20

Clarke's measurements of the 500 meter drag coefficient normalized by Lettau's empirical value for neutral conditions, versus bulk stability.

with inertial effects such as the low level jet, a common occurrence over land in clear skies and a phenomenon unpredictable by steady state models.

The diabatic model can be extended to the flow over the sea surface by regarding z_o as an unknown and adding the specification (3.21) to the system of equations. Blackadar has included the effects of baroclinicity by assuming that the geostrophic wind is a linear function of height. We may fit the internal boundary conditions to the non-neutral boundary layer model with an internally prescribed roughness in essentially the same way by introducing the following parameter, defined at h in the surface layer:

$$P = \frac{U_h}{(\partial U/\partial z)_h} = \frac{B_o G}{F\phi_u(h/L')} \cdot [\ln B_o R_o - \psi(h/L')] \qquad (4.15)$$

The requirement of continuity of wind shear can be written

$$U_h = P\left(\frac{\partial \vec{G}}{\partial z} + \frac{\partial W}{\partial z}\right)_h$$

the geometrical implications of which are shown in the diagram that applies at h :
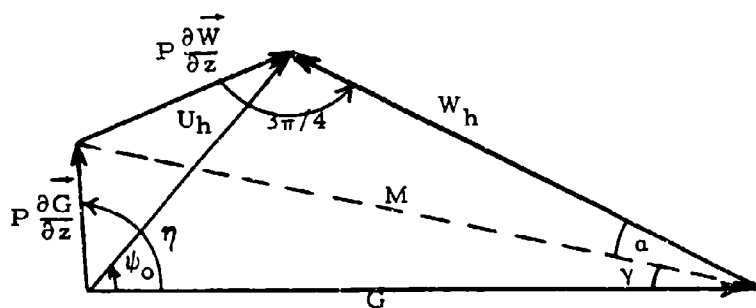
By the differentiation of (4.6) one can write at h

$$\left|\frac{\partial W}{\partial z}\right|_h = \sqrt{2}\, a\, |W_h|$$

so that one can write

$$P\left|\frac{\partial W}{\partial z}\right|_h = \sqrt{2}\, P'\, |W_h|$$

where P' is a dimensionless parameter.

$$P' = \frac{B_o G}{\phi_u(h/L')} \sqrt{\frac{\phi_u(h/L')}{2K_* B_o G}}\,[\ln B_o R_o - \psi(h/L')] \tag{4.16}$$

If the thermal wind vector is replaced by its dimensionless magnitude

$$r = \frac{1}{F}\left|\frac{\partial \vec{G}}{\partial z}\right|$$

and the parameter

$$r' = r\, B_o\, (\ln B_o R_o - \psi(h/L')) \tag{4.17}$$

is introduced, one can write

$$P\left|\frac{\partial \vec{G}}{\partial z}\right| = r'G$$

From the law of cosines applied to each of the two smaller triangles in the diagram that has M on one side, one can write

$$M^2 = |W_h|^2 s^2 = G^2 q^2 \tag{4.18}$$

where

$$s^2 = (1 + 2P' + 2P'^2) \tag{4.19}$$

and

$$q^2 = (1 + r'^2 - 2r' \cos \eta) \tag{4.20}$$

From the law of sines is obtained

$$\sin \alpha = P'/s \tag{4.21}$$

$$\sin \gamma = r' \sin \eta / q \tag{4.22}$$

From the larger triangle in the diagram is obtained the following relations:

$$U_h = \left| W_h \right| \sin(\alpha + \gamma)/\sin \psi_o \tag{4.23}$$

$$U_h^2 = G^2 + \left| W_h \right|^2 - 2G \left| W_h \right| \cos(\alpha + \gamma) \tag{4.24}$$

$$\left| W_h \right|^2 = U_h^2 + G^2 - 2U_h G \cos \psi_o \tag{4.25}$$

Since we are interested mainly in the surface boundary layer wind characteristics we can form the following two equations from (4.11), (4.21), (4.22), (4.23), (4.24), and (4.25):

$$\tan \psi_o = \frac{\sin(\alpha + \gamma)}{s/q - \cos(\alpha + \gamma)} \tag{4.26}$$

$$U_* = \frac{[KGq \sin(\alpha + \gamma)/s \sin \psi_o]}{[\ln B_o R_o - \psi(h/L')]} \tag{4.27}$$

If we add to these equations (3.21) and (3.39), there is obtained a system of equations that may be solved for U_* and ψ_o from the input parameters: G, F, $(\theta_a - \theta_s)$, $|\partial V_g / \partial z|$, and η, all of which can be easily calculated from a knowledge of sea level pressure, air temperature, sea surface temperature, and latitude.

After considerable experimentation, the iterative procedure adopted to solve this highly implicit set of equations was as follows:

1. Set $r' = \eta = 0$, $L' = \infty$ and adopt a trial value for

   $U_* = U_*(n)$, $n = 1$.

2. Compute z_o, L', P, A, P', r', s, q, a, γ, ψ_o' and

   $U_*(n + 1)$ using (3.21), (3.39), (4.15), (4.10), (4.16),

   (4.17), (4.19), (4 20), (4.21), (4.22), (4.26), and (4.27)

   respectively.

3. Set $U_*(n) = U_*(n + 1)$ and repeat the procedure until

   $$U_*(n) - U_*(n - 1) < \epsilon$$

   where ϵ is some preassigned convergence criterion.

4. Set r' and η to their actual values and using the last

   computed U_* repeat 2 and 3.

Basically, the above procedure solves a problem encountered
in the convergence of the baroclinic solution by suitably restricting U_*
and ψ_o through solution of the barotropic case. The procedure as pro-
grammed in Appendix II is free of computational instability and con-
verges rapidly for all reasonable choices of $U_*(1)$. From the finally
computed U_*, and the corresponding values of z_o and L', the entire
surface boundary layer profile is specified below the level h.

4.3 Some characteristics of the marine surface boundary layer

It is difficult to establish, through observation the success with
which the planetary boundary layer model presented in Section 4.2
specifies the surface boundary layer wind distribution over the sea sur-
face from the large-scale synoptic parameters. The problem, however,
has been of sufficient practical importance in that there is some obser-
vational evidence against which the model can be compared. In particular,

the ratio of the anemometer level wind speed to the geostrophic wind speed (geostrophic wind ratio) and the angle between the surface wind direction and the surface isobaric orientation (inflow angle) over the ocean have been topics of concern to meteorologists and oceanographers for several generations.

There have been numerous attempts via the statistical analysis of a large number of observations to determine the geostrophic wind ratio over the oceans since Shaw employed climatological means to specify the ratio for the British Isles, including the North Sea. For the latter location Shaw proposed that the ratio varies from 65% for light winds to 58% for strong winds (Lettau, 1959). Though the climatological means no doubt incorporated situations in which the planetary boundary layer wind was non-steady and affected by non-neutral stratification, those effects would tend to average out for the North Sea so that the ratios are probably representative of steady neutral conditions.

Several investigators have deliberately attempted to exclude the effects of a non-steady pressure pattern in the determination at the geostrophic wind ratio. Bleeker (Bijvoet, 1957) determined the geostrophic wind ratio for cases of quasi-stationary pressure patterns with straight isobars at the position of a North Sea light vessel. The relation found between the geostrophic wind speed and the air-sea temperature difference represents an average over all observed wind speeds and is shown in Figure 21a. Johnson (1954) studied the ratio of the anemometer level wind at certain North Atlantic weather ships to the gradient wind for cases of stationary wind conditions during 1952. He concluded that the gradient wind ratio varied with both wind speed

and air-sea temperature difference. Excerpts for two wind spee from Johnson's general relation are shown in Figure 21A. Also shown is a relation published in the U.S. Navy Hydrographic Office "Techniques for Forecasting Wind, Waves and Swell" (H.O. Pub. No. 604) which is again a relation averaged over all wind speeds.

All of the above relations indicate a linear variation with re- markably similar slopes. The scatter of the data from which the re- lations were derived was probably considerable and the linearity perhaps reflects this fact. The relations of Johnson straddle the averaged re- lations and agree at neutral conditions with the ratios of Shaw.

For comparison, the planetary boundary layer model was employed to generate relationships between the ratio of the 20 meter wind to geo- strophic wind and air-sea temperature difference for two wind speeds and fo- mid-latitudes. The relationships shown in Figure 21b are distinctly nonlinear, reflecting the fact that in the model, unstable con- ditions are less effective in altering the geostrophic wind ratio than are stable conditions. The model predicts the geostrophic wind radio to decrease with increasing wind speed at all stabilities and except for the nonlinearity, agrees with the observed relationships within the un- certainties introduced solely by the differences in the levels at which the surface wind was measured.

Investigators have only rarely recognized the significance of baroclinicity in the boundary layer and though the statistical relations may effectively reflect stationary wind conditions, they may include the effects of baroclinicity. To demonstrate the effects of baroclinicity upon the geostrophic wind ratio, the 30 knot relationship was recomputed for the case $r = 45$, $\eta = 45°$, which corresponds to a horizontal temperature
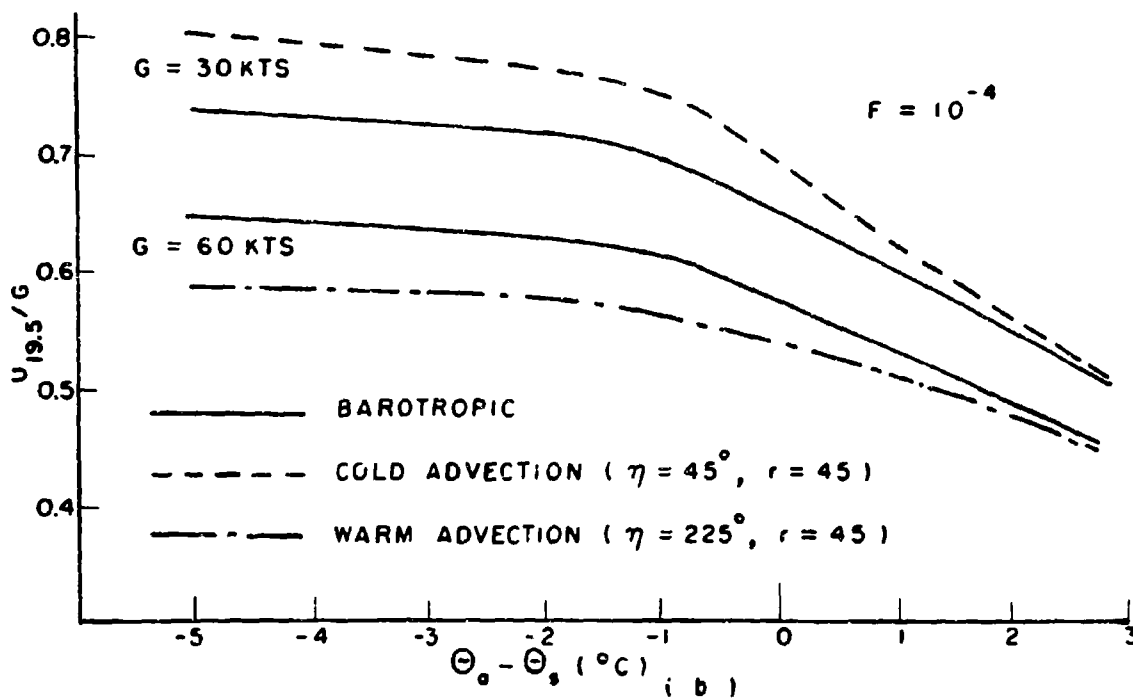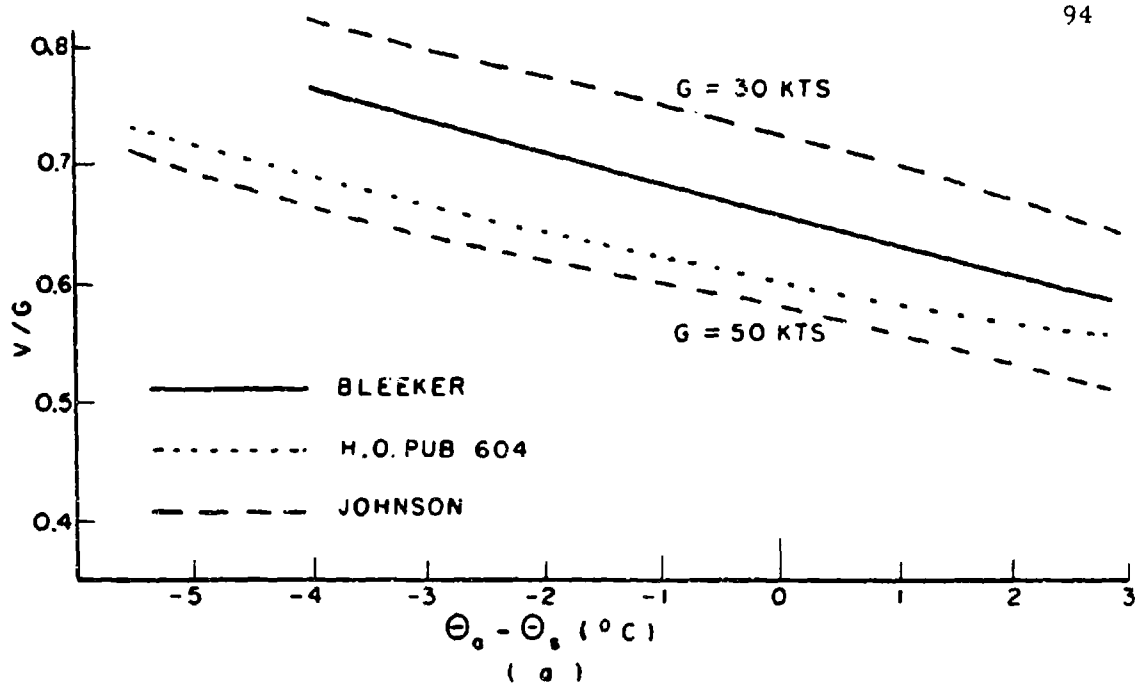
FIG. 21

(a) Published empirical relationships between the ratio of the anemometer level wind speed to the geostrophic wind speed and the air-sea temperature difference. (b) Two-layer model predictions of the dependence of the ratio of the 19.5 meter wind speed to the geostrophic wind speed upon air-sea temperature difference and thermal advection.

gradient of 1.3°C/100 kilometers oriented such that cold advection prevails, and the 60 knot case has been recomputed for the same thermal gradient but with the gradient oriented ($\eta = 225°$) such that warm advection prevails. It is seen in Figure 21b that the effects of baroclinicity increase as stability decreases and that cold advection increases the ratio while warm advection decreases it. The temperature gradient chosen is somewhat greater than average but less than that commonly found in frontal zones so that the effect is significant for neutral or unstable conditions. Also, since baroclinicity affects the solution through the dimensionless parameter

$$r \simeq \frac{g}{F^2 T} |\nabla_h T|$$

even small horizontal temperature gradients become significant at lower latitudes.

It is interesting to note that over the oceans baroclinicity and stability are highly correlated, such that unstable conditions are associated with cold advection and vice versa[*]. The effect of this association on the barotropic relationships in Figure 21a would be to raise the geostrophic wind ratio increasingly with decreasing stability ane effectively "straighten out" the relationship. We may speculate then that the statistical relationships have a built-in correction for the average correlation between stability and baroclinicity.

The influence of baroclinicity and stability on the directional characteristics of the wind in the planetary boundary layer has been

[*]Intuitively, one expects this but statistical evidence supporting this statement may be taken from Mendenhall's (1967) analysis of average lapse rates in the layer surface-950 mb at Ship N. The results showed that the smallest lapse rates occur with southerly winds and the largest with northerly winds.

studied by Mendenhall (196 7). He concluded that over the mid-latitude oceans, the diurnal variation of frictional veering of the wind with height was negligible, but that lapse rate and baroclinicity were important. Their combined effects at Ship N are shown in Figure 22a which shows the averaged observed veering of the layer 1000-900 mb as a function of the geostrophic veering in the lowest 1000 meters (computed on the basis of surface layer horizontal temperature gradient assumed constant throughout the lower 1000 meters) and the mean lapse rate in the layer surface-900 mb.

For comparison, Figure 22b shows the predictions of the model for the case $F = 10^{-4}$, $G = 40$ knots. The degree of geostrophic veering was specified by orienting the temperature gradient along the surface geostrophic wind direction and varying its sign and magnitude. Average observed veering was computed as the angular difference between the surface wind direction and the geostrophic wind direction at 1000 meters. The agreement with Mendenhall's data is qualitatively good and suggests that baroclinicity is more significant than stability in determining the directional nature of the planetary boundary layer wind distribution. Both Figures 22a and 22b indicate that in situations of strong cold advection, particularly when accompanied by unstable stratification, the actual wind may, in fact, back (negatively veer) with height. This supports also the results of Sheppard, Charnock and Francis (1952) who studied the variation of wind with height in the first few hundred meters over the Northeast Atlantic during ten winter days of westerly wind. They showed that on over 30% of the cases analyzed, the 300 meter wind was backed on the surface wind and these cases corresponded
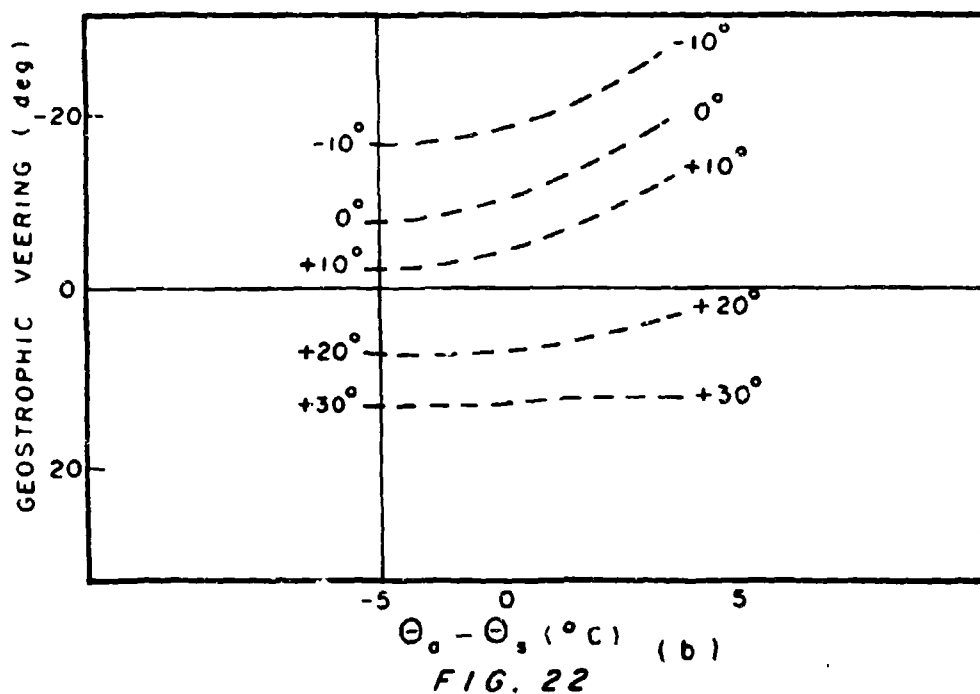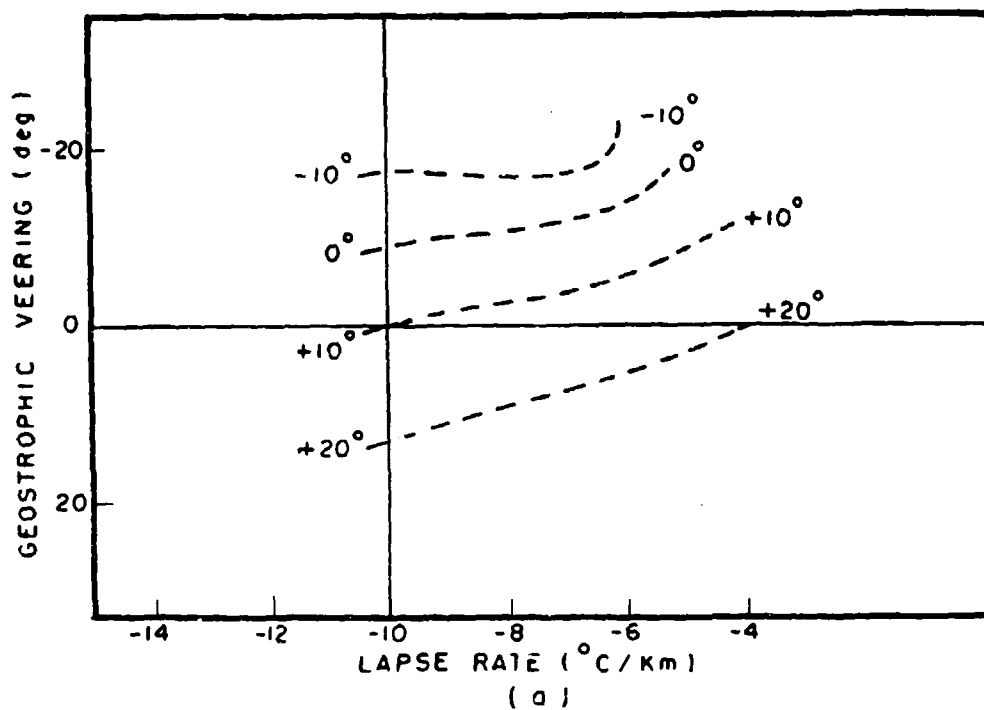
(a) Isolines of average observed veering (surface-900 mb) at ship N as a function of lapse rate and geostrophic veering, from Mendenhall (1967). Sample size 2386 observations. (b) Two-layer model predictions of average veering (surface-1000 m) as a function of air-sea temperature difference and geostrophic veering.

to situations when the thermal wind was backed appreciably upon the actual wind.

We may infer from these limited comparisons that the simple boundary layer model derived above provides a reasonable framework for the specification of the surface boundary layer parameters required for wave forecasting from the routinely available larger-scale synoptic parameters. It appears capable of isolating the influences of wind speed, latitude, stability, and baroclinicity on the surface boundary layer with more success than has been possible through purely statistical approaches.

5. A Wind Specification Program

5.1 Introduction

This section describes how the surface and planetary boundary layer models presented above may be applied, in an objective computerized format to the specification of the wind distribution over the North Pacific Ocean as required for the calculation of a wave spectrum climatology. Such a task requires the analysis of one year's ship data and the calculation of wave hindcasts with the Inoue (1967) spectral growth model and a wave propagation system such as that proposed by Baer (1967).

The analysis scheme presented here is a generalization of an earlier wind analysis program which was used to generate a wave spectrum climatology for the North Atlantic Ocean (Bunting, 1966). The new scheme provides the three numbers directly required in the wave growth calculation: 19.5 meter wind speed, surface layer wind direction, and friction velocity. The analyses are generated at six-hour intervals on a grid mesh corresponding to the JNWP grid (Cressman, 1959) but with the grid spacing halved and the grid boundaries extended to the equator. The procedure is directly extendable to global oceanic analysis. Further, an abbreviated form of the analysis program provides the necessary meteorological input for a true wave forecasting procedure.

Aside from being able to satisfy the meteorological requirements of present and possibly even more complex future wave prediction models, the new analysis technique eliminates some of the deficiencies of the earlier scheme. In particular, the technique features an improved specification of the wind field at low latitudes, a more accurate standardi-

zation of wind measurements to 19.5 meters, and a new treatment of
Beaufort estimates of the wind speed.

5.2 Objective analysis approach

The use of profile theory as formulated in Section 3 allows
one to apply standard objective analysis techniques to ship observations
of wind and air-sea temperature differences to obtain, effectively, an
objective analysis of the wind distribution in the marine surface boundary
layer.

Many types of objective analysis schemes have been proposed but
the one most widely used is the so-called successive approximation
technique (SAT) developed at the Joint Numerical Weather Prediction
Center and described by Cressman (1959). The technique was applied
to the analysis of wind over oceanic regions by Thomasell and Welsh
(1962), who later proposed and applied a technique known as the con-
ditional relaxation analysis method (CRAM). It has been shown that
SAT and CRAM can produce nearly equivalent results with the same
set of observations, but that CRAM is more efficient, particularly over
sparse data regions (Harris, Thomasell and Welsh, 1966).

The basic aim of objective analysis is to produce a consistent
and organized field of a physical parameter on a regularly spaced
grid system from a set of irregularly spaced data. In CRAM this is
accomplished by requiring that grid point (i, j) values of the analysis
parameter, say Q(i, j), satisfy Poisson's equation

$$\nabla^2 Q(i, j) = F(i, j) \tag{5.1}$$

where ∇^2 is the two-dimensional finite difference Laplacian operator,
subject to the constraints of the observations acting as internal boundary

points and a set of perimeter boundary points. The forcing function $F(i, j)$ defines the shape of the Q field and may be computed from some initial guess field of the parameter, $Q_g(i, j)$ as

$$F(i, j) = \nabla^2 Q_g(i, j)$$

The initial guess field determines the values of Q along the boundary of the grid system and may also be employed to translate observations to grid points prior to CRAM. If the grid spacing is small enough, this may be done accurately by interpolating the initial guess field to the position of the observation through curvilinear surface fitting to the four grid points surrounding the observation and translating the difference between the observed and interpolated values to the nearest grid point, thereby creating an internal boundary point.

After all observations have been translated to grid points, equation (5.1) is solved by a relaxation procedure. The small-scale noise in the resulting analysis due to fitting erroneous or unrepresentative data can be partially eliminated by applying a smoothing operator as (Shuman, 1957)

$$Q(i, j) = \frac{Q(i, j) + b\overline{Q}(i, j)}{1 + b} \tag{5.2}$$

where b is a parameter controlling the degree of smoothing, and

$$\overline{Q}(i, j) = \frac{1}{4}[Q(i + 1, j) + Q(i - 1, j) + Q(i, j+1) + Q(i, j- 1)]$$

In this study, CRAM is applied to the analysis of the wind distribution in the surface layer through the analysis of the meridional and zonal components and the 19.5 meter wind separately. These analyses combined with an analysis of the air-sea temperature difference

fully define the wind field in the surface layer.

The standardization of the initial guess wind field to 19.5 meters is easily accomplished by applying the planetary boundary layer model to objectively analyzed fields of sea level pressure and temperature. The standardization of ship reports of wind speed, however, requires that each report be treated in a way consistent with the way in which the observation was made.

5.3 Treatment of ship reports

Wind observations at sea consist of either measurements from some kind of anemometer or estimates derived from observations of the Beaufort force. Both types of observations are subject to a gross error inherent in the method, the Beaufort estimates most commonly because of the taking of observations by inexperienced personnel and the anemometer measurements because of instrumental errors and the errors arising from an incorrect transformation of relative wind to absolute wind. In either case there is little one can do with a "bad" observation other than attempt to prevent its use through a computerized error recognition scheme.

The accuracy of wind observations at sea varies greatly with anemometer determinations being potentially more accurate than the Beaufort estimates. Anemometer winds from fixed ocean station vessels are the most accurate data available with decreasing accuracy as one proceeds through observations from anemometer-equipped military vessels, lightships, merchant vessels, and finally, to merchant ships without anemometers. The use of ship data is further complicated by the fact that anemometer heights vary over a great range and that the height at which the observation is made is not included as part of the report.

Further, when dealing with historical data to generate analyses for wave hindcasting, two sources of ship reports are available: radio transmitted observations and ship report inventories compiled from ships' weather logs stored in national meteorological centers. Observations in the latter category have already been subjected to some forms of error check; while those in the former category are subject to errors of coding and transmission. Interestingly, while one might expect the former category to form a subset of observations from the latter, in practice the two data sets tend to complement each other with only about a 20% duplication in reports.

In order that ship reports can be standardized to 19.5 meters in a way consistent with the type of observations and that internal boundary points be determined by the most accurate and reliable ship report in its circle of influence, the part of the analysis program concerned with data handling first places ship reports in a priority listing into one of the following four categories:

1. Ocean station vessel on station

2. Wind measured-anemometer height known

3. Wind measured-anemometer height unknown

4. Wind estimated.

Within each category, ship reports are listed according to source, reports derived from ships' logs being given higher priority. After correlation of the observations to 19.5 meters, the program incorporated ships into the analysis in the order of listing. The procedure ensures that in case a grid point lies near two or more reports, only the most reliable report is chosen, and also that where the two data sets overlap, the report from the more reliable source is chosen.

Ships in categories 1 and 2 are easily corrected to 19.5 meters using the reported wind speed, air-sea temperature difference and anemometer height and applying the surface boundary model to the calculation of the stability and wind profile at the position of the ship. Since vessels on station at weather stations report the call sign of the station, the anemometer height for category 1 vessels is determined from a knowledge of the anemometer heights of all ships manning the stations and a knowledge of the sailing schedules.

In connection ith this study, an extensive effort was initiated by the U.S. Naval Oceanographic Office to obtain information on the anemometer heights of all ships so equipped and which report meteorological observations routinely. The listing in Appendix III shows the results of this effort to date. Anemometer heights vary from 7 to 37 meters, the average height being 21 meters. The great majority of the vessels are military vessels and one would not expect as much variation in anemometer height on these vessels due to variations in loading as on merchant vessels. The listing also includes the Canadian, U.S., and British vessels which man ocean station vessels so that observations from these vessels can be utilized while the ships are in transit.

Until a complete listing of anemometer heights for ships so equipped is compiled, there will remain ships in category 3. In the data for the Pacific hindcasts (March, 1966-March, 1967), ships could be identified in this category only from the ship reports compiled from ships' logs, as a provision is made there to indicate whether the reported wind is measured or estimated. The new form of the synoptic ode for ships (effective 1 January 1968) also includes this provision.

For the lack of any better information, winds from ships in this category are placed at 19.5 meters, a level close to the mean height of anemometer levels for ships in categories 1 and 2..

The majority of ship wind reports routinely available today still consists of the Beaufort winds. That is, the wind speed is determined from an observation of Beaufort number through a set of Beaufort number-wind speed equivalents supposed to yield the wind speed as would be measured at 10 meters above mean sea level. If such equivalents were indeed correct, it would be a simple matter to correct the observations to 19.5 meters on the basis of the profile formulas derived above. There is mounting evidence, however, that the current official equivalents are in error. The development of a new set of equivalents is a question under active consideration by the World Meteorological Organization.

The history of the Beaufort scale can be found in a paper by Kinsman (196?) and the evaluation of the current wind speed equivalents is discussed in a paper by Verploegh (1956). It suffices here to state that the source of the difficulty with the current equivalents, which were drafted by G. C. Simpson in 1906 from observations at some English coastal stations, is that the observations were made at locations unrepresentative of deep ocean conditions and that the series reflects largely the conception of the Beaufort scale of only two observers.

The inadequacy of the current series was clearly indicated in a wave hindcast program designed to generate a wave spectrum climatology for the Atlantic Ocean. In the preparation of the wind fields for that program, Beaufort estimate winds were first treated as though they were representative of the standard 10 meter height and were raised to 19.5 meters on the basis of a logarithmic profile and Sheppard's drag coefficient.

Resulting hindcasts, verified by measured wave heights, were consistently high. The forced assumption that Beaufort winds uncorrected were representative of 19.5 meters removed much of the bias in the resultant hindcasts (Pierson, Tick, and Baer, 1966).

Verploegh (1956) has proposed a new conversion scale based on a combination of all prior existing studies of the Beaufort force wind speed equivalents including the studies of Simpson and some 19th century studies. Frost (1966) has criticized the way in which the studies were combined and the series has not yet been accepted by W. M. O. The proposed series differs from the current one (see Table I) in that it yields higher winds for Beaufort numbers 1-5 and lower winds for Beaufort numbers 7-12. Verploegh also states that the new equivalents apply in the height range 10-15 meters above sea level. The anemometer levels in the nine sets of data from which the series were determined ranged from 7 to 32 meters and no attempt was made to reduce the data to one level.

Since the publication of Verploegh's paper, measurements of the wind speed equivalents of Beaufort numbers have continued to accumulate. The most extensive series of measurements was made on the British weather ships between 1960 and 1964 and the results were reported by Frost (1966). A large set of measurements has also been accumulated at the position of the Canadian weather ship in the North Pacific Ocean between April 1962 and May 1963. Since the anemometer level on the Canadian weather ships is 19.3 meters, and that on the British weather ships is 19.5 meters, these data can be used directly to determine a set of Beaufort number wind equivalents for 19.5 meters for use in the wave forecasting wind analysis model.

Table I. Wind speed equivalents of Beaufort force
estimates from British and Canadian
weather ship measurements.

Beaufort number	19.5 meter wind speed	No. of observations	Verploegh (1956)	Current
1	2.0	181	1.5	.8
2	4.1	444	3.4	2.4
3	6.2	830	5.6	4.3
4	8.4	959	7.8	6.7
5	10.6	816	10.2	9.4
6	12.9	748	12.6	12.3
7	15.3	755	15.1	15.5
8	18.0	518	17.7	18.9
9	21.5	175	20.4	22.6
10	25.1	51	23.3	26.4
11	27.4	13	26.5	30.9
12	29.0	9	28.2	>32.4

Table I shows the Beaufort number wind speed equivalents determined by combining the British and Canadian data. The 19.5 meter equivalents are in good agreement with Verploegh's proposed series, provided his series is representative of a level less than 19.5 meters, and both series differ from the current series in the same way. The 19.5 meter equivalents are also shown in Figure 23 where it is seen that they may be well approximated by the relation

$$U_{19.5} = 1.62 \ B^{7/6} \tag{5.3}$$

where B is the Beaufort number. Also shown in the figure are the current 10 meter equivalents. The curves intersect near Beaufort number 7 and indicate that between Beaufort numbers 5 and 8 (roughly 20 to 40 knots), currently reported wind speeds can be taken to be representative of 19.5 meters with little error, in essential agreement with the forced assumption noted above.

The current set of equivalents is well represented by the relation

$$U_r = .836 \ B^{3/2} \tag{5.4}$$

and this relation can be combined with (5.3) to yield a relation that converts currently reported winds, U_r, to the 19.5 meter equivalents. For wind speeds in knots the relation is

$$U_{19.5} = 2.16 \times U_r^{7/9} \tag{5.5}$$

Observers frequently interpolate between Beaufort numbers or take into account effects of fetch, duration, stability, and tidal effects by choosing wind speeds at the extremes of the ranges of the current equivalents. The use of (5.5) correctly expresses such considerations

CURRENT 10 m EQUIVALENTS

$U_{19.5} = 1.62 \ B^{7/6}$

BEAUFORT FORCE

FIG. 23
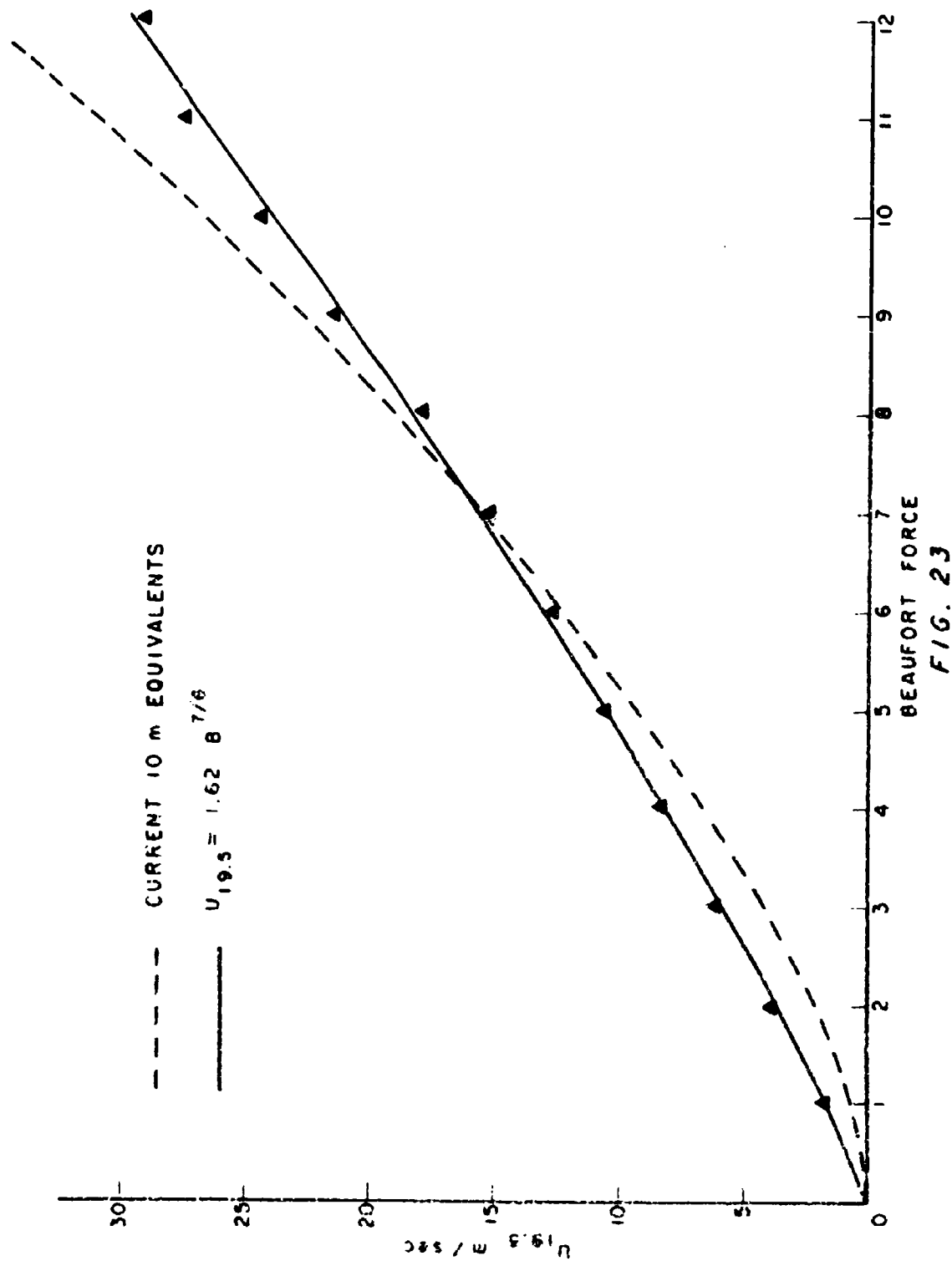
Beaufort number 19.5 meter height wind speed equivalents from observations on British and Canadian weather ships.

in terms of the 19.5 meter equivalents.

5.4 The analysis procedure

The general flow of the proposed analysis procedure is indicated in Figure 24. Objectively analyzed fields of sea level pressure, air temperature and sea surface temperature serve as the basic meteorological input along with the ships' observations of wind speed and direction. The analyzed fields are routinely available on the standard JNWP grid from both the U. S. Navy Fleet Weather Facility (sea level pressure, air temperature, sea temperature) and ESSA (sea level pressure and temperature).

The first step in the procedure is the computation of the initial evaluation of the boundary layer wind distribution from the analyzed fields. The sea level pressure field and air temperature analysis are used to compute the surface geostrophic wind speed and direction, the thermal wind speed and direction, and the angle between the thermal wind and geostrophic wind. These quantities along with the air-sea temperature differences are sufficient to compute the characteristics of the surface boundary layer through the application of the planetary boundary layer model developed above. Indeed, in a true wave forecasting procedure, the model yields directly the specific information required by the spectral growth formulation. In this instance, the input fields may be prognostic fields of sea level pressure and boundary layer temperature such as are currently being produced by primitive equation prediction models (Shuman and Hovermale, 1968), and a sea surface temperature analysis, a sufficiently conservative field for short-range forecasting.
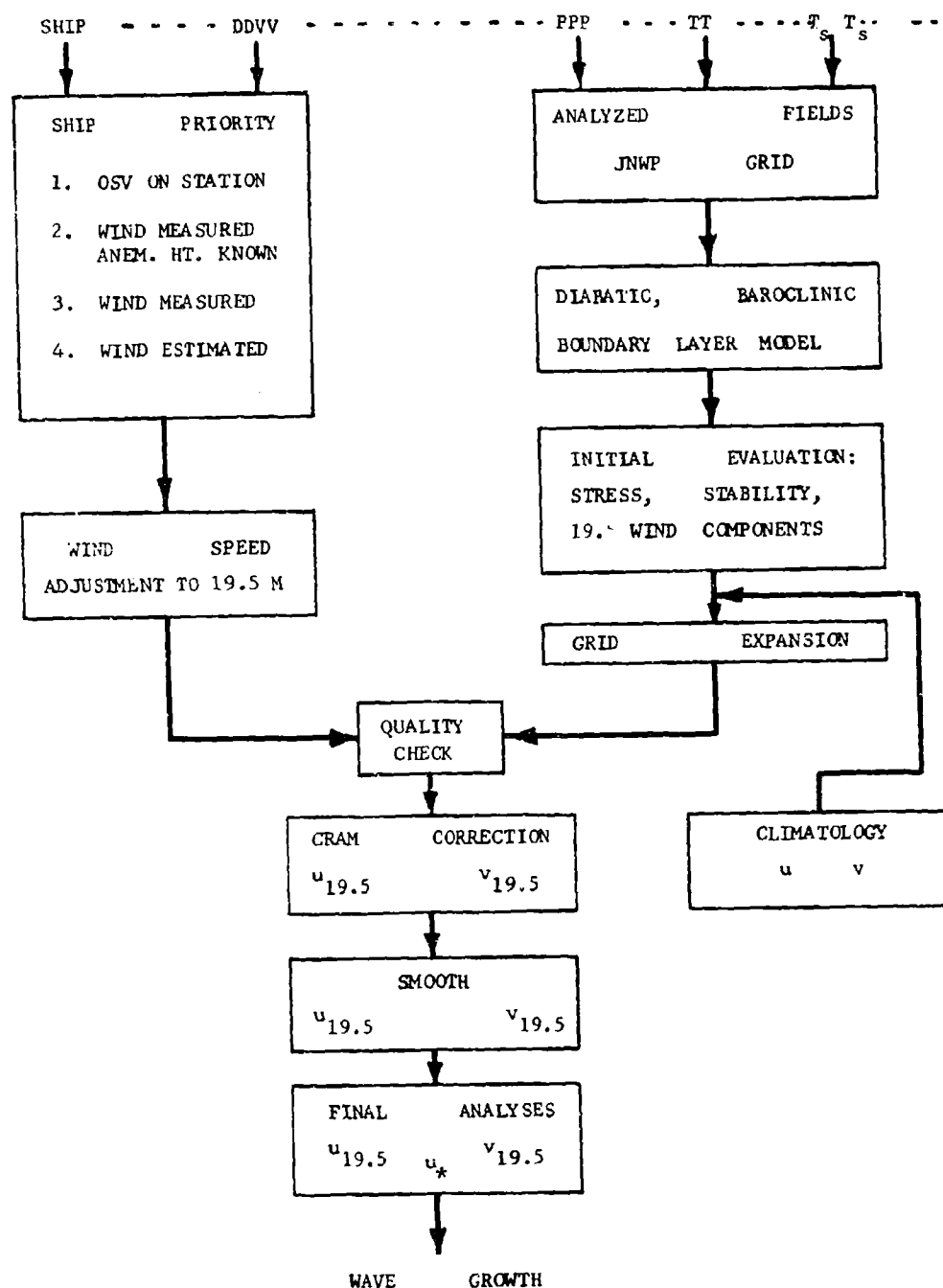
FIG. 24

Flow diagram of proposed analysis scheme.

In a hindcasting situation, the analysis can be carried further in terms of the wind components at any level in the surface layer, since the air-sea temperature difference is regarded as given. The 19.5 meter level is well within the surface layer for wind speeds of practical interest so that the meridional and zonal components of the 19.5 meter wind are the only output of the model retained.

It is generally desirable for wave forecasting purposes to provide a meteorological i' out extending through the trade wind zones to near the equator. However, analyzed and prognostic fields of sea level pressure and air temperature are generally limited by the octagonal boundary of the JNWP gird and even if available would not be useful for wind field calculations since the planetary boundary layer model is bound to fail as lower latitudes are approached. To provide the necessary input then, the first guess meridional and zonal 19.5 meter wind components are merged with a climatological wind field and extended to the equator. The climatology used for this purpose consists of the mean monthly surface zonal and meridional wind components as compiled on the JNWP grid extended to include the entire Northern Hemisphere.*

The merger of the climatological wind field with the computed initial guess fields is accomplished simply by overlapping the two outer rings of computed winds with climatological winds and averaging for each component. More elaborate merging procedures could be applied but since the fields have yet to pass through CRAM and smoothing, the

---

*Climatological source: Components of the 1000-mb winds (or surface winds) of the Northern Hemisphere (1966): NAVAIR 50-1C-51 .

fields will be automatically integrated further by these operations.

To allow a more accurate incorporation of observations into the initial guess field and also to allow for the possibility of a smaller scale analysis where the data permit, the initial guess field is expanded to a grid system in which the JNWP grid spacing has been halved, creating four times as many grid points (125 x 125). In the procedure, new grid point information is generated by fitting a curvilinear surface to the four grid points surrounding the generated grid point and interpolating the surface to the position of the grid point.

The incorporation of ship reports into the analysis is done on a priority basis. At this stage, a final error check may be made on observations by comparing the reported wind speed and direction to that interpolated to the position of the ship from the initial guess field. If the difference of either element exceeds a preset limit, the observation is discarded; otherwise, the difference is translated to the nearest grid point, thereby creating an internal boundary point. The application of CRAM and a smoothing then yields analyzed fields of $U_{19.5}$, $V_{19.5}$, from which, combined with the air-sea temperature difference, fields of the 19.5 meter wind speed, direction, and friction velocity are computed for transferral to the wave prediction grid and use in the wave growth subroutine.

6. Summary and Conclusions

The past decade has witnessed the development of numerical ocean wave specification procedures to the point where realistic wave generation theories are being used to model the way in which the wave spectrum develops in response to the low level wind field near the sea surface. Limited evaluation of the models has indicated that their practical utility is limited mainly by the inadequacy of the meteorological input supplied to these models by existing meteorological analysis techniques. In particular, what is required by an operational state of the art wave specification model is a description of the surface boundary layer wind distribution in the marine atmosphere on the synoptic time and space scales. For the purposes of wave hindcasting this description must be computed from conventional ships' observations while for wave forecasting the description must be computed from routinely available meteorological prognostic fields. The latter problem is solved in this study through the development of a planetary boundary layer model appropriate to the marine atmosphere. The results of this study may be stated as follows.

1. Though considerable progress has been made in the past decade in our understanding of the distribution of wind in the planetary boundary layer, none of the theoretical models proposed prior to this study could be applied to the non-neutral baroclinic boundary layer over the sea.

2. One of the more successful models was extended to include the effects of a non-neutral stratification and an internally prescribed description of the lower boundary. Baroclinicity was included in a

way such that its effect could be specified from conventional analyses
of surface air temperature, and the stability influence was formulated
so that its effects could be specified from the air-sea temperature
difference.

3. The characteristics of the surface boundary layer wind distribution
were found to depend significantly upon the geostrophic wind speed,
the air-sea temperature difference, the magnitude and orientation
of the horizontal temperature gradient and latitude. The ratio of the
typical anemometer level wind to the geostrophic wind can range from
40% to 90% over typical ranges of wind speed and air-sea temperature
difference. Baroclinicity and air-sea temperature were also found to
affect the directional characteristics of the boundary layer wind dis-
tribution.

4. Existing statistical studies of the speed and directional character-
istics of the anemometer level wind over the sea were found to be
special cases (in terms of latitude, height at which wind speed was
measured, range of wind speeds and stabilities involved and con-
siderations of the average correlation between stability and baro-
clinicity) of the model. When the model parameters were suitably
restricted, the theoretical relationships compared very well with the
statistically derived relations.

5. The boundary layer model approach makes possible the calculation
of the input parameters required by wave specification models from
routinely available prognostic fields.

6. Should spacecraft sources of surface wind information become
available, the model may be utilized in reverse to specify the distri-

bution of wind and pressure to the top of the planetary boundary layer from surface layer information alone.

The planetary boundary layer model is consistent, as the surface is approached, with a surface boundary layer model constructed around the similarity profile forms that have been shown to describe the distribution of wind and temperature in the lowest 10-100 meters of atmosphere over land and the sea. The following conclusions could be drawn from research on this aspect of the model.

1. A combination of inferences from recent theoretical work on wave generation and evidence from recent field experiments in wave generation and in turbulence studies over water leads naturally to the conclusion that at least for situations of active wave generation, the profile method can be applied to the calculation of the turbulent fluxes of momentum in the surface boundary layer over the sea.

2. Within this restriction, the main difference between the surface boundary layer over land and that over the ocean lies in the complexity of the roughness parameter specification for the latter. In this study, the roughness parameter is prescribed internally in terms of physical constants and the surface shearing stress. The proposed relation interpolates between aerodynamically smooth and rough flows and is consistent with a large body of observational evidence.

3. The surface boundary layer model effectively separates the effects of wind speed, stability and anemometer height on the ratio of the surface shearing stress to the anemometer level wind speed. The predictions of the model compare favorably with recently obtained direct measurements of the turbulent Reynolds stress over the open ocean over a wide

range of wind speeds and stabilities.

4. A technique has been developed w....reby the surface boundary layer
wind distribution may be specified from single layer measurements of
wind and air temperature and sea surface temperature measurements.
The procedure was successfully tested with the limited amount of ob-
servational data capable of evaluating such a technique.

The incorporation of stability effects in the meteorological
specification makes possible the inclusion of such effects in wave pre-
diction. As a part of this study, the wave spectral growth formulation
of the wave prediction model under development at N. Y. U. was general-
ized to include certain effects of stability in the following way.

1. The effect of stability upon the Miles-Phillips instability mechanism
was investigated and it was demonstrated that the existing relation be-
tween growth rate and surface shear stress was of sufficient generality
to describe the effects of stability on growth rate, provided a stability
dependence was incorporated into the calculation of the shear stress
from the wind field.

2. The Pierson-Moskowitz fully developed spectral form was effectively
generalized to non-neutral conditions by relating the fully developed
form to the low level wind profile, instead of to the wind high above the
surface. Within the context of the spectral growth formulation, this
effect allows stability to further affect the growth rate as well as the
maximum height to which a spectral component can grow for a given
anemometer level and speed, fetch and duration.

3. Through the application of the surface boundary layer model, the
stability modifications were tested by generating model predictions for

conditions corresponding to those encountered in observational studies
of the dependence of wave generation on air-sea temperature difference.
The calculations compared quite favorably with the observational evidence.

4.   The effects of stability on wave generation are significant with the
extremes of air-sea temperature frequency encountered over large areas
of the major oceans. For example, the range of air-sea temperature
difference, -8°C to +4°C, produces deviations in significant wave height
over neutral conditions that average ±20% over the wind speed range
20-40 knots. In terms of the spectrum, these changes correspond to
significant shifts in the spectral peak and larger changes in the spectral
density of wave components at frequencies near and below that of the
spectral peak.

Finally, as a part of this study, an analysis scheme is ou ined
which demonstrates how standard objective analysis techniques can be
combined with the surface and planetary boundary layer models summar-
ized above in an objective computerized format. Also discussed are
solutions to some very practical problems associated with the full
utilization of the different kinds of ships' weather observations routinely
available.

References

Adelfang, S.I. (1969): Measurements of atmospheric turbulence a few meters above the sea surface with a three component thrust anemometer. Scientific report, New York University, School of Engineering and Science, GSL-69-3.

Appleby, J.F., and W. Ohmstede (1966): Numerical solutions of the distribution of wind and turbulence in the planetary boundary layer. Met. Res. Note. No. 8, Meteor. Dept., U.S. Army Electronics Research and Development Activity, Fort Huachuca, Arizona.

Baer, L. (1962): An experiment in numerical forecasting of deep water ocean waves. Lockheed Missile and Space Co., Sunnyvale, Calif.

Baer, L. (1967): Pacific Ocean wave forecasting study. Lockheed Report No. 20856, Lockheed California Company.

Barnett, T.P. (1967): On the generation, dissipation and prediction of ocean wind waves. U.S. Naval Ocean. Office, Wash., D.C.

Barnett, T.P., and J.C. Wilkerson (1966): On the interpretation of fetch-limited wave spectra as measured by an airborne sea-swell recorder. U.S. Naval Ocean. Office, Wash., D.C.

Belinski, V.A. (1948): Dynamic Meteorology. State Publishing House of Technical-Theoretical Literature, Moscow.

Bijvoet, H.C. (1957): A new overlay for the determination of the surface wind over the sea from surface weather charts. Mededelingen en Verhandelingen. Koninklijk Nederlands Meteorologisch Instituut.

Blackadar, A.K. (1962): The vertical distribution of wind and turbulent exchange in a neutral atmosphere. J. Geophys. Res., 67, 3095-3102.

Blackadar (1965a): A simplified two-layer model of the baroclinic neutral atmospheric boundary layer. Final Report: Flux of Heat and Momentum in the Planetary Boundary Layer of the Atmosphere. Penn. State University.

Blackadar, A.K. (1965b): A single layered theory of the vertical distribution of wind and turbulence in a baroclinic neutral atmospheric boundary layer. Final Report: Flux of Heat and Momentum in the Planetary Boundary Layer of the Atmosphere. Penn. State University.

Blackadar, A.K., and J.K.S. Ching (1965): Wind distribution in a steady state planetary boundary layer of the atmosphere with upward turbulent heat flux. Final Report: Flux of Heat and Momentum in the Planetary Boundary Layer of the Atmosphere. Penn. State University.

Blanchard, D. C. (1963): The electrification of the atmosphere by particles from bubbles in the sea. Progr. Oceanog., 1, 71-202.

Brocks, K. M. (1959): Measurement of wind profiles over the sea and drag at the sea surface. International Oceanographic Congress, New York.

Brooke-Benjamin (1959): Shearing flow over a wavy boundary. J. Fluid Mech., 6, 161-205.

Bunting, D. C. (1966): Wave hindcast project North Atlantic Ocean. U.S. Naval Oceanographic Office, Washington, D. C.

Businger, J. A. (1966): Transfer of momentum and heat in the planetary boundary layer. Proc. Symp. Arctic Heat Budget and Atmospheric Circulation, Rm-5233-Nsf, Rand Corp, 305.

Charnock, H. (1955): Wind stress on a water surface. Quart. J. Roy. Meteorol. Soc., 81, 639.

Cressman, C. P. (1959): An operational objective analysis system. Mo. Wea. Rev., 87, 367.

Deacon, E. L. (1962): Aerodynamic roughness of the sea. J. Geophys. Res., 67, 3167.

Deacon, E. L., and E. K. Webb (1962): Small scale interactions. In The Sea, Vol. I, 43-87, Wiley, New York.

Deardorff, J. W. (1962): An operational ocean buoy for air-sea transfer studies. Occasional Report No. 13. Department of Meteorology and Climatology, University of Washington.

DeLeonibus, P. S. (1966): Momentum flux observations from an ocean tower. U.S. Naval Oceanographic Office (unpublished manuscript), Washington, D. C.

Ellison, T. H. (1956): Atmospheric turbulence. In Survey in Mechanics, ed. by G. K. Batchelor and R. M. Davies, Cambridge University Press, New York, 400-430.

Estoque, M. A. (1959): A preliminary report on a boundary layer numerical experiment. G. R. D. Res. Notes No. 20, 29 pp.

Fleagle, R. G. (1956): Note on the effect of air-sea temperature difference on wave generation. Trans. A. G. U., 37, 275-277.

Fleagle, R. G., J. W. Deardorff, and F. I. Badgley (1958): Vertical distribution of wind speed, temperature and humidity above a water surface. J. Marine Res., 17, 141-155.

Frost, R. (1966): The relation between Beaufort force wind speed and wave height. Sci. Paper No. 25, Meteorological Office, London.

Harris, R. G. , A. Thomasell, and J. Welsh (1966): Studies of techniques for the analysis and prediction of temperature in the ocean. Part III Automated analysis and prediction. Report 7421-213, Travelers Research Center, Inc.

Hasse, L. K. , K. Brocks, M. Dunckel, and U. Gorner (1966): Eddy flux measurements at sea. Beitr. Phys. Atmos., 39, 254-257.

Hires, R. I. (1968): An experimental study of wind-wave interactions. Tech. Report 37, Chesapeake Bay Institute, Johns Hopkins University.

Hoerber, H. (1968): Einige Ergebnisse von windprofil Messungen uber see bei stabiler Schictung. Tellus, 20, 1.

Inoue, T. (1967): On the growth of the spectrum of a wind generated sea according to a modified Miles-Phillips mechanism and its application to wave forecasting. Scientific report, New York University, School of Engineering and Science, GSL-67-5.

Johnson, P. (1954): The ratio of the sea-surface wind to the gradient wind. Proc. of the First Conference on Ships and Waves, ed. J. W. Johnson, Hoboken, New Jersey.

Kinsman, B. (1969): An exploration of the origin and persistence of the Beaufort wind force scale. Tech. Reprt. 39, Chesapeake Bay Institute, Johns Hopkins University.

Kitaigorodskii, S. A. (1961): Application of the theory of similarity to the analysis of wind generated wave motion as a stochastic process. Izv. Akad. Nauk. SSSR, Ser. Geofiz., 1, 105-117.

Kitaigorodskii, S. A. , and Y. A. Volkov (1965): On the roughness parameter of the sea surface and the calculation of momentum flux in the water layer of the atmosphere. Izv. Atm. and Ocean. Phys. Ser. 1, 973-988.

Kraus, E. B. (1966): The aerodynamic roughness of the sea surface. J. Atmos. Sci., 23, 443-445.

Lettau, H. H. (1950): A re-examination of the Leipzig wind profile considering some relations between wind and turbulence in the friction layer. Tellus, 2, 125-129,

Lettau, H. H. (1959): Wind profile, surface stress and geostrophic drag coefficients in the atmospheric surface layer. In Advances in Geophysics, 6, 241-257, Academic Press.

Lettau, H. H. (1962): Theoretical wind spirals in the boundary layer of a barotropic atmosphere. Beitr. zur Physik der Atmos., 35, 195-212.

Lumiey, J.L., and H.A. Panofsky (1964): The Structure of Atmospheric Turbulence. Interscience Publishers, New York.

McVehil, G.E. (1964): Wind and temperature profiles near the ground in stable stratification. Quart. J. Roy. Meteor. Soc., 90, 136-146.

Mendenhall, B.R. (1967): A statistical study of frictional wind veering in the planetary boundary layer. Atmospheric Science Paper No. 116, Department of Atmospheric Science, Colorado State University, Fort Collins, Colorado.

Miles, J.W. (1957): On the generation of surface waves by shear flows. J. Fluid Mech., 3, 185-204.

Miles, J.W. (1959): On the generation of surface waves by shear flows. Part II, J. Fluid Mech., 6, 568-582.

Miles, J. W. (1960): On the generation of surface waves by turbulent shear flows. J. Fluid Mech., 7, 469-478.

Miles, J.W. (1962): On the generation of surface waves by shear flows. Part III, J. Fluid Mech., 13, 433-448.

Miles, J.W. (1965): A note on the interaction between surface waves and wind profiles. J. Fluid Mech., 22, 823-827.

Monahan, E.C. (1966): Sea spray and its relationship to low elevation wind speed. Ph.D. Thesis, Massachusetts Institute of Technology, Cambridge, 175 pp.

Monahan, E.C. (1969): Fresh water whitecaps. To be published in J. Atmos. Science.

Moore, R.K., and W.J.Pierson (1967): Measuring sea state and estimating surface winds from a polar orbiting satellite. In Electromagnetic Sensing of the Earth from Satellites (R. Zirkland, ed.) R1-R28, Polytechnic Press, Brooklyn.

Moskowitz, L. (1964): Estimates of the power spectrums for fully developed seas for wind speeds of 20-40 knots. J. Geophys. Res., 69, 5161-5179.

Motzfeld, H. (1937): Die turbulente Stromung an welligen Wanden. Z. f. Angewandte Mathematik u. Mechanik, 17, 193-212.

Munk, W.H. (1955): Wind stress on water: an hypothesis. Quart. J. Roy. Meteor. Soc., 81, 320-332.

Neumann, G. (1953): On ocean wave spectra and a new method of forecasting wind generated seas. Tech. Memo. No. 43, Beach Erosion Board, Corps. of Engineers, Washington, D.C.

Neumann, G. (1956): Wind stress on water surface. Bull. A.M.S., 37, 211.

Nikuradse, J. (1933): Stromungsgesetze in rauhen Rohren. Forschungs-Arb. Ing.-Wesen, No. 361.

Pandolfo, J. (1966): Wind and temperature profiles for constant-flux boundary layers in lapse conditions with a variable eddy con-ductivity to eddy viscosity ratio. J. Atmos. Sci., 23, 495.

Panofsky, H.A. (1963): Determinations of stress from wind and tempera-ture measurements. Quart. J. Roy. Meteor. Soc., 88, 85.

Paulson, C.A. (1967): Profiles of wind speed, temperature and humidity over the sea. Sci. Rept. NSF GP-2418, Department of Atmospheric Sciences, University of Washington.

Phillips, O.M. (1957): On the generation of waves by turbulent wind. J. Fluid Mech., 2, 417-445.

Phillips, O.M. (1958): The equilibrium range in the spectrum of wind generated waves. J. Fluid Mech., 4, 426-434.

Phillips, O.M. (1966): The Dynamics of the Upper Ocean. Cambridge University Press, London.

Pierson, W.J. (1964): The interpretation of wave spectrums in terms of the wind profile instead of the wind measured at a constant height. J. Geophys. Res., 6, 5191-5203.

Pierson, W.J., G. Neumann, and R.W. James (1955): Practical methods for observing and forecasting ocean waves by means of wave spectra and statistics. H.O. Pub. 603, U.S. Navy Hydrographic Office, Washington, D.C.

Pierson, W.J., and W. Marks (1952): The power spectrum analysis of ocean wave records. Trans. A.G.U., 33, 834-844.

Pierson, W.J., and L. Moskowitz (1964): A proposed spectral form for fully developed wind seas based on the similarity theory of S.A. Kitaigorodskii. J. Geophys. Res., 69, 5181-5190.

Pierson, W.J., L.J. Tick, and L. Baer (1966): Computer based pro-cedures for preparing global wave forecasts and wind field analyses capable of using wave data obtained by a spacecraft. Preprint, Proc. Sixth Naval Hydrodynamics Symposium.

Plate, E.J., P.C. Chang, and G.M. Hidy (1969): Experiments on the generation of small water waves by wind. J. Fluid Mech., 35, 625-565.

Priestley, C.H.B. (1967): Handover in scale of the fluxes of momentum, heat, etc. in the atmosphere boundary layer. Phys. of Fluids, 10, S38-S46.

Priestly, J. T. (1965): Correlation studies of pressure fluctuations on the ground beneath a turbulent boundary layer. National Bureau of Standards, NBS Report 8942, 92 pp., U.S. Dept. of Commerce.

Roll, H. U. (1952): Über Grössenauterschiede der Meereswellen bei warm und kalt Luft. Deut. Hydrogr. Zeit., 5, 111-114.

Roll, H. U. (1965): Physics of the Marine Atmosphere, Intern. Geophys. Ser., Vol. 7, ed. by J. Von Mieghem, Academic Press, New York.

Rossby, C. G., and R. B. Montgomery (1935): The layer of frictional influence in wind and ocean currents. Papers in Phy. Ocean. and Meteor., M. I. T. and Woods Hole Oceanog. Inst., 3, pp. 101.

Saunders, P. M. (1967): The temperature at the ocean air interface. J. Atmos. Sci., 24, 269.

Schlichting, H. (1951): Boundary Layer Theory. Pergamon Press, London.

Seesholtz, J. R. (1968): A field investigation of the air-flow immediately above ocean surface waves. M. I. T., Dept. of Meteor.

Shemdin, O. H. (1967): Experimental and analytical investigation of the air velocity profile above progressive waves. Tech. Rept. No. 82, Dept. of Civil Engineering, Stanford University, 57 pp.

Shemdin, O. H., and E. Y. Hsu (1966): The dynamics of wind in the vicinity of progressive water waves. Tech. Rept. No. 66, Dept. of Civil Engineering, Stanford University, 209 pp.

Sheppard, P. A. (1958): Transfer across the Earth's surface through the air above. Quart. J. Roy. Meteor. Soc., 84, 204-224.

Sheppard, P. A., H. Charnock, and J. R. D. Francis (1952): Observations of the westerlies over the sea. Quart. J. Roy. Meteor. Soc., 78, 563.

Shuman, F. G. (1957): Numerical methods in weather prediction: II Smoothing and filtering. Mo. Wea. Rev., 85, 357-361.

Shuman, F. G., and J. B. Hovermale (1968): An operational six-layer primitive equation model. J. Appl. Meteor., 7, 525-547.

Smith, S. P. (1966): Thrust anemometer measurements of wind velocity fluctuations, spectra and stress over the sea. Report BIO 66-8 Bedford Institute of Oceanography, Dartmouth, N.S., Canada.

Snyder, R. (1965): The wind generation of ocean waves. Ph. D. dissertation, Univ. of Calif., San Diego, 393 pp.

Snyder, R., and C.S. Cox (1966): A field study of the wind generation of ocean waves. J. Mar. Res., 24, 141-177.

Stewart, R.W. (1966): The wave drag of wind over water. J. Fluid Mech., 10, 189-194.

Sutton, O.G. (1953): Micrometeorology, McGraw-Hill, New York.

Sverdrup, H.U., and W.H. Munk (1947): Wind, sea and swell: theory of relations for forecasting. U.S. Hydrographic Office H.O. Pub. 601, 44 pp.

Takeda, A. (1963): Wind profiles over sea waves. J. Ocean. Soc. Japan, 19, 16-22.

Thomasell, A., and J.G. Welsh (1962): Objective analysis of surface pressure temperature, dewpoint and wind. Travelers Research Center, Inc.

Thomasell, A., and J.G. Welsh (1963): Studies of the specification of surface winds over the ocean. Travelers Research Center, Inc.

Van Dorn, W.G. (1953): Wind stress on an artificial pont. J. Mar. Res., 12, 249-276.

Verploegh, G. (1956): The equivalents velocities for the Beaufort estimates of the wind force at sea. Mededelingen Verhandelingen 66, Koninklijk Nederlands Meteorologisch Instituut.

Weiler, H.S., and R.W. Burling (1967): Direct measurements of stress and spectra of atmospheric turbulence in the boundary layer over the sea. J. Atmos. Sci., 24, 653-664.

Wilson, B. (1960): Note on surface wind stress over water at low and high wind speeds. J. Geophys. Res., 65, 3377-3381.

Wu, J. (1969): Froude number scaling of wind-stress coefficients. J. Atmos. Sci., 26, 408-413.

Zubkovski and Kravchenko (1967): Direct measurements of some characteristics of atmospheric turbulence in the near water layer. Izv. Atmospheric and Ocean. Physics, 3, 127-135.

APPENDIX I: Fortran V subprogram for the computation of
friction velocity, roughness parameter and
stability length from wind speed and air-sea
temperature difference data.

```
      SUBROUTINE PROPAR (UM, ZM, TD, ZTM, VST, ZO, SLN)
C     INPUTS: UM=WIND SPEED(FT/SEC), ZM=ANEMOMETER
C             HEIGHT (FT), TD=AIR-SEA TEMP DIFFERENCE
C             (CELSIUS), ZTM=THERMOMETER HEIGHT (FT)
C     OUTPUT: VST=FRICTION VELOCITY (FT/SEC), ZO=
C             ROUGHNESS PARAMETER (FT), SLN=STABILITY
C             LENGTH (FT)

      DATA A/7.3627E-04/B/1.3045E-03/C/-1.4534E-03/CF/54.3478/
      VST=.04*UM
      IF(ABS(TD).GT.1.0) GO TO 2000
1000  VSTN=(.4*UM)/(LOG(ZM/(A/VST+B*VST**2+C)))
      IF(ABS(VSTN-VST).LT.05) GO TO 1400
1200  VST=VSTN
      GO TO 1000
C       FOR NEUTRAL CONDITIONS SLN RETURNS  0 .
1400  SLN=0.
      GO TO 12
2000  SLG=VST**2*CF*(LOG(ZTM/(A/VST+B*VST**2+C)))/TD
  1   VSTN=(.4*UM)/(LOG(ZM/(A/VST+B*VST**2+C))-PSI(ZM/SLG))
      IF(ABS(VSTN-VST).LT..05) GO TO 4
  2   VST=VSTN
      GO TO 1
  4   SL=SLG
  5   SLN=CF*VSTN**2*(LOG(ZTM/(A/VSTN+B*VSTN**2+C))-PSI(ZTM/SL))/TD
      IF(ABS(SLN-SL).LT.1.) GO TO 8
  6   SL=SLN
      GO TO 5
  8   IF(ABS(SLN-SLG).LT.1.) GO TO 12
      SLG=SLN
      GO TO 1
  12  ZO=A/VST+B*VST**2+C
      END


      FUNCTION PSI(P)
      IF (P. GT.O.) GO TO 40
  5   S=SHR(P)
      PSI=1.-S-3.*LOG(S)+2.*LOG((1.+S)/2)+2.*ATAN(S)-1.5708+
     1LOG((1.+S**2)/2.)
          RETURN
  40  PSI= -7. * P

      END
```

APPENDIX I continued:

```
      FUNCTION SHR(PS)
      IF(PS.GT.O.) GO TO 40
   5  RI=PS
  10  RINEW=PS*(1.0-18.*RI)**(1./4.)
      IF(ABS(RINEW-RI).LT..001) GO TO 30
  20  RI=RINEW
      GO TO 10
  30  SHR=1./(1.-18.*RINEW)**(1./4.)
      RETURN
  40  SHR=1.+7.*PS
      END
```

APPENDIX II: Fortran V subprogram for the computation of friction velocity, inflow angle, roughness parameter and stability length from the large scale synoptic parameters.

```
      SUBROUTINE ITRATE(G, F, TD, TH, ETAH, VST, PHI, ZO, PARAM)
C     INPUTS:G=GEOSTROPHIC WIND SPEED(FT/SEC), F=CORIOLIS
C            PARAMETER(1/SEC), TD=AIR-SEA TEMPERATURE
C            DIFFERENCE(CELSIUS), TH=DIMENSIONLESS THERMAL
C            WIND MAGNITUDE, ETAH=ANGLE BETWEEN GEOSTROPHIC
C            WIND AND THERMAL WIND.
C     OUTPUT:VST=FRICTION VELOCITY(FT/SEC), PHI=INFLOW ANGLE
C            (RADIANS), ZO=ROUGHNESS PARAMETER(FT), PARAM=
C            STABILITY LENGTH(FT).
C NOTE: FUNCTIONS SHR AND PSI ARE USED AS IN APPENDIX I
      DATA C1/7.3627E-04/C2/1.3045E-03/C3/-1.4534E-03/B/3.E-04/TA/280./

      VST=.0245*G
      T=0.
      ETA=0.
      INDEX=1
      IF(ABS(TD).GT.1.) GO TO 4
    3 ZONL=0.
      PARAM=0.
      FI=0.
      S=1.
      GO TO 1110
    4 PARAM=TA*VST**2/(.16*32.2*.1*TD)
    6 ZONL=((B*G)/F)/PARAM
      FI=PSI(ZONL)
      S=SHR(ZONL)
 1110 CONTINUE
      CPA=(B*G/F*S)*(LOG(B*G/(F*(C1/VST+C2*VST**2+C3)))-FI)
      BET=SQRT(S*F**2/(2*VST*.4*B*G))
      P=SQRT(1.+2.*CPA**2*BET**2+2.*CPA*BET)
      R=SQRT(1.+(F**2*T**2*CPA**2)/G**2-(2.*F*T*CPA*COS(ETA))/G)
      ALPH=ASIN(CPA*BET/P)
      ARGUM=(F*T*CPA*SIN(ETA)/(R*G))
      GAMMA=ASIN(ARGUM)
 1114 PHI=ATAN(SIN(ALPH+GAMMA)/(P/R-COS(ALPH+GAMMA)))
      VSTN=((.4*G*R*SIN(ALPH+GAMMA))/(P*SIN(PHI)))/(LOG(B*G/F*(C1/VST
     1+C2*VST**2+C3)))-FI
      TEST=ABS(VSTN-VST)
      IF(TEST-.05)1130,1130,1120
 1120 VST=VSTN
      GO TO 1110
 1130 IF(ZONL-0.)1140,1150,1140
 1140 FE=PSI(33./PARAM)
      PARMNU=(VST**2*TA*(LOG(33./(C1/VST+C2*VST**2+C3))-FE))/5.15*TD
      IF(ABS(PARMNU-PARAM).LT.5) GO TO 1150
 1142 PARAM=PARMNU
      GO TO 6
```

Appendix II continued

```
1150   IF(INDEX-2)1152, 1155, 1152
1152   T=TH
       ETA=ETAH
       INDEX=2
1155   ZO=C1/VST+C2*VST**2+C3
       END
```

Appendix II continued

```
1150   IF(INDEX-2)1152, 1155, 1152
1152   T=TH
       ETA=ETAH
       INDEX=2
1155   ZO=C1/VST+C2*VST**2+C3
       END
```

APPENDIX III: Anemometer height listing.

Call Sign	Height (ft)	Call Sign	Height (ft)
(U.S. Coast Guard)		NRUS	80
NRUO	78	NRUA	66
NBYG	78	NBTM	80
NRPA	42	NRDS	93
NODG	52	NBWJ	76
NODH	52	NRDC	79
NODI	52	NICB	84
NRPX	52	NLUR	99
NRPK	52	(MSTS* VESSELS)	
NODC	78	NCML	76
NRPN	54	NQWO	55
NRCQ	80	NZAE	62
NMJH	49	NBEI	83
NMGP	49	NCHI	89
NMJA	49	NODQ	60
NEWP	49	NYCE	110
NKVY	49	NLZF	103
NMDN	49	NJSK	79
NRVA	60	NLOO	79
NODO	60	NTPA	79
NPPY	52	NNUD	84
NRZI	52	NUGS	70
NRUC	70	NYSS	90
NRXO	60	NTFH	60
NNHB	79	NRKO	90
WRUD	80	NPFG	60
NODB	78	NUUG	54
NRUP	56	NRXE	60
NRFJ	72	NHXN	79
NRUU	56	NXDM	79
NRDT	89	NHYK	79
NRUJ	80	NKBF	100
NRUB	80	(Scripps Institute)	
NRUN	80	KEYI	64
NBNP	80	KLFK	48
NBXL	79	KKDZ	72
NRDB	95	KSLF	55
NBZF	82	KGWU	59
NBOZ	80	(Pacific Far East Lines)	
NYLW	80	KFCJ	69
NRDD	70	KIBA	69
NBQR	80	NCVN	97
NEJL	75	NSCR	55
NRDL	89	(Chevron Shipping)	
NICC	80	6ZRC	95
NODA	75	6ZJE	95

*Military Sea Transportation Service

APPENDIX III continued

Call Sign	Height (ft)
(States Line Shipping)	
WJBA	103
WJHA	103
KKFW	103
WPHI	103
KGTP	103
WEBW	103
(U.S. Bureau of Comm. Fish.)	
WTDK	60
WTDF	48
WTDL	84
(British Weather Ships)	
MDBE	64
MYDN	64
MEDD	64
MEDE	64
(British Antarctic Survey)	
ZDLB	30
ZDLA	30
(Others)	
GRLU	74
MHKV	58
GSZY	46
GLNE	80
MLBG	29
BKBO	63
6ZHL	120
WTES	92
DZYB	50
WFNA	52

DOCUMENT CONTROL DATA - R&D		
(Security classification of title, body of abstract and indexing annotation must be entered when the overall report is classified)		

1. ORIGINATING ACTIVITY (Corporate author)	2a. REPORT SECURITY CLASSIFICATION
New York University School of Engineering and Science, Research Div.	Unclassified
	2b. GROUP

3. REPORT TITLE

Specification of the Wind Distribution in the Marine Boundary Layer for
Wave Forecasting

4. DESCRIPTIVE NOTES (Type of report and inclusive dates)

5. AUTHOR(S) (Last name, first name, initial)

Cardone, Vincent J.

6. REPORT DATE	7a. TOTAL NO. OF PAGES	7b. NO. OF REFS
December 1969	x + 131 + 6	99

8a. CONTRACT OR GRANT NO. Nonr 285(57)	9a. ORIGINATOR'S REPORT NUMBER(S)
+ N62306-1589, Task Order no. 3 + N62306-68-C-0249	
b. PROJECT NO. 1103	GSL-69-1
+ 1301 and 1534 c.	9b. OTHER REPORT NO(S) (Any other numbers that may be assigned this report)
d.	

10. AVAILABILITY/LIMITATION NOTICES

Qualified requesters may obtain copies of this report from DDC

11. SUPPLEMENTARY NOTES	12. SPONSORING MILITARY ACTIVITY

13. ABSTRACT ⸺The operational application of sophisticated spectral ocean wave specification models to wave forecasting requires that an adequate meteorological input to these models consist of a specification of the wind distribution in the marine surface boundary layer. This study demonstrates how this requirement can be satisfied in a computerized objective format from routinely available meteorological data and prognostic fields.

Wave generation theory is employed to develop a quantitative formulation for the effects of atmospheric stability upon the development of the wave spectrum. In terms of this stability dependent spectral growth formulation, the effects of stability on wave generation are found to be significant and compare well with observational studies of the dependence of wave height and whitecap production on air-sea temperature difference.

A simple model of the non-neutral, baroclinic planetary boundary layer over a sea surface described in terms of an internally prescribed roughness parameter is derived. The model is shown to provide a suitable framework for the diagnosis of the marine surface boundary layer wind distribution from prognostic fields of sea level pressure, air temperature and sea surface temperature. The model is consistent, as the surface is approached, with a surface boundary layer model constructed around the similarity profile forms that are shown to be applicable, at least under active wave generating conditions, to the flow near the sea surface. Finally, it is shown how these models can be objectively applied to ships'weather observations and routine prognostic fields to satisfy the requirements of wave hindcasting and forecasting.

DD FORM 1473
1 JAN 64

14. KEY WORDS	LINK A		LINK B		LINK C	
	ROLE	WT	ROLE	WT	ROLE	WT
Air-sea interaction						
Wave forecasting						
Wave hindcasting						
Planetary boundary layer						
Marine boundary layer						

INSTRUCTIONS

1. ORIGINATING ACTIVITY: Enter the name and address of the contractor, subcontractor, grantee, Department of Defense activity or other organization (corporate author) issuing the report.

2a. REPORT SECURITY CLASSIFICATION: Enter the overall security classification of the report. Indicate whether "Restricted Data" is included. Marking is to be in accordance with appropriate security regulations.

2b. GROUP: Automatic downgrading is specified in DoD Directive 5200.10 and Armed Forces Industrial Manual. Enter the group number. Also, when applicable, show that optional markings have been used for Group 3 and Group 4 as authorized.

3. REPORT TITLE: Enter the complete report title in all capital letters. Titles in all cases should be unclassified. If a meaningful title cannot be selected without classification, show title classification in all capitals in parenthesis immediately following the title.

4. DESCRIPTIVE NOTES: If appropriate, enter the type of report, e.g., interim, progress, summary, annual, or final. Give the inclusive dates when a specific reporting period is covered.

5. AUTHOR(S): Enter the name(s) of author(s) as shown on or in the report. Enter last name, first name, middle initial. If military, show rank and branch of service. The name of the principal author is an absolute minimum requirement.

6. REPORT DATE: Enter the date of the report as day, month, year; or month, year. If more than one date appears on the report, use date of publication.

7a. TOTAL NUMBER OF PAGES: The total page count should follow normal pagination procedures, i.e., enter the number of pages containing information.

7b. NUMBER OF REFERENCES: Enter the total number of references cited in the report.

8a. CONTRACT OR GRANT NUMBER: If appropriate, enter the applicable number of the contract or grant under which the report was written.

8b, 8c, & 8d. PROJECT NUMBER: Enter the appropriate military department identification, such as project number, subproject number, system numbers, task number, etc.

9a. ORIGINATOR'S REPORT NUMBER(S): Enter the official report number by which the document will be identified and controlled by the originating activity. This number must be unique to this report.

9b. OTHER REPORT NUMBER(S): If the report has been assigned any other report numbers (either by the originator or by the sponsor), also enter this number(s).

10. AVAILABILITY/LIMITATION NOTICES: Enter any limitations on further dissemination of the report, other than those imposed by security classification, using standard statements such as:

(1) "Qualified requesters may obtain copies of this report from DDC."

(2) "Foreign announcement and dissemination of this report by DDC is not authorized."

(3) "U. S. Government agencies may obtain copies of this report directly from DDC. Other qualified DDC users shall request through

_____ ."

(4) "U. S. military agencies may obtain copies of this report directly from DDC. Other qualified users shall request through

_____ ."

(5) "All distribution of this report is controlled. Qualified DDC users shall request through

_____ ."

If the report has been furnished to the Office of Technical Services, Department of Commerce, for sale to the public, indicate this fact and enter the price, if known.

11. SUPPLEMENTARY NOTES: Use for additional explanatory notes.

12. SPONSORING MILITARY ACTIVITY: Enter the name of the departmental project office or laboratory sponsoring (paying for) the research and development. Include address.

13. ABSTRACT: Enter an abstract giving a brief and factual summary of the document indicative of the report, even though it may also appear elsewhere in the body of the technical report. If additional space is required, a continuation sheet shall be attached.

It is highly desirable that the abstract of classified reports be unclassified. Each paragraph of the abstract shall end with an indication of the military security classification of the information in the paragraph, represented as (TS), (S), (C), or (U).

There is no limitation on the length of the abstract. However, the suggested length is from 150 to 225 words.

14. KEY WORDS: Key words are technically meaningful terms or short phrases that characterize a report and may be used as index entries for cataloging the report. Key words must be selected so that no security classification is required. Identifiers, such as equipment model designation, trade name, military project code name, geographic location, may be used as key words but will be followed by an indication of technical context. The assignment of links, rules, and weights is optional.

DD FORM 1 JAN 64 1473 (BACK)